Janne Kokkala

Quantum computing with itinerant microwave photons

School of Science

Thesis submitted for examination for the degree of Master of Science in Technology.

Espoo 27.03.2013

Thesis supervisor:

Prof. Risto Nieminen

Thesis instructor:

Adj. Prof. Mikko Möttönen

Aalto University
School of Science

AALTO UNIVERSITY
SCHOOL OF SCIENCE

ABSTRACT OF THE
MASTER'S THESIS

Author: Janne Kokkala

Title: Quantum computing with itinerant microwave photons

Date: 27.03.2013 Language: English Number of pages: 6+69

School of Science

Department of Applied Physics

Professorship: Engineering Physics Code: Tfy-105

Supervisor: Prof. Risto Nieminen

Instructor: Adj. Prof. Mikko Möttönen

Microwave photons in superconducting circuits is a promising approach for quantum computing due to long coherence times and the easy controllability of superconducting devices. However, as the search of the ultimate design of a quantum computer is still ongoing, various suggestions for the realization of a quantum bit, qubit, exist even in the area of superconducting circuits.

In this thesis, we study theoretically quantum computing using itinerant microwave photons as qubits. Basic tools for treating the reflection of wave packets and the noise generated by resistive elements in a circuit are derived starting from a widely used model for superconducting transmission lines. We also present simple quantum devices that can act as quantum gates for microwave qubits, including a novel suggestion for a tunable phase shifter. A tunable phase shifter is a useful component in the study of microwave photons in general as well as in quantum computing. The tunable phase shifter consists of three superconducting quantum interference devices (SQUIDs) that can be treated as tunable inductors in the low-power regime.

The results of this thesis can be used both in applications related to quantum computing and in the general study of quantum mechanics in circuits. In particular, we conclude that there exist feasible system parameters, for which it should be possible to demonstrate the tunable phase shifter utilizing available experimental techniques. We also show the principle how the possible nonlinearity of the phase shifter can be used in a two-qubit gate providing interactions between microwave photons.

Keywords: quantum computing, microwave photon, superconducting circuit, tunable phase shifter, SQUID

AALTO-YLIOPISTO
PERUSTIETEIDEN KORKEAKOULU

DIPLOMITYÖN
TIIVISTELMÄ

Tekijä: Janne Kokkala

Työn nimi: Kvanttilaskenta kiertävillä mikroaaltofotoneilla

Päivämäärä: 27.03.2013 Kieli: englanti Sivumäärä: 6+69

Perustieteiden korkeakoulu

Teknillisen fysiikan laitos

Professuuri: Teknillinen fysiikka Koodi: Tfy-105

Valvoja: prof. Risto Nieminen

Ohjaaja: dos. Mikko Möttönen

Mikroaaltofotonien käyttö suprajohtavissa piiresissä on pitkien koherenssiaikojen ja suprajohtavien laitteiden hallittavuuden ansiosta lupaava lähestymistapa kvanttilaskennalle. Kvanttitietokoneen lopullinen rakenne ei ole vielä tiedossa, ja myös suprajohtavissa piireissä on esitetty useita vaihtoehtoja kvanttibitin, kubitin, toteuttamiseksi.

Tässä työssä tutkimme teoreettisesti kiertävien mikroaaltofotonien käyttöä kvanttilaskennassa. Johdamme yleisestä suprajohtavan siirtolinjan mallista lähtien perustyökaluja aaltopakettien heijastumisen ja resistiivisistä komponenteista aiheutuvan kohinan käsittelyyn. Esittelemme myös yksinkertaisia kvanttilaitteita, joita voidaan käyttää kvanttiportteina mikroaaltokubiteille. Yksi laitteista on uudenlainen säädettävä vaiheensiirrin, jota voidaan käyttää kvanttilaskennan lisäksi myös yleisesti mikroaaltofotonien tutkimiseen. Säädettävä vaiheensiirrin koostuu kolmesta suprajohtavasta kvantti-interferenssilaitteesta (SQUIDistä), joita voidaan matalilla tehoilla käsitellä säädettävinä induktoreina.

Työn tuloksia voidaan käyttää sekä kvanttilaskentaan liittyvissä sovelluksissa että yleisesti kvanttimekaniikan tutkimiseen virtapiireissä. Näytämme työssä, että on olemassa kokeellisesti toteutettavissa olevat parametrit, joilla säädettävän vaiheensiirtimen toiminta voidaan osoittaa tällä hetkellä käytettävissä olevilla kokeellisilla tekniikoilla. Näytämme myös, miten vaiheensiirtimen mahdollista epälineaarisuutta voidaan käyttää kaksikubittiportissa, joka mahdollistaisi mikroaaltofotonien välisen vuorovaikutuksen.

Avainsanat: kvanttilaskenta, mikroaaltofotoni, suprajohtava virtapiiri, säädettävä vaiheensiirrin, SQUID

Acknowledgements

This thesis was written in Quantum Computing and Devices group (QCD) of the Centre of Excellence in Computational Nanoscience (COMP) in the Department of Applied Physics of Aalto University. I thank the leader of COMP, Prof. Risto Nieminen, for acting as the supervisor of this thesis. I also thank the leader of QCD, Adj. Prof. Mikko Möttönen, who has instructed this thesis.

Finally, I want to thank the people at Ristin kilta for being friends to me throughout my student life in Otaniemi, especially Johannes Haataja for being a physicist to a physicist, Hannu Hartikainen for celebrating 1337, and Paavo Leinonen for sharing his knowledge of electrical engineering during my thesis work; `#kiltis` for providing opinions on thesis writing and physics in general; Tuomo Tanttu for constantly commenting on the progress of my work; and my family for their support.

Otaniemi, 27.03.2013

Janne Ilmari Kokkala

Contents

Chapter 1

Introduction

The concept of quantum computing was introduced in 1982 when Richard Feynman suggested that a computer based on quantum mechanics would be efficient in simulating quantum mechanical systems [1]. David Deutsch described the concept of universal quantum computer further and argued that any physical system could be simulated efficiently by it [2]. Quantum computing attracted widespread interest finally when Peter Shor discovered polynomial-time algorithms for discrete logarithm and factoring of integers, much faster than any known classical algorithm, showing the superior power of quantum computers in certain classical problems compared with classical computers [3].

An important aspect of quantum information theory is quantum communication, the ability to transmit quantum states while preserving their coherence. An example of the benefits of quantum communication is the distribution of secret keys, called quantum key distribution (QKD). In QKD, a third party eavesdropping the communication can be detected, based on the quantum mechanical principle that observation of a system affects the system. Quantum key distribution over distances exceeding 40 km has been demonstrated experimentally. [4]

The ideal quantum computer should be both controllable and isolated from the environment to maintain coherence for the time of the operation. Naturally, these two requirements contradict and thus provide a challenge for realizing a quantum computer. To date, various realizations of quantum bits have been proposed, ranging from nuclear spins in a liquid to solid state Josephson junction arrays [4].

Single photons provide a possible scheme for quantum computing. The study of single photons in a cavity interacting with atoms, so-called cavity quantum electrodynamics, is a wide field with applications also outside quantum computing [5]. In quantum computing, photons can either be used directly as qubits or to provide interaction between atoms acting as qubits. Further, optical photons are a convenient scheme for quantum communication channels for their ability to travel long distances maintaining coherence.

However, since optical photons do not interact directly with each other and only very weak nonlinear effects have been observed in so-called Kerr medium, using them as qubits is not a convenient choice for multi-qubit operations. A scheme for probabilistic linear optical quantum computing has been proposed [6] but probabilistic quantum computing is not the ideal solution due to its large overhead in resources. Furthermore, cavity quantum electrodynamics at optical frequencies suffers from the difficulty of controlling single atoms and from the limited lifetime of the atoms in the cavity, leading to the question whether the ideas of optical quantum computing can be used in other systems.

Superconducting circuits provide a promising approach for quantum computing due to in-situ tunability and integrability with classical electronics [7]. The ideas of optical quantum electrodynamics can be used in systems copuling artificial atoms with microwave photons in superconducting waveguides. Circuit quantum electrodynamics is a growing field of research which is used for studying both quantum information and topics related to quantum optics. [8]

In this thesis, we focus on itinerant microwave photons in superconducting transmission lines. We review the formalism for single-photon wave packets starting from the quantization of the transmission line and we briefly study the photon reflection in the case of a transmission line terminated by an impedance. In addition, we review some devices for superconducting microwave circuits and present a novel idea for a tunable phase shifter which can be used both in quantum computing and in the study of microwaves in superconducting circuits.

The thesis is structured as follows: In Ch. 2, we present the theoretical principles of quantum computing, optical quantum computing, and superconducting devices. In Ch. 3, we focus on the properties of superconducting transmission lines in the single-photon regime by presenting the model of a superconducting transmission line and reviewing some special cases. Further, in Ch. 4, we present devices that can be used as quantum logic gates for microwave photons in superconducting circuits. Finally, we conclude the observations made in this thesis in Ch. 5.

Chapter 2

Background

In this chapter, we introduce the main concepts of quantum computing, optical quantum computing, and quantum electrodynamics. We continue by giving a short introduction to superconductivity and the properties of the superconducting quantum interference device. Finally, we outline some ideas on circuits for microwave photons.

2.1 Quantum computing

2.1.1 Qubit

A classical bit is a system with two possible states, denoted by 0 and 1. A qubit is a quantum system with two basis states, denoted by $|0\rangle$ and $|1\rangle$. The basis states correspond to the two possible values of the classical bit. In contrast to the classical bit, the qubit is a quantum system and thus it can be in a superposition of the basis states. The state of a qubit $|\psi\rangle$ can be expressed as

$$|\psi\rangle = \alpha|0\rangle + \beta|1\rangle, \tag{2.1}$$

where $|\alpha|^2 + |\beta|^2 = 1$. In quantum mechanics, the global phase of the system is irrelevant, and the general form of the state of a qubit can be expressed as

$$|\psi\rangle = \cos\theta|0\rangle + e^{i\varphi}\sin\theta|1\rangle. \tag{2.2}$$

Thus the state of one qubit can be represented as a vector on a unit sphere, where φ is the azimuthal angle and θ is the polar angle.

In an ideal measurement of the state of the qubit in the computational basis $\{|0\rangle, |1\rangle\}$, the result 0 is obtained with probability $|\alpha|^2$ and the result 1 is obtained with probability $|\beta|^2$. The measurement projects the state of the qubit into the basis state $|0\rangle$ or $|1\rangle$ corresponding to the obtained result.

A system with n classical bits has 2^n different states. On the other hand, the state of a quantum system with n qubits lies in the Hilbert space with 2^n basis states. Usually, the basis states are denoted by $|x_1\rangle \otimes |x_2\rangle \otimes \ldots \otimes |x_n\rangle = |x_1 x_2 \ldots x_n\rangle$, where $x_i \in \{0,1\}$ refers to the state of the ith qubit. The general state of an n-qubit system is given by

$$|\psi\rangle = \sum_{x \in \{0,1\}^n} \alpha_{x_1 x_2 \ldots x_n} |x_1 x_2 \ldots x_n\rangle, \tag{2.3}$$

where $\sum |\alpha_{x_1 x_2 \ldots x_n}|^2 = 1$ and we used the notation $x = (x_1, x_2, \ldots, x_n)$.

Measuring the state of the ith qubit in the n-qubit system yields $k \in \{0,1\}$ with probability $\sum_{\substack{x \in \{0,1\}^n \\ x_i = k}} |\alpha_{x_1 x_2 \ldots x_n}|^2$, and the measurement projects the state of the qubit into

$$\frac{1}{\sqrt{\sum_{\substack{x \in \{0,1\}^n \\ x_i = k}} |\alpha_{x_1 x_2 \ldots x_n}|^2}} \sum_{\substack{x \in \{0,1\}^n \\ x_i = k}} \alpha_{x_1 x_2 \ldots x_n} |x_1 x_2 \ldots x_n\rangle. \tag{2.4}$$

The ideal measurement of a qubit or an n-qubit state after which the state is projected to a corresponding eigenstate, thereby yielding the same result if the measurement is instantly repeated, is called a quantum nondemolition (QND) measurement [9].

The state of a single qubit can be expressed as a 2-dimensional vector,

$$\alpha|0\rangle + \beta|1\rangle \hat{=} \begin{pmatrix} \alpha \\ \beta \end{pmatrix}, \tag{2.5}$$

and the state of an n-qubit system can be expressed as a 2^n-dimensional vector,

$$\sum_{x \in \{0,1\}^n} \alpha_{x_1 x_2 \ldots x_n} |x_1 x_2 \ldots x_n\rangle \hat{=} \begin{pmatrix} \alpha_{00\ldots000} \\ \alpha_{00\ldots001} \\ \alpha_{00\ldots010} \\ \alpha_{00\ldots011} \\ \vdots \end{pmatrix}, \tag{2.6}$$

where the vector representation of a basis state $|x_1 x_2 \ldots x_n\rangle$ is the Kronecker product of the vector representations of the single qubit basis states $|x_1\rangle, |x_2\rangle, \ldots, |x_n\rangle$.

In this thesis, we consider only *pure states* of quantum systems. A *mixed state* of a quantum system is a statistical ensemble of pure states, which can be used to describe systems with decoherence.

2.1.2 Entanglement

The state $|\Psi\rangle$ of a n-qubit system is *separable* if it can be written as

$$|\Psi\rangle = |\psi_1\rangle \otimes |\psi_2\rangle \otimes \ldots \otimes |\psi_n\rangle, \tag{2.7}$$

where $|\psi_i\rangle$ is the single-qubit state of the ith qubit. Measuring the state of the ith qubit projects the system into state

$$|\Psi\rangle = |\psi_1\rangle \otimes |\psi_2\rangle \otimes \ldots \otimes |\psi_{i-1}\rangle \otimes |\tilde{\psi}_i\rangle \otimes |\psi_{i+1}\rangle \otimes \ldots \otimes |\psi_n\rangle, \tag{2.8}$$

where $|\tilde{\psi}_i\rangle$ is the state of the ith qubit corresponding to the result of the measurement. Thus when multiple qubits are measured, the outcomes are independent. If the pure state of an n-qubit system is not separable, it is *entangled*. For engtangled states, the outcomes of the measurements of multiple qubits are generally not independent.

The general form of a pure separable 2-qubit state is

$$|\Psi\rangle = (\alpha|0\rangle + \beta|1\rangle)(\gamma|0\rangle + \delta|1\rangle) = \alpha\gamma|00\rangle + \alpha\delta|01\rangle + \beta\gamma|10\rangle + \beta\delta|11\rangle. \tag{2.9}$$

For example the state $\frac{1}{\sqrt{2}}(|00\rangle + |11\rangle)$ is not separable since it cannot be expressed as a product of two single-qubit states. When either qubit is measured, the state of the system becomes either $|00\rangle$ or $|11\rangle$, depending on the outcome of the first measurement. Therefore, the possible outcomes on measuring both qubits are only 00 and 11.

2.1.3 Quantum logic gates

The evolution of a coherent quantum system is always unitary, and thus the valid operations on qubits, i.e., quantum gates, are mappings $|\psi\rangle \to \hat{U}|\psi\rangle$, where $\hat{U}$ is a unitary operator. In the vector representation, the quantum gate from n to n qubits can be expressed as a multiplication by a unitary matrix U of size $2^n \times 2^n$. Because unitary, a quantum gate is always linear and reversible. Thus, a quantum gate can be defined by its effect on the basis states. Because the global phase of the state of the n-qubit system is physically irrelevant, the global phase of a n-qubit gate is irrelevant.

Many of the gates used in classical computers have two input bits and one output bit. They are not reversible, and thus they do not have exactly equivalent quantum counterparts. Nevertheless, for example the classical NAND gate can be implemented as a 3-qubit gate with an additional fixed input qubit where two of the output qubits are ignored [4]. In classical computing, any function from $\{0,1\}^n$ to $\{0,1\}^m$ can be realized combining simple logic gates. In quantum computing, classical functions can be realized using reversible quantum gates with additional input and output qubits. For example, a classical function $f : \{0,1\}^n \to \{0,1\}^m$ can be realized as a $(n+m)$-bit quantum gate which maps $|x\rangle|y\rangle$ where $x \in \{0,1\}^n$ and $y \in \{0,1\}^m$ to $|x\rangle|y \oplus f(y)\rangle$ where $\oplus$ is elementwise sum modulo 2.

Applying multiple n-qubit gates $\hat{U}_1, \hat{U}_2, \ldots \hat{U}_m$ to a n-qubit system successively maps the state $|\psi\rangle$ to $\hat{U}_m \ldots \hat{U}_1|\psi\rangle$. Therefore, the operation of multiple gates combined can be presented as a single gate. On the other hand, a complicated gate can be decomposed into product of simpler gates. A set S of n-qubit gates is called

universal if all n-qubit gates can be expressed as product of gates in S. For physical realization of quantum computer, the concept of universal gates is useful: if it is shown that a universal set of n-qubit gates can be realized physically, any n-qubit gate can be realized combining the elementary gates. For example, the single-qubit gates and the CNOT gate, which are presented below, constitute a universal set.

2.1.4 Single-qubit gates

In classical computing, the only nontrivial one-bit gate is the NOT gate which maps 0 to 1 and vice versa. The quantum equivalent to the classical NOT gate maps $|0\rangle$ to $|1\rangle$ and $|1\rangle$ to $|0\rangle$. It is represented by the matrix

$$X = \begin{pmatrix} 0 & 1 \\ 1 & 0 \end{pmatrix}, \tag{2.10}$$

and thus it maps the state $\alpha|0\rangle + \beta|1\rangle$ to $\beta|0\rangle + \alpha|1\rangle$.

Another useful single qubit gate is the Hadamard gate represented by

$$H = \frac{1}{\sqrt{2}} \begin{pmatrix} 1 & 1 \\ 1 & -1 \end{pmatrix}, \tag{2.11}$$

which is the size-2 discrete Fourier transform. It maps the states $|0\rangle$ and $|1\rangle$ to the states $|+\rangle = \frac{1}{\sqrt{2}}(|0\rangle + |1\rangle)$ and $|-\rangle = \frac{1}{\sqrt{2}}(|0\rangle - |1\rangle)$, respectively. The Hadamard gate is also its own inverse, $HH = I$. In other words, applying the Hadamard gate twice to a qubit results in the initial state of the qubit.

Another single qubit gate is the phase shift gate defined by $|0\rangle \to |0\rangle$ and $|1\rangle \to e^{i\phi}|1\rangle$. It is represented by the matrix

$$R(\phi) = \begin{pmatrix} 1 & 0 \\ 0 & e^{i\phi} \end{pmatrix}. \tag{2.12}$$

Any single qubit gate can be represented as a unitary 2×2 matrix. A general unitary matrix U can be written as

$$U = e^{i\varphi_1} \begin{pmatrix} \cos\theta & e^{i\varphi_2}\sin\theta \\ -e^{i\varphi_3}\sin\theta & e^{i(\varphi_3+\varphi_2)}\cos\theta \end{pmatrix}. \tag{2.13}$$

The matrix U can be further decomposed into

$$\begin{aligned} U &= e^{i\varphi_1} \begin{pmatrix} \cos\theta & e^{i\varphi_2}\sin\theta \\ -e^{i\varphi_3}\sin\theta & e^{i(\varphi_3+\varphi_2)}\cos\theta \end{pmatrix} \\ &= e^{i\varphi_1} \begin{pmatrix} \cos\theta & -e^{i(\varphi_2+\frac{\pi}{2})}i\sin\theta \\ -e^{i(\varphi_3-\frac{\pi}{2})}i\sin\theta & e^{i(\varphi_3+\varphi_2)}\cos\theta \end{pmatrix} \\ &= e^{i\varphi_1} \begin{pmatrix} 1 & 0 \\ 0 & e^{i(\varphi_3-\frac{\pi}{2})} \end{pmatrix} \begin{pmatrix} \cos\theta & -i\sin\theta \\ -i\sin\theta & \cos\theta \end{pmatrix} \begin{pmatrix} 1 & 0 \\ 0 & e^{i(\varphi_2+\frac{\pi}{2})} \end{pmatrix} \end{aligned}$$

$$= e^{i\varphi_1} \begin{pmatrix} 1 & 0 \\ 0 & e^{i(\varphi_3 - \frac{\pi}{2})} \end{pmatrix} \frac{1}{\sqrt{2}} \begin{pmatrix} 1 & 1 \\ 1 & -1 \end{pmatrix} e^{-i\theta} \begin{pmatrix} 1 & 0 \\ 0 & e^{i2\theta} \end{pmatrix} \frac{1}{\sqrt{2}} \begin{pmatrix} 1 & 1 \\ 1 & -1 \end{pmatrix} \begin{pmatrix} 1 & 0 \\ 0 & e^{i(\varphi_2 + \frac{\pi}{2})} \end{pmatrix}$$
$$= e^{i(\varphi_1 - \theta)} R(\varphi_3 - \frac{\pi}{2}) H R(2\theta) H R(\varphi_2 + \frac{\pi}{2}). \tag{2.14}$$

The global phase $e^{i(\varphi_1 - \theta)}$ is meaningless, and thus any single qubit gate can be constructed using only phase shift gates and Hadamard gates. For example, the NOT gate introduced earlier can be expressed as $X = HR(\pi)H$. In other words, the NOT operation can be performed by applying a Hadamard gate, a phase shift of π, and another Hadamard gate in this order.

2.1.5 Multi-qubit gates

It can be shown that any n-qubit gate can be implemented using a universal set consisting only of 2-qubit gates [4]. Here, we restrict our attention to 2-qubit gates.

The simplest 2-qubit gates are the ones that treat each qubit separately. Applying an operator $\hat{U}_1$ to the first qubit and an operator $\hat{U}_2$ to the second qubit separately maps $|x_1 x_2\rangle = |x_1\rangle \otimes |x_2\rangle$ to $\hat{U}_1|x_1\rangle \otimes \hat{U}_2|x_2\rangle$. This is equal to applying the operator $\hat{U} = \hat{U}_1 \otimes \hat{U}_2$ to the 2-qubit system.

However, the simple gates cannot create entangled states from separable states, and quantum computing requires other types of 2-qubit gates, too. The simplest nontrivial 2-qubit gate is the controlled not gate, CNOT : $|x_1 x_2\rangle \rightarrow |x_1, x_2 \oplus x_1\rangle$, where $\oplus$ is addition modulo 2. It performs the NOT operation to the second qubit if the first qubit is $|1\rangle$. In matrix representation, CNOT can be written as

$$CN = \begin{pmatrix} 1 & 0 & 0 & 0 \\ 0 & 1 & 0 & 0 \\ 0 & 0 & 0 & 1 \\ 0 & 0 & 1 & 0 \end{pmatrix}. \tag{2.15}$$

Another common 2-qubit gate is the controlled phase shift, CZ : $|x_1 x_2\rangle \rightarrow (-1)^{x_1 x_2} |x_1 x_2\rangle$, which shifts the phase of the 2-qubit system by π only if both of the qubits are at $|1\rangle$. The matrix representation is

$$CZ = \begin{pmatrix} 1 & 0 & 0 & 0 \\ 0 & 1 & 0 & 0 \\ 0 & 0 & 1 & 0 \\ 0 & 0 & 0 & -1 \end{pmatrix}. \tag{2.16}$$

By simple matrix multiplication, we find that

$$CN = (I \otimes H) CZ (I \otimes H), \tag{2.17}$$

meaning that the CNOT gate can be constructed using Hadamard gates for the second qubit and a CZ gate.

A CNOT or a CZ gate along with single-qubit gates is a universal set of 2-qubit gates [4].

2.2 Optical quantum computing

Using photons as qubits is an attractive choice for quantum computing. Optical photons can travel long distances in optical fibers and single qubit gates can be easily created using commercial beam splitters and phase shifters. However, photons do not interact directly with each other, which is a challenge for implementing nontrivial two-qubit gates. Nevertheless, optical photons can be made to interact with each other via nonlinear medium.

2.2.1 Realization of a qubit

In an electromagnetic cavity, the energy is quantized in units of $\hbar\omega$ and the quantum of energy is called a photon. The quantum properties of photons have been widely studied. The state of a cavity with a single photon mode can be expressed in terms of the Fock states, where $|n\rangle$ is the state with $n \geq 0$ photons in the chosen mode. The bosonic annihilation and creation operators are denoted by $\hat{a}$ and $\hat{a}^\dagger$, for which

$$\hat{a}|n\rangle = \sqrt{n}|n-1\rangle, \tag{2.18}$$

$$\hat{a}^\dagger|n\rangle = \sqrt{n+1}|n+1\rangle, \tag{2.19}$$

$$[\hat{a}, \hat{a}^\dagger] = 1. \tag{2.20}$$

The Hamiltonian of a cavity with a single mode of frequency ω is

$$\hat{H} = \hbar\omega\hat{a}^\dagger\hat{a}, \tag{2.21}$$

where the zero-point energy $\hbar\omega/2$ is omitted. In this thesis, we focus on itinerant photons, i.e., photons travelling in a waveguide from a source to a detector, instead of photons confined in a cavity. Nevertheless, considering only photons of single frequency, the Hamiltonian can be approximated by that of a cavity.

A trivial choice for a qubit would be a cavity where the Fock states $|0\rangle$ and $|1\rangle$ correspond to the qubit states. However, one cavity cannot be approximated as a two-level system because the energy gap between $|0\rangle$ and $|1\rangle$ is equal to the energy gap between $|1\rangle$ and $|2\rangle$. Therefore, operations on the cavity may easily result in a state which is not a superposition of only the qubit states.

A more convenient way of defining a qubit is using the dual-rail representation shown in Fig. 2.1: there are two independent photon modes with equal frequency ω, and the qubit states $|0_Q\rangle, |1_Q\rangle$ correspond to a single photon being in one mode or in the other. Let $|mn\rangle$ be the state where the first waveguide is in Fock state $|m\rangle$ and

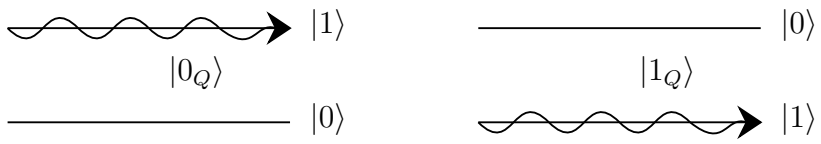

Figure 2.1: Dual-rail representation of a qubit. The photon being on the first mode corresponds to the qubit state $|0_Q\rangle$ and the photon being on the second mode corresponds to the qubit state $|1_Q\rangle$.

the second waveguide is in Fock state $|n\rangle$. The logical states of the qubit are then defined by

$$|0_Q\rangle = |10\rangle, \qquad |1_Q\rangle = |01\rangle. \tag{2.22}$$

Let $\hat{a}_0$ and $\hat{a}_1$ be the bosonic annihilation operators for the first and second waveguide, respectively. The Hamiltonian of the system is

$$\hat{H} = \hbar\omega(\hat{a}_0^\dagger \hat{a}_0 + \hat{a}_1^\dagger \hat{a}_1). \tag{2.23}$$

Both $|10\rangle$ and $|01\rangle$ are eigenstates of $\hat{H}$ with energy $\hbar\omega$. Thus, the state of the qubit $|\psi\rangle = c_0|0_Q\rangle + c_1|1_Q\rangle$ changes only by an overall phase in time evolution. In the dual-rail-representation, single-qubit operations conserving the photon number keep the system in a state that corresponds to a qubit state.

For optical photons, the two modes in the Hamiltonian (2.23) can also be different polarization directions [10]. In coplanar waveguides considered in this thesis however, there is only one polarization direction, and thus we use photons in two separate waveguides.

2.2.2 Single-qubit gates

An optical phase shifter of an angle ϕ on a single waveguide slows down the time evolution of the phase of a photon. Compared to a waveguide with index of refraction n_0, it takes $(n - n_0)d/c$ more time for light to propagate a distance d in a medium with index of refraction n, and the obtained phase shift for a single photon is $\phi = \omega(n - n_0)d/c$. Therefore, the phase shifter induces a transform from the Fock state $|n\rangle$ to $e^{in\phi}|n\rangle$. As illustrated in Fig. 2.2, in the dual-rail representation, a phase shifter on only the second waveguide yields evolution from $c_0|10\rangle + c_1|01\rangle$ to $c_0|10\rangle + e^{i\phi}c_1|01\rangle$, which performs the phase shift gate $R(\phi)$.

An optical beam splitter has two input modes $\hat{a}_{0,1}^{\text{in}}$ and two output modes $\hat{a}_{0,1}^{\text{out}}$. The inputs and outputs are related by

$$\begin{pmatrix} \hat{a}_0^{\text{out}} \\ \hat{a}_1^{\text{out}} \end{pmatrix} = S \begin{pmatrix} \hat{a}_0^{\text{in}} \\ \hat{a}_1^{\text{in}} \end{pmatrix}, \tag{2.24}$$

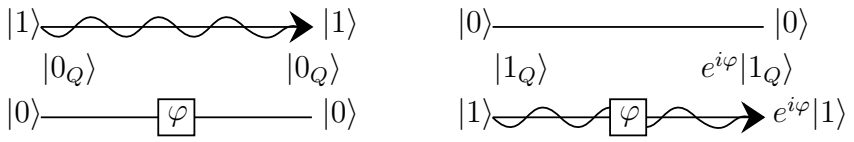

Figure 2.2: Phase shift gate with one optical phase shifter of φ. A photon on the first mode, corresponding to qubit state $|0_Q\rangle$, obtains no phase shift, and a photon on the second mode, corresponding to qubit state $|1_Q\rangle$, obtains a phase shift of φ.

where

$$S = \begin{pmatrix} \cos\theta & ie^{-i\varphi}\sin\theta \\ ie^{i\varphi}\sin\theta & \cos\theta \end{pmatrix}, \tag{2.25}$$

is the scattering matrix of the beam splitter [10]. The Fock states can be defined in the input and output sides of the beam splitter separately: Let $|mn\rangle_{\text{in(out)}}$ be the state with m photons in the mode $\hat{a}_0^{\text{in(out)}}$ and n photons in the mode $\hat{a}_1^{\text{in(out)}}$. The ground state of the system is $|00\rangle_{\text{in}} = |00\rangle_{\text{out}} =: |00\rangle$.

Let $|\psi\rangle = c_0|10\rangle_{\text{in}} + c_1|01\rangle_{\text{in}}$ be the state of the system. Using the unitarity of S, the state can be rewritten as

$$\begin{aligned} |\psi\rangle &= c_0|10\rangle_{\text{in}} + c_1|01\rangle_{\text{in}} = [c_0(\hat{a}_0^{\text{in}})^\dagger + c_1(\hat{a}_1^{\text{in}})^\dagger]|00\rangle \\ &= \begin{pmatrix} \hat{a}_0^{\text{in}} \\ \hat{a}_1^{\text{in}} \end{pmatrix}^\dagger \begin{pmatrix} c_0 \\ c_1 \end{pmatrix} |00\rangle = \begin{pmatrix} \hat{a}_0^{\text{in}} \\ \hat{a}_1^{\text{in}} \end{pmatrix}^\dagger S^\dagger S \begin{pmatrix} c_0 \\ c_1 \end{pmatrix} |00\rangle = \begin{pmatrix} \hat{a}_0^{\text{out}} \\ \hat{a}_1^{\text{out}} \end{pmatrix}^\dagger S \begin{pmatrix} c_0 \\ c_1 \end{pmatrix} |00\rangle \\ &= [\tilde{c}_0(\hat{a}_0^{\text{out}})^\dagger + \tilde{c}_1(\hat{a}_1^{\text{out}})^\dagger]|00\rangle = \tilde{c}_0|10\rangle_{\text{out}} + \tilde{c}_1|01\rangle_{\text{out}}, \end{aligned} \tag{2.26}$$

where

$$\begin{pmatrix} \tilde{c}_0 \\ \tilde{c}_1 \end{pmatrix} = S \begin{pmatrix} c_0 \\ c_1 \end{pmatrix}. \tag{2.27}$$

In the input side, the state of the system can be interpreted as the qubit being in state $c_0|0_Q\rangle + c_1|1_Q\rangle$. In the output side, the state of the system can be interpreted as the qubit being in state $\tilde{c}_0|0_Q\rangle + \tilde{c}_1|1_Q\rangle$. Therefore, the beam splitter performs the single qubit gate described by the matrix S.

Combined with a phase shift gate $R(\phi)$, the transform is

$$U = R(\phi)S = \begin{pmatrix} \cos\theta & ie^{-i\varphi}\sin\theta \\ ie^{i(\varphi+\phi)}\sin\theta & e^{i\phi}\cos\theta \end{pmatrix}, \tag{2.28}$$

which is equivalent to the general unitary matrix in Eq. (2.13).

2.2.3 Two-qubit gates

As explained in Sec. 2.1.5, a CZ or a CNOT gate with single qubit gates is sufficient for realizing arbitrary two-qubit gates. However, for photonic qubits, realizing a two-qubit gate is a challenging task, and any two-qubit gate would be a significant

step towards an optical quantum computer. A two-qubit gate requires interaction between photons, and the simplest way is to use nonlinear medium [10]. In a Kerr medium, the classical index of refraction depends on the total intensity of light I,

$$n(I) = n_1 + n_2 I. \tag{2.29}$$

Therefore, two beams of light will acquire an extra phase shift depending on the intensity of the other beam. Quantum mechanically, this effect can be described by the unitary transform $e^{i\chi L \hat{a}^\dagger \hat{a} \hat{b}^\dagger \hat{b}}$, where χ is a coefficient related to n_2, L is the length of the nonlinear component, and $\hat{a}$ and $\hat{b}$ are the annihilation operators of the two modes. In the dual-rail representation for two-qubit system, we may connect the modes corresponding to the $|1_Q\rangle$ state of both qubits by a Kerr medium, and choosing $L = \pi/\chi$ this would yield the CZ gate. However, the Kerr coefficient χ is usually very small, and the length L cannot be increased enough because the known Kerr media are highly absorptive. Thus, using Kerr medium in optical quantum computing is impractical.

In 2000, it was proved [6] that scalable optical quantum computing is possible using only linear components. The KLM scheme relies on probabilistic gates where the result of a single operation is correct with a probability $p < 1$. With direct approach, a calculation using N gates succeeds with probability p^N and it should be repeated on the order of p^{-N} times. Nevertheless, in the KLM scheme, using teleportation tricks the computation can be done with only polynomial error probability. However, probabilistic quantum computing is not the ideal solution for scalable quantum computer due to its large overhead in resources, and hence is not considered in this thesis. [10]

2.3 Cavity quantum electrodynamics

Cavity quantum electrodynamics is the study of individual atoms interacting with only a few optical modes confined between mirrors. In an optical cavity with high quality factor, photons interact long time with the atoms before escaping. Here, a two-level atom with energy eigenstates $|g\rangle$ and $|e\rangle$ is described by the Hamiltonian

$$\hat{H}_\mathrm{a} = \frac{1}{2}\hbar\omega_\mathrm{a}\hat{\sigma}_z, \tag{2.30}$$

where $\hbar\omega_\mathrm{a}$ is the transition energy of the states and $\hat{\sigma}_z = |e\rangle\langle e| - |g\rangle\langle g|$. The Hamiltonian of the cavity with a single mode of frequency ω_c is the Hamiltonian of a harmonic oscillator,

$$\hat{H}_\mathrm{c} = \hbar\omega_\mathrm{c}\left(\hat{a}^\dagger\hat{a} + \frac{1}{2}\right), \tag{2.31}$$

where $\hat{a}$ is the annihilation operator of a photon with frequency ω_c. The interaction between the states is described by

$$\hat{H}_\mathrm{int} = \hbar g(\hat{a} + \hat{a}^\dagger)(|g\rangle\langle e| + |e\rangle\langle g|), \tag{2.32}$$

where g is the interaction strength. The total Hamiltonian of the system is

$$\hat{H} = \hat{H}_{\mathrm{a}} + \hat{H}_{\mathrm{c}} + \hat{H}_{\mathrm{int}}. \tag{2.33}$$

In the Jaynes–Cummings model, we use the rotating wave approximation to neglect the rapidly oscillating terms of the interaction Hamiltonian to obtain the Jaynes–Cummings Hamiltonian

$$\hat{H}_{\mathrm{JCM}} = \hbar\omega_{\mathrm{a}}\hat{\sigma}_z + \hbar\omega_{\mathrm{c}}\left(\hat{a}^\dagger\hat{a} + \frac{1}{2}\right) + \hbar g\left(\hat{a}|e\rangle\langle g| + \hat{a}^\dagger|g\rangle\langle e|\right). \tag{2.34}$$

This Hamiltonian is usually the starting point in studies of interaction between light and matter, and also for interaction between microwaves and superconducting qubits, as explained in Sec. 2.5.

The cavity QED approach can be used in quantum computing by either treating the atoms as qubits and using photons to couple them, or by storing the information into the cavity states and using the atoms as nonlinear medium to provide interaction between photons. [4]

2.4 Superconductivity

In some materials, a sudden disappearance of resistivity can be observed when the material is cooled below a critical temperature. The BCS theory, named after John Bardeen, Leon Cooper, and John Schrieffer, describes superconductivity as a condensate of electron pairs, so called Cooper pairs. The system is analogous to the Bose-Einstein condensate of bosons at low temperatures. Within the mean field approximation, the condensate can be described by the Ginzburg-Landau order parameter $\psi(\vec{r}) = |\psi(\vec{r})|\, e^{i\phi(\vec{r})}$, where the Cooper pair density is described by $|\psi(\vec{r})|^2$ and the phase $\phi(\vec{r})$ is related to the supercurrents. [11]

2.4.1 Josephson effect

A Josephson junction is a small insulating barrier or some other type of weak link between two superconducting leads. The capacitance C of the junction yields a charging energy $4e^2/(2C)$ for a Cooper pair. In addition, Cooper pairs can tunnel through the barrier resulting in a supercurrent even without any applied bias voltage. The Josephson effect is described by the following relations for the current I and voltage V across the junction:

$$I = I_c \sin\varphi, \tag{2.35}$$

$$V = \frac{\Phi_0}{2\pi}\partial_t\varphi, \tag{2.36}$$

where $\Phi_0 = h/2e$ is the flux quantum, φ is the superconductor phase difference across the junction, and I_c is the critical current of the junction which depends on the physical properties of the junction. The phase difference φ is a quantum operator $\hat{\varphi}$ whose conjugate is the number of Cooper pairs $\hat{n}$ transferred through the junction. Assuming small charging energy in the junction, the state of the system is close to an eigenstate of $\hat{\varphi}$ and thus we may treat the phase difference as a classical variable [12].

Integrating VI over time yields the energy associated with the Josephson effect,

$$U_J(\varphi) = -E_J \cos\varphi, \tag{2.37}$$

where $E_J = \frac{\Phi_0 I_c}{2\pi}$ is called the Josephson energy of the junction.

2.4.2 Superconducting quantum interference device

A superconducting quantum interference device (SQUID) consists of two parallel Josephson junctions forming a loop, as shown in Fig. 2.3. An external magnetic field contributes to the phase change around the ring by $2\pi\Phi/\Phi_0$, where Φ is the external magnetic flux threading the loop. Because the order parameter has to be single valued, the total phase change in a loop is a multiple of 2π. Thus we have

$$-\varphi_1 + \varphi_2 + 2\pi\frac{\Phi}{\Phi_0} = 2n\pi, \quad n \in \mathbb{Z}. \tag{2.38}$$

For this equation to be satisfied, a supercurrent I_s circulates in the ring, generating a difference on the currents through the Josephson junctions. The energetically

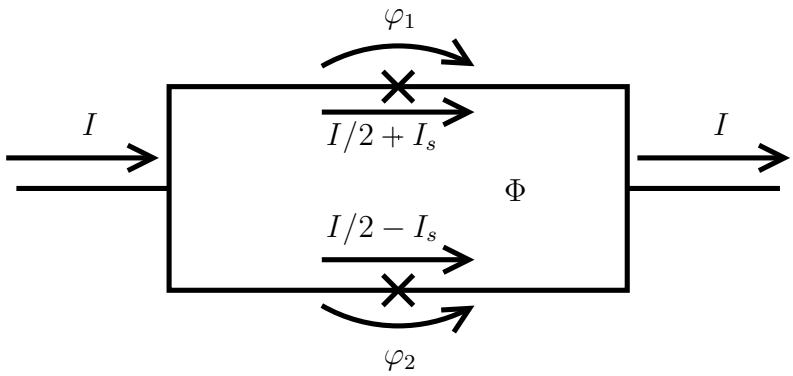

Figure 2.3: Superconducting quantum interference device (SQUID) consisting of two parallel Josephson junctions forming a loop. The current through the SQUID is I, and the external magnetic flux threading the loop is Φ. The phase differences across the Josephson junctions are φ_1 and φ_2 and the currents through the junctions are $I/2 + I_s$ and $I/2 - I_s$, where I_s is the loop current caused by the magnetic field.

optimal I_s is obtained when $|\varphi_1 - \varphi_2|$ is smallest. Hence

$$\begin{aligned} & \frac{\varphi_1 - \varphi_2}{2} = \pi\frac{\Phi}{\Phi_0} - n\pi \\ \Leftrightarrow \quad & \cos\left(\frac{\varphi_1 - \varphi_2}{2}\right) = (-1)^n \cos\left(\pi\frac{\Phi}{\Phi_0}\right) \\ \Leftrightarrow \quad & \cos\left(\frac{\varphi_1 - \varphi_2}{2}\right) = \left|\cos\left(\pi\frac{\Phi}{\Phi_0}\right)\right|, \end{aligned} \tag{2.39}$$

where on the last line we used the fact that the smallest solution for $|\varphi_1 - \varphi_2|$ is obtained when $|\varphi_1 - \varphi_2| < \pi$, and thus the left-hand-side of the equation is positive.

Assuming negligible self-indcutance of the loop and symmetric SQUID with identical Josephson junctions with critical currents I_{c0}, the total phase difference over the SQUID is $\varphi = (\varphi_1 + \varphi_2)/2$, and the total current assumes the form

$$\begin{aligned} I &= I_{c0}\sin\varphi_1 + I_{c0}\sin\varphi_2 = 2I_{c0}\cos\left(\frac{\varphi_1 - \varphi_2}{2}\right)\sin\left(\frac{\varphi_1 + \varphi_2}{2}\right) \\ &= 2I_{c0}\left|\cos\left(\pi\frac{\Phi}{\Phi_0}\right)\right|\sin\varphi. \end{aligned} \tag{2.40}$$

Defining the critical current of the SQUID as

$$I_c(\Phi) = 2I_{c0}\left|\cos\left(\pi\frac{\Phi}{\Phi_0}\right)\right|, \tag{2.41}$$

the total current assumes the form

$$I = I_c(\Phi)\sin\varphi. \tag{2.42}$$

If a voltage V is applied across the SQUID, the same voltage occurs across both Josephson junctions, yielding

$$\frac{\Phi_0}{2\pi}\partial_t\varphi = \frac{\Phi_0}{4\pi}(\partial_t\varphi_1 + \partial_t\varphi_2) = V. \tag{2.43}$$

Equations (2.42) and (2.43) are the Josephson relations for a Josephson junction with a critical current $I_c(\Phi)$. Therefore, the SQUID is equivalent to a tunable Josephson junction whose critical current depends on the external magnetic flux as in Eq. (2.41). A real SQUID is not exactly symmetric, and thus there is a small minimum value for the critical current.

SQUID as a tunable inductor

Noting that $\partial_t I = I_c(\Phi)\cos\varphi\partial_t\varphi$ in the Josephson equations, the equations become similar to the voltage-current equation of an inductor,

$$V = \frac{\Phi_0}{2\pi}\partial_t\varphi = \frac{\Phi_0}{2\pi I_c(\Phi)\cos\varphi}\partial_t I. \tag{2.44}$$

For $\varphi \in [-\pi/2, \pi/2]$, Eq. (2.44) becomes

$$V = \frac{\Phi_0}{2\pi I_c(\Phi)\cos\varphi}\partial_t I = \frac{\Phi_0}{2\pi\sqrt{I_c(\Phi)^2 - I^2}}\partial_t I. \tag{2.45}$$

Thus the SQUID acts as a nonlinear inductor with current-dependent inductance

$$L_J(\Phi, I) = \frac{\Phi_0}{2\pi\sqrt{I_c^2 - I^2}}. \tag{2.46}$$

Expanding the inductance to the second power in $I = I_c(\Phi)\sin\varphi$ around $I_0 = I_c(\Phi)\sin\varphi_0$, we obtain

$$L_J(\Phi, I) = \frac{\Phi_0}{2\pi I_c(\Phi)\cos\varphi_0}\left[1 - \left(\frac{I - I_0}{\sqrt{2}I_c(\Phi)\cos\varphi_0}\right)^2\right]. \tag{2.47}$$

This expansion can be used to study the nonlinear effects of the SQUID [13, 14].

Assuming vanishing loop-inductance and small fluctuations in the current I and the total phase difference φ, that is, $|I - I_0| \ll \sqrt{2}I_c(\Phi)\cos\varphi_0$, a SQUID can be treated as a tunable linear inductor, inductance L_J of which is a function of the external magnetic flux threading the loop Φ, [15]

$$L_J(\Phi) = \frac{\Phi_0/2\pi}{I_c(\Phi)\cos\varphi_0}. \tag{2.48}$$

If the total capacitance of the SQUID C_J is small such that the plasma frequency of the SQUID $\omega_p = 1/\sqrt{L_J C_J}$ is high compared to the frequency of the relevant dynamics of the studied system, the SQUID can be characterized by the inductance. This model has been used, e.g., for analyzing the dynamical Casimir effect [12] and tunable heat conduction [16] in superconducting waveguides.

If a dc bias current I_b is applied across the SQUID, the current varies around $I_0 = I_c(\Phi)\sin\varphi_0 = I_b$. Thus the inductance of the SQUID can be tuned also by a dc bias current. Using a bias tee for the bias current, the dc bias current does not have other effects on the dynamics of the system for the photons.

2.5 Circuits for microwave photons

Superconducting circuits consisting of waveguides for microwave photons and devices acting as artificial atoms can be treated using the same theoretical methods as in optical quantum computing and optical cavity QED [7, 8, 17]. In superconducting circuits, the parameters of the system can be tuned to larger extent. In particular, the lifetime of the atom inside the cavity is infinite, and for example, using nonlinear elements in microwave circuits may provide stronger Kerr cross nonlinearity than in optical quantum computing [14]. Therefore, circuit cavity quantum

electrodynamics is a promising approach for quantum computing. A scalable fault-tolerant architechture for a quantum computer with superconducting circuits using microwave cavities has been proposed [18], and generation of single photons [19] and Fock states [20] has been demonstrated. In Ref. [14], a nondemolition measurement scheme for microwave resonators based on the Kerr cross nonlinearity caused by the nonlinearity of SQUIDs was proposed.

A commonly used superconducting artificial atom is the Cooper pair box (CPB) consists of a superconducting island connected to a reservoir via a Josephson junction through which Cooper pairs can tunnel and to a gate voltage V_g via a capacitance C_g. The Hamiltonian of the CPB is

$$\hat{H}_{\mathrm{CPB}} = 4E_c \left(\hat{n} - \frac{V_g}{2C_g e} \right)^2 + E_J \sum_n (|n+1\rangle\langle n| + |n\rangle\langle n+1|), \tag{2.49}$$

where E_c is the charging energy of a single electron on the island, $\hat{n}$ is the Cooper pair number operator of the island, and E_J is the Josephson energy of the Josephson junction. For $V_g \approx C_g e$, the system can be approximated as a two-state system with $n = 0, 1$. If the gate is connected to a superconducting cavity with a single mode, the gate voltage becomes an operator $\hat{V}_g = V_{g0} + \hat{V}$, where V_{g0} is the DC gate voltage and $\hat{V}$ is the voltage induced by the photons in the cavity. In Sec. 3.1, we derive $\hat{V} = A(\hat{a} + \hat{a}^\dagger)$, where $\hat{a}$ is the annihilation operator of a photon in the cavity, and A is a constant depending on the system. Combining these, we obtain the cavity QED Hamiltonian in Eq. (2.33). [8]

The transmon qubit [8,21] has a design similar to a Cooper pair box where $E_J \gg E_c$ to reduce the harmful effect of charge noise on the device operation. In this regime, the system cannot be approximated by two charge states. However, the transmon can be made sufficiently anharmonic for it to behave as a two-state system for the lowest energy eigenstates, and the transmon qubit coupled to a cavity can be described by the Jaynes–Cummings Hamiltonian.

Somewhat less studied approach is using itinerant microwave photons instead of photons confined in a cavity. Single photon generation has been demonstrated [19] and the quantum properties have been studied [22,23]. In addition, a single photon router has been demonstrated [24] and a scheme for nondemolition measurement of itinerant photons has been proposed [25].

For traveling photons, we may define field operators $\hat{\psi}_L(x)$ and $\hat{\psi}_R(x)$ for left- and right-moving photons for which the voltage at the waveguide is

$$\hat{V}(x) = B[\hat{\psi}_L(x) + \hat{\psi}_R(x) + \hat{\psi}_L^\dagger(x) + \hat{\psi}_R^\dagger(x)], \tag{2.50}$$

where B is a constant depending on the system [26]. Using similar approach than in the Jaynes–Cummings Hamiltonian, one may study the interaction between photons and qubits. For example, a microwave photon detector based on this approach has been proposed [27]. In Ch. 3, we define the field operators starting from the quantization of the transmission line.

In this thesis, we focus mostly on microwave photons not interacting with artificial atoms. Nevertheless, the devices and phenomena discussed here can be used directly in systems that are treated with circuit QED. In addition, the ideas from circuit QED can possibly be used to treat the nonlinear effects in the tunable phase shifter to be discussed in Ch. 4.

Chapter 3

Superconducting transmission lines

In this chapter, we present the general model for superconducting transmission lines and derive explicitely the Hamiltonian and the single photon operators and the field operators, which are used for circuit cavity quantum electrodynamics, for the simplest case, the infinite transmission line. Our derivation follows Refs. [28, 29]. We continue by using this model to derive theoretical tools for studying the reflection of single photons in a semi-infinite transmission line terminated by an impedance. We conclude this chapter by discussing our approach on complex networks of transmission lines mostly based on Ref. [28] and presenting some examples of simple networks.

3.1 Infinite transmission line

In this Section, we present our model for the transmission line in the infinite case where no boundary conditions affect the dynamics or the quantization of the transmission line.

3.1.1 Classical case

The transmission line, such as a coaxial cable, consists of a centre conductor that is capacitively coupled with a conductor that is connected to ground. In superconducting circuits, the transmission lines are realized as coplanar waveguides where the centre pin is coupled to two conductors that are in the ground potential. We model the transmission line as a discrete set of capacitors with capacitance C and inductors with inductance L [8, 29, 30] as shown in Fig. 3.1. Because the resistance of a superconducting transmission line is zero, there are no dissipative elements in our model. We denote the current (from left to right) on the inductor between the

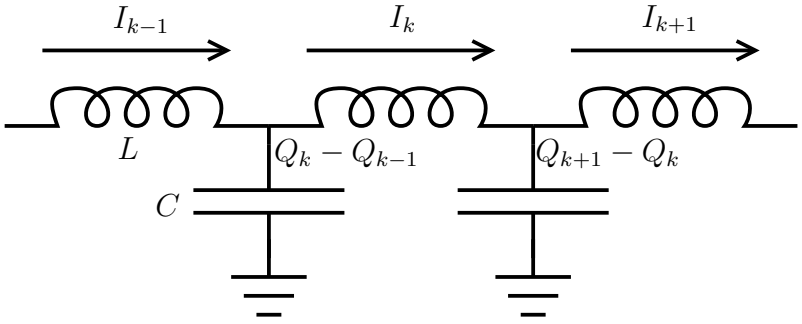

Figure 3.1: Discrete model of the transmission line consisting of capacitors with capacitance C and inductors with inductance L. The current at the kth inductor is I_k, and the charge at the kth capacitor is $Q_k - Q_{k-1}$.

kth and $(k+1)$th capacitors by I_k, and define the charge variable Q_k such that $\partial_t Q_k = -I_k$. By Kirchoff's law the charge of the kth capacitor is $Q_k - Q_{k-1}$. The variable Q_k is the total charge to the left of the kth capacitor plus a constant which is irrelevant in the case of an infinite transmission line.

The voltage on the kth capacitor is $V_k = (Q_k - Q_{k-1})/C$. This yields the equation of motion

$$L\partial_t^2 Q_k = -L\partial_t I_k = V_{k+1} - V_k = \frac{Q_{k+1} + Q_{k-1} - 2Q_k}{C}. \tag{3.1}$$

Let the length of an LC element of the discrete model be Δx. For the capacitors and the inductors, we may write $C = c\Delta x$ and $L = l\Delta x$, where c and l are the capacitance and inductance per unit length, respectively. Taking the limit $\Delta x \to 0$ and denoting $Q_k = Q(k\Delta x)$ yields

$$l\partial_t^2 Q(x,t) = \frac{1}{c}\partial_x^2 Q(x,t). \tag{3.2}$$

This is the wave equation for Q with velocity $v = 1/\sqrt{lc}$. The solution can be expressed in terms of left- and right-going waves,

$$Q(x,t) = Q_L(t + x/v) + Q_R(t - x/v). \tag{3.3}$$

For the voltage and current, we obtain

$$V(x,t) = \frac{1}{c}\partial_x Q(x,t), \tag{3.4}$$

$$I(x,t) = -\partial_t Q(x,t). \tag{3.5}$$

We can define left- and right-going voltage waves,

$$V_L(x,t) = \frac{d}{dx}\frac{1}{c}Q_L(t + x/v) = Z_c Q_L'(t + x/v), \tag{3.6}$$

$$V_R(x,t) = \frac{d}{dx}\frac{1}{c}Q_R(t - x/v) = -Z_c Q_R'(t - x/v), \tag{3.7}$$

where $'$ denotes the derivative of the functions of one variable and $Z_c = \frac{1}{cv} = \sqrt{\frac{l}{c}}$ is the characteristic impedance of the transmission line. In terms of these definitions, the total voltage and current can be written as

$$V(x,t) = V_L(t + x/v) + V_R(t - x/v), \tag{3.8}$$

$$\begin{aligned} I(x,t) &= -\partial_t Q(x,t) = -[Q'_L(t + x/v) + Q'_R(t - x/v)] \\ &= -\frac{1}{Z_c}\left[V_L(t + x/v) - V_R(t - x/v)\right]. \end{aligned} \tag{3.9}$$

For quantization of the trasmission line, we need the Lagrangian. The continuum limit can also be obtained from the Lagrangian of the discrete case,

$$\mathcal{L} = \sum_k \frac{L}{2}\dot{Q}_k^2 - \frac{1}{2C}(Q_k - Q_{k-1})^2. \tag{3.10}$$

The continuum limit of this is

$$\mathcal{L} = \int dx\, \mathcal{L}(x) = \int dx \left\{\frac{l}{2}\dot{Q}(x)^2 - \frac{1}{2c}[\partial_x Q(x)]^2\right\}, \tag{3.11}$$

for which the Euler-Lagrange equation is Eq. (3.2).

The conjugate of Q is $\Pi_Q := \frac{\partial \mathcal{L}}{\partial \dot{Q}} = l\dot{Q}$, which is the magnetic flux per unit length threading the transmission line. The Hamiltonian is given by

$$\mathcal{H} = \int dx \left[\dot{Q}\Pi_Q - \mathcal{L}(x)\right] = \int dx \left\{\frac{l}{2}\dot{Q}(x)^2 + \frac{1}{2c}[\partial_x Q(x)]^2\right\}. \tag{3.12}$$

In terms of Q and Π_Q, the Hamiltonian is expressed as

$$\mathcal{H} = \int dx \left\{\frac{1}{2l}[\Pi_Q(x)]^2 + \frac{1}{2c}[\partial_x Q(x)]^2\right\}. \tag{3.13}$$

This form is the starting point for the quantum treatment of the transmission line.

3.1.2 Coordinate transforms

The coordinate system for the physical transmission line depends of the choices of the location of the origin and the direction of positive x axis. The relation between two coordinate systems is

$$\tilde{x} = \alpha x + d, \quad \alpha = \pm 1, \tag{3.14}$$

where the $\alpha = 1$ if the directions of the x axis and the $\tilde{x}$ axis are equal and $\alpha = -1$ if the directions are opposite. Here, we derive the transformation for the new charge variable $\tilde{Q}$ corresponding to the coordinate transform.

Consider a point P in the transmission line, and define x_0 such that the point P is at $x = x_0$ in the original coordinates. In the new coordinates, the point P is thus at $\tilde{x} = \alpha x_0 + d$.

The value of $Q(x)$ at $x = x_0$ is the total charge on the transmission line from point P to infinity in the direction of the negative x axis, whereas the value of $\tilde{Q}(\tilde{x})$ at $\tilde{x} = \alpha x_0 + d$ is the total charge on the transmission line from point P to infinity in the direction of the negative $\tilde{x}$ axis. If $\alpha = 1$, this yields $Q(x_0) = \tilde{Q}(x_0 + d)$. If $\alpha = -1$, the total charge in the transmission line, which is a constant, can be written as $Q(x) + \tilde{Q}(-x_0 + d)$. Because an arbitrary constant can be added to Q, we may choose $-Q(x_0) = \tilde{Q}(-x_0 + d)$. Combining both cases, we obtain

$$\tilde{Q}(\tilde{x}) = \tilde{Q}(\alpha x + d) = \alpha Q(x), \quad \alpha = \pm 1. \tag{3.15}$$

With this coordinate transform, the treatment of the transmission line does not depend on the choice of coordinates, e.g., the actual physical quantities, current and voltage, can be obtained from $\tilde{Q}$ by $\tilde{I}(\tilde{x}) = -\partial_t \tilde{Q}(\tilde{x})$ and $\tilde{V}(\tilde{x}) = \frac{1}{c}\partial_{\tilde{x}} \tilde{Q}(\tilde{x})$, which are similar to the equations in the original coordinate system.

3.1.3 Quantization

We quantize the transmission line following Ref. [28]. Here, Q and its canconincal conjugate Π_Q become operators $\hat{Q}$ and $\hat{\Pi}_Q$ satisfying the bosonic equal-time commutation relations in the Heisenberg picture[1]

$$[\hat{Q}(x,t), \hat{Q}(x',t)] = 0, \tag{3.16}$$

$$[\hat{\Pi}_Q(x,t), \hat{\Pi}_Q(x',t)] = 0, \tag{3.17}$$

$$[\hat{Q}(x,t), \hat{\Pi}_Q(x',t)] = i\hbar\delta(x - x'). \tag{3.18}$$

Thus the Hamiltonian assumes the form

$$\hat{\mathcal{H}}(t) = \int dx \left\{ \frac{1}{2l} \hat{\Pi}_Q(x,t)^2 + \frac{1}{2c} [\partial_x \hat{Q}(x,t)]^2 \right\}. \tag{3.19}$$

[1] In the Schrödinger picture, the state of the system $|\Psi(t)\rangle_S$ evolves according to the Schrödinger equation $-i\hbar\partial_t |\Psi(t)\rangle_S = \hat{H}|\Psi(t)\rangle_S$, and the expectation value of an observable $\hat{O}_S$ is ${}_S\langle\Psi(t)|\hat{O}_S|\Psi(t)\rangle_S$. In the Heisenberg picture, the operators are defined by $\hat{O}_H(t) = \hat{U}(t)^\dagger \hat{O}_S \hat{U}(t)$ where $i\hbar\partial_t \hat{U}(t) = \hat{H}\hat{U}(t)$ and $\hat{U}(0) = \hat{I}$, and the expectation value of the operator is thus ${}_H\langle\Psi|\hat{O}_H(t)|\Psi\rangle_H$, where $|\Psi\rangle_H = |\Psi(0)\rangle_S$. The equation of motion for operator $\hat{O}_H$ is $i\hbar\partial_t \hat{O}_H(t) = [\hat{O}_H(t), \hat{H}]$.

The equations of motion are

$$\begin{aligned}
\partial_t \hat{Q}(x,t) &= -\frac{i}{\hbar}\left[\hat{Q}(x,t), \hat{\mathcal{H}}(t)\right] \\
&= -\frac{i}{\hbar}\int dx' \left\{\frac{1}{2l}\left[\hat{Q}(x,t), \hat{\Pi}_Q(x',t)^2\right] + \frac{1}{2c}\left[\hat{Q}(x,t), [\partial_x \hat{Q}(x',t)]^2\right]\right\} \\
&= -\frac{i}{\hbar}\int dx' \frac{1}{2l}\left[\hat{Q}(x,t), \hat{\Pi}_Q(x',t)^2\right] \\
&= -\frac{i}{\hbar}\int dx' \frac{1}{2l}\left[\left[\hat{Q}(x,t), \hat{\Pi}_Q(x',t)\right], \hat{\Pi}_Q(x',t)\right]_+ \\
&= -\frac{i}{\hbar}\int dx' \frac{1}{2l} 2i\hbar\delta(x-x')\hat{\Pi}_Q(x',t) = \frac{1}{l}\hat{\Pi}_Q(x,t), \qquad (3.20) \\
\partial_t \hat{\Pi}_Q(x,t) &= -\frac{i}{\hbar}\left[\hat{\Pi}_Q(x,t), \hat{\mathcal{H}}(t)\right] \\
&= -\frac{i}{\hbar}\int dx' \left\{\frac{1}{2l}\left[\hat{\Pi}_Q(x,t), \hat{\Pi}_Q(x',t)^2\right] + \frac{1}{2c}\left[\hat{\Pi}_Q(x,t), [\partial_x \hat{Q}(x,t)]^2\right]\right\} \\
&= -\frac{i}{\hbar}\int dx' \frac{1}{2c}\left[\hat{\Pi}_Q(x,t), [\partial_x \hat{Q}(x',t)]^2\right] \\
&= -\frac{i}{\hbar}\int dx' \frac{1}{2c}\left[\left[\hat{\Pi}_Q(x,t), \partial_x \hat{Q}(x',t)\right], \partial_x \hat{Q}(x',t)\right]_+ \\
&= \frac{i}{\hbar}\int dx' \frac{1}{2c}\left[\left[\hat{\Pi}_Q(x,t), \hat{Q}(x',t)\right], \partial_x^2 \hat{Q}(x',t)\right]_+ \\
&= \frac{i}{\hbar}\int dx' \frac{1}{2c}(-2)i\hbar\delta(x-x')\partial_x^2 \hat{Q}(x',t) = \frac{1}{c}\partial_x^2 \hat{Q}(x,t), \qquad (3.21)
\end{aligned}$$

where $[\hat{A}, \hat{B}]_+ = \hat{A}\hat{B} + \hat{B}\hat{A}$ is the anticommutator. Here, we used integration by parts and have assumed that $\lim_{x\to\pm\infty} \hat{Q}(x,t) = 0$. This is not necessarily true in the case of an infinite waveguide but is a good approximation for physical situations.

Combining these, we obtain a wave equation similar to the classical case,

$$l\partial_t^2 \hat{Q}(x,t) = \frac{1}{c}\partial_x^2 \hat{Q}(x,t). \qquad (3.22)$$

The solution to the wave equation can be written as

$$\hat{Q}(x,t) = \hat{Q}_L(t + x/v) + \hat{Q}_R(t - x/v). \qquad (3.23)$$

Fourier expanding $\hat{Q}_{L,R}$ yields

$$\hat{Q}(x,t) = \sqrt{\frac{\hbar}{4\pi Z_c}}\int_{-\infty}^{\infty} d\omega \frac{1}{\sqrt{|\omega|}}\left(\hat{A}_{L\omega} e^{-i\omega(t+x/v)} - \hat{A}_{R\omega} e^{-i\omega(t-x/v)}\right), \qquad (3.24)$$

where $\hat{A}_{L\omega}$ and $\hat{A}_{R\omega}$ are time-independent operators corresponding to the left- and right-moving waves, and the normalization factor is chosen to simplify equations

below. The minus sign is for convenience in the coordinate transform $\tilde{x} = -x$. As explained in Sec. 3.1.2,

$$\begin{aligned}\hat{\tilde{Q}}(\tilde{x},t) &= -\hat{Q}(-\tilde{x},t) \\ &= \sqrt{\frac{\hbar}{4\pi Z_c}}\int_{-\infty}^{\infty} d\omega \frac{1}{\sqrt{|\omega|}}\left(\hat{\tilde{A}}_{L\omega}e^{-i\omega(t+\tilde{x}/v)} - \hat{\tilde{A}}_{R\omega}e^{-i\omega(t-\tilde{x}/v)}\right), \end{aligned} \tag{3.25}$$

where $\hat{\tilde{A}}_{L\omega} = \hat{A}_{R\omega}$ and $\hat{\tilde{A}}_{R\omega} = \hat{A}_{L\omega}$.

Because $\hat{Q}$ corresponds to a physical observable, it is Hermitian. Thus $\hat{A}_{\alpha(-\omega)} = \hat{A}^\dagger_{\alpha\omega}$, where $\alpha = L, R$, and we may rewrite $\hat{Q}$ in terms of only positive frequencies as

$$\hat{Q}(x,t) = \sqrt{\frac{\hbar}{4\pi Z_c}}\int_0^{\infty} d\omega \frac{1}{\sqrt{\omega}}\left(\hat{A}_{L\omega}e^{-i\omega(t+x/v)} - \hat{A}_{R\omega}e^{-i\omega(t-x/v)} + \text{h.c.}\right), \tag{3.26}$$

where h.c. denotes Hermitian conjugate.

Here, $\hat{A}_{\alpha\omega}$ and $\hat{A}^\dagger_{\alpha\omega}$ with $\alpha = L, R$ are the annihilation and creation operators for the left- and right-moving photons, respectively. They satisfy the bosonic commutation relations [28]

$$[\hat{A}_{\alpha\omega}, \hat{A}^\dagger_{\alpha'\omega'}] = \delta_{\alpha\alpha'}\delta(\omega - \omega'), \tag{3.27}$$

where $\alpha = L, R$. The commutation relation follows from the Fourier transform of Eqs. (3.16)–(3.18).

It is useful to write down the voltage and current (from left to right) at a point in the transmission line in terms of the operators $\hat{A}$,

$$\begin{aligned}\hat{V}(x,t) &= \frac{1}{c}\partial_x \hat{Q}(x,t) \\ &= -i\sqrt{\frac{\hbar Z_c}{4\pi}}\int_0^{\infty} d\omega\sqrt{\omega}\left(\hat{A}_{L\omega}e^{-i\omega(t+x/v)} + \hat{A}_{R\omega}e^{-i\omega(t-x/v)} - \text{h.c.}\right), \end{aligned} \tag{3.28}$$

$$\begin{aligned}\hat{I}(x,t) &= -\partial_t \hat{Q}(x,t) \\ &= i\sqrt{\frac{\hbar}{4\pi Z_c}}\int_0^{\infty} d\omega\sqrt{\omega}\left(\hat{A}_{L\omega}e^{-i\omega(t+x/v)} - \hat{A}_{R\omega}e^{-i\omega(t-x/v)} - \text{h.c.}\right), \end{aligned} \tag{3.29}$$

where we used $\frac{1}{cv\sqrt{Z_c}} = \frac{\sqrt{lc}}{c\sqrt{Z_c}} = \sqrt{Z_c}$ on the first equation.

In terms of the time-independent operators $\hat{A}_{R\omega}$ and $\hat{A}_{R\omega}$, the Hamiltonian can be written in the Heisenberg picture as

$$\begin{aligned}\hat{\mathcal{H}}(t) &= \int dx \left[\frac{1}{2l}\hat{\Pi}_Q(x,t)^2 + \frac{1}{2c}[\partial_x \hat{Q}(x,t)]^2\right] \\ &= \int dx \left[\frac{l}{2}[\partial_t \hat{Q}(x,t)]^2 + \frac{1}{2c}[\partial_x \hat{Q}(x,t)]^2\right] \end{aligned}$$

$$
\begin{aligned}
=&\frac{\hbar}{4\pi Z_c}\int dx\int_0^\infty d\omega\int_0^\infty d\omega'\frac{1}{\sqrt{\omega\omega'}}\Big\{\\
&\frac{l}{2}\left[-i\omega\left(\hat{A}_{L\omega}e^{-i\omega(t+x/v)}-\hat{A}_{R\omega}e^{-i\omega(t-x/v)}-\text{h.c.}\right)\right]\\
&\times\left[-i\omega'\left(\hat{A}_{L\omega'}e^{-i\omega'(t+x/v)}-\hat{A}_{R\omega'}e^{-i\omega'(t-x/v)}-\text{h.c.}\right)\right]\\
&+\frac{1}{2c}\left[\frac{-i\omega}{v}\left(\hat{A}_{L\omega}e^{-i\omega(t+x/v)}+\hat{A}_{R\omega}e^{-i\omega(t-x/v)}-\text{h.c.}\right)\right]\\
&\times\left[\frac{-i\omega'}{v}\left(\hat{A}_{L\omega'}e^{-i\omega'(t+x/v)}+\hat{A}_{R\omega'}e^{-i\omega'(t-x/v)}-\text{h.c.}\right)\right]\Big\}\\
=&\frac{\hbar l}{8\pi Z_c}\int dx\int_0^\infty d\omega\int_0^\infty d\omega'(-\sqrt{\omega\omega'})\Big\{\\
&\left(\hat{A}_{L\omega}e^{-i\omega(t+x/v)}-\hat{A}_{R\omega}e^{-i\omega(t-x/v)}-\text{h.c.}\right)\\
&\times\left(\hat{A}_{L\omega'}e^{-i\omega'(t+x/v)}-\hat{A}_{R\omega'}e^{-i\omega'(t-x/v)}-\text{h.c.}\right)\\
&+\left(\hat{A}_{L\omega}e^{-i\omega(t+x/v)}+\hat{A}_{R\omega}e^{-i\omega(t-x/v)}-\text{h.c.}\right)\\
&\times\left(\hat{A}_{L\omega'}e^{-i\omega'(t+x/v)}+\hat{A}_{R\omega'}e^{-i\omega'(t-x/v)}-\text{h.c.}\right)\Big\}\\
=&\frac{\hbar l}{4\pi Z_c}\int dx\int_0^\infty d\omega\int_0^\infty d\omega'(-\sqrt{\omega\omega'})\Big\{\\
&\hat{A}_{L\omega}\hat{A}_{L\omega'}e^{-i(\omega+\omega')(t+x/v)}-\hat{A}_{L\omega}\hat{A}^\dagger_{L\omega'}e^{-i(\omega-\omega')(t+x/v)}\\
&-\hat{A}^\dagger_{L\omega}\hat{A}_{L\omega'}e^{-i(-\omega+\omega')(t+x/v)}+\hat{A}^\dagger_{L\omega}\hat{A}^\dagger_{L\omega'}e^{i(\omega+\omega')(t+x/v)}\\
&+\hat{A}_{R\omega}\hat{A}_{R\omega'}e^{-i(\omega+\omega')(t-x/v)}-\hat{A}_{R\omega}\hat{A}^\dagger_{R\omega'}e^{-i(\omega-\omega')(t-x/v)}\\
&-\hat{A}^\dagger_{R\omega}\hat{A}_{R\omega'}e^{-i(-\omega+\omega')(t-x/v)}+\hat{A}^\dagger_{R\omega}\hat{A}^\dagger_{R\omega'}e^{i(\omega+\omega')(t-x/v)}\Big\}\\
=&\frac{\hbar l v}{2Z_c}\int_0^\infty d\omega\int_0^\infty d\omega'(-\sqrt{\omega\omega'})\Big\{\\
&\hat{A}_{L\omega}\hat{A}_{L\omega'}e^{-i(\omega+\omega')t}\delta(\omega+\omega')-\hat{A}_{L\omega}\hat{A}^\dagger_{L\omega'}e^{-i(\omega-\omega')t}\delta(\omega-\omega')\\
&-\hat{A}^\dagger_{L\omega}\hat{A}_{L\omega'}e^{-i(-\omega+\omega')t}\delta(\omega-\omega')+\hat{A}^\dagger_{L\omega}\hat{A}^\dagger_{L\omega'}e^{i(\omega+\omega')t}\delta(\omega+\omega')\\
&+\hat{A}_{R\omega}\hat{A}_{R\omega'}e^{-i(\omega+\omega')t}\delta(\omega+\omega')-\hat{A}_{R\omega}\hat{A}^\dagger_{R\omega'}e^{-i(\omega-\omega')t}\delta(\omega-\omega')\\
&-\hat{A}^\dagger_{R\omega}\hat{A}_{R\omega'}e^{-i(-\omega+\omega')t}\delta(\omega-\omega')+\hat{A}^\dagger_{R\omega}\hat{A}^\dagger_{R\omega'}e^{i(\omega+\omega')t}\delta(\omega+\omega')\Big\}\\
=&\frac{\hbar}{2}\int_0^\infty d\omega\omega\left(\hat{A}_{L\omega}\hat{A}^\dagger_{L\omega}+\hat{A}^\dagger_{L\omega}\hat{A}_{L\omega}+\hat{A}_{R\omega}\hat{A}^\dagger_{R\omega}+\hat{A}^\dagger_{R\omega}\hat{A}_{R\omega}\right)\\
=&\int_0^\infty d\omega\hbar\omega\left(\hat{A}^\dagger_{L\omega}\hat{A}_{L\omega}+\hat{A}^\dagger_{R\omega}\hat{A}_{R\omega}\right)+\text{const.},
\end{aligned}
\tag{3.30}
$$

which is the Hamiltonian of an infinite combination of harmonic oscillators with a continuous spectrum.

In the infinite transmission line, a single photon with well-defined frequency is not localized. A physical single-photon wave packet of finite spatial extend is a super-

position of photons with different frequencies. In the next section, we present the field operators that can be used to analyze realistic wave packets.

3.1.4 Field operators

We define $|0\rangle$ to be the ground state, i.e., the state for which $\hat{A}_{L\omega}|0\rangle = \hat{A}_{R\omega}|0\rangle = 0$ for every ω. A single-photon state with only left-going photons can be described at $t = 0$ by

$$|s_L\rangle = \int_0^\infty d\omega\, X_L(\omega)\hat{A}^\dagger_{L\omega}|0\rangle, \tag{3.31}$$

where $X_L : [0,\infty) \to \mathbb{C}$ is normalized to satisfy

$$\begin{aligned} 1 = \langle s_L|s_L\rangle &= \int_0^\infty d\omega \int_0^\infty d\omega' X_L(\omega)^* X_L(\omega')\langle 0|\hat{A}_{L\omega}\hat{A}^\dagger_{L\omega'}|0\rangle \\ &= \int_0^\infty d\omega\, X_L(\omega)^* X_L(\omega). \end{aligned} \tag{3.32}$$

We extend X_L to all real numbers by defining $X_L(\omega) = 0$ for $\omega < 0$ and define

$$\xi_L(x) = \frac{1}{\sqrt{2\pi v}}\int_0^\infty d\omega\, e^{-i\omega x/v} X_L(\omega) = \frac{1}{\sqrt{2\pi v}}\int_{-\infty}^\infty d\omega\, e^{i\omega x/v} X_L(-\omega), \tag{3.33}$$

similar to the inverse Fourier transform formula in Eq. (A.7), yielding

$$X_L(\omega) = \frac{1}{\sqrt{2\pi v}}\int_{-\infty}^\infty dx\, e^{i\omega x/v}\xi_L(x), \tag{3.34}$$

for $\omega > 0$. Thus the single photon state assumes the form

$$|s_L\rangle = \int_{-\infty}^\infty dx\, \xi_L(x)\frac{1}{\sqrt{2\pi v}}\int_0^\infty d\omega\, e^{i\omega x/v}\hat{A}^\dagger_{L\omega}|0\rangle. \tag{3.35}$$

Defining the field operator for left-going photons as

$$\hat{\psi}_L(x) = \frac{1}{\sqrt{2\pi v}}\int_0^\infty d\omega\, e^{-i\omega x/v}\hat{A}_{L\omega}, \tag{3.36}$$

we may write

$$|s_L\rangle = \int_{-\infty}^\infty dx\, \xi_L(x)\hat{\psi}^\dagger_L(x)|0\rangle. \tag{3.37}$$

Here, $\xi_L(x)$ contains no negative frequency terms.

Similarly, we may define the field operator for right-going photons as

$$\hat{\psi}_R(x) = \frac{1}{\sqrt{2\pi v}}\int_0^\infty d\omega\, e^{i\omega x/v}\hat{A}_{R\omega}, \tag{3.38}$$

and write

$$|s_R\rangle = \int_0^\infty d\omega\, X_R(\omega)\hat{A}^\dagger_{R\omega}|0\rangle = \int_{-\infty}^\infty dx\, \xi_R(x)\hat{\psi}^\dagger_R(x)|0\rangle, \tag{3.39}$$

to describe the single-photon state with only right-going photons. Here, ξ_R is defined by

$$\xi_R(x) = \frac{1}{\sqrt{2\pi v}}\int_0^\infty d\omega\, e^{i\omega x/v} X_R(\omega), \tag{3.40}$$

and contains no positive frequency terms.

The general single-photon state can be written as

$$|s\rangle = \int_{-\infty}^\infty dx \left[\xi_L(x)\hat{\psi}^\dagger_L(x) + \xi_R(x)\hat{\psi}^\dagger_R(x)\right]|0\rangle, \tag{3.41}$$

where ξ_L contains only negative-frequency terms and ξ_R contains only positive-frequency terms. Because $\psi^\dagger_L$ contains only negative frequency terms, using Eq. (A.14), we may write

$$\int_{-\infty}^\infty dx\, \xi_R(x)\hat{\psi}^\dagger_L(x)|0\rangle = 0, \tag{3.42}$$

and similarly,

$$\int_{-\infty}^\infty dx\, \xi_L(x)\hat{\psi}^\dagger_R(x)|0\rangle = 0. \tag{3.43}$$

Thus we may define $\xi(x) = \xi_L(x) + \xi_R(x)$ and write a general single-photon state as

$$|s\rangle = \int_{-\infty}^\infty dx\, \xi(x)\hat{\psi}^\dagger(x)|0\rangle, \tag{3.44}$$

where $\hat{\psi}(x) = \hat{\psi}_L(x) + \hat{\psi}_R(x)$ is the total bosonic field operator. The function ξ is the wave function of the single-photon wave packet, and its negative frequency terms are associated with left-moving photons and positive frequency terms are associated with right-moving photons.

In the Heisenberg picture,

$$\hat{\psi}_L(x,t) = \frac{1}{\sqrt{2\pi v}}\int_0^\infty d\omega\, e^{-i\omega(t+x/v)}\hat{A}_{L\omega}, \tag{3.45}$$

$$\hat{\psi}_R(x,t) = \frac{1}{\sqrt{2\pi v}}\int_0^\infty d\omega\, e^{-i\omega(t-x/v)}\hat{A}_{R\omega}, \tag{3.46}$$

$$\hat{\psi}(x,t) = \frac{1}{\sqrt{2\pi v}}\int_0^\infty d\omega\, e^{-i\omega t}\left[e^{-i\omega x/v}\hat{A}_{L\omega} + e^{i\omega x/v}\hat{A}_{R\omega}\right]. \tag{3.47}$$

The equal-time commutation relations for $\hat{\psi}$ are

$$\begin{aligned}\left[\hat{\psi}(x,t),\hat{\psi}(x',t)\right] =&\frac{1}{\sqrt{2\pi v}}\int_0^\infty d\omega\frac{1}{\sqrt{2\pi v}}\int_0^\infty d\omega' e^{-i(\omega+\omega')t}\\ &\times\left[e^{-i\omega x/v}\hat{A}_{L\omega}+e^{i\omega x/v}\hat{A}_{R\omega},e^{-i\omega' x'/v}\hat{A}_{L\omega'}+e^{i\omega' x'/v}\hat{A}_{R\omega'}\right]\\ =&0 \qquad (3.48)\\ \left[\hat{\psi}(x,t),\hat{\psi}^\dagger(x',t)\right] =&\frac{1}{\sqrt{2\pi v}}\int_0^\infty d\omega\frac{1}{\sqrt{2\pi v}}\int_0^\infty d\omega' e^{-i(\omega-\omega')t}\\ &\times\left[e^{-i\omega x/v}\hat{A}_{L\omega}+e^{i\omega x/v}\hat{A}_{R\omega},e^{i\omega' x'/v}\hat{A}^\dagger_{L\omega'}+e^{-i\omega' x'/v}\hat{A}^\dagger_{R\omega'}\right]\\ =&\frac{1}{2\pi v}\int_0^\infty d\omega\int_0^\infty d\omega' e^{-i(\omega-\omega')t}\\ &\times\left\{e^{-i(\omega x-\omega' x')/v}\left[\hat{A}_{L\omega},\hat{A}^\dagger_{L\omega'}\right]+e^{i(\omega x-\omega' x')/v}\left[\hat{A}_{R\omega},\hat{A}^\dagger_{R\omega'}\right]\right\}\\ =&\frac{1}{2\pi v}\int_0^\infty d\omega\left(e^{-i\omega(x-x')/v}+e^{i\omega(x-x')/v}\right)=\delta(x-x'). \qquad (3.49)\end{aligned}$$

The normalization condition for the single photon state descibed in Eq. (3.44) is

$$\begin{aligned}1=\langle s|s\rangle &= \int_{-\infty}^{\infty}dx\int_{-\infty}^{\infty}dx'\xi(x)^*\xi(x')\langle 0|\hat{\psi}(x)\hat{\psi}^\dagger(x')|0\rangle\\ &=\int_{-\infty}^{\infty}dx\int_{-\infty}^{\infty}dx'\xi(x)^*\xi(x')\langle 0|\left\{[\hat{\psi}(x),\hat{\psi}^\dagger(x')]+\hat{\psi}^\dagger(x')\hat{\psi}(x)\right\}|0\rangle\\ &=\int_{-\infty}^{\infty}dx\int_{-\infty}^{\infty}dx'\xi(x)^*\xi(x')\left\{\langle 0|\delta(x-x')|0\rangle+\langle 0|\hat{\psi}^\dagger(x')\hat{\psi}(x)|0\rangle\right\}\\ &=\int_{-\infty}^{\infty}dx\,\xi(x)^*\xi(x). \qquad (3.50)\end{aligned}$$

Assuming a narrow frequency band near ω_0, the variable $\hat{Q}$ can be approximated as

$$\begin{aligned}\hat{Q}(x,t) &= \sqrt{\frac{\hbar}{4\pi Z_c}}\int_0^\infty d\omega\frac{1}{\sqrt{\omega}}\left(\hat{A}_{L\omega}e^{-i\omega(t+x/v)}-\hat{A}_{R\omega}e^{-i\omega(t-x/v)}+\text{h.c.}\right),\\ &\approx\sqrt{\frac{\hbar v}{2Z_c\omega_0}}\frac{1}{\sqrt{2\pi v}}\int_0^\infty d\omega\left(\hat{A}_{L\omega}e^{-i\omega(t+x/v)}-\hat{A}_{R\omega}e^{-i\omega(t-x/v)}+\text{h.c.}\right),\\ &=\sqrt{\frac{\hbar}{2l\omega_0}}\left[\hat{\psi}_L(x,t)-\hat{\psi}_R(x,t)+\hat{\psi}^\dagger_L(x,t)-\hat{\psi}^\dagger_R(x,t)\right], \qquad (3.51)\end{aligned}$$

and voltage and current can be approximated as

$$\begin{aligned}\hat{V}(x,t) &= -i\sqrt{\frac{\hbar Z_c}{4\pi}}\int_0^\infty d\omega\sqrt{\omega}\left(\hat{A}_{L\omega}e^{-i\omega(t+x/v)}+\hat{A}_{R\omega}e^{-i\omega(t-x/v)}-\text{h.c.}\right)\\ &\approx -i\sqrt{\frac{\hbar\omega_0}{2c}}\left[\hat{\psi}_L(x,t)+\hat{\psi}_R(x,t)-\hat{\psi}^\dagger_L(x,t)-\hat{\psi}^\dagger_R(x,t)\right], \qquad (3.52)\end{aligned}$$

$$\hat{I}(x,t) = i\sqrt{\frac{\hbar}{4\pi Z_c}}\int_0^\infty d\omega\sqrt{\omega}\left(\hat{A}_{L\omega}e^{-i\omega(t+x/v)} - \hat{A}_{R\omega}e^{-i\omega(t-x/v)} - \text{h.c.}\right),$$
$$\approx i\sqrt{\frac{\hbar\omega_0}{2l}}\left[\hat{\psi}_L(x,t) - \hat{\psi}_R(x,t) - \hat{\psi}_L^\dagger(x,t) + \hat{\psi}_R^\dagger(x,t)\right]. \quad (3.53)$$

These approximations have been used in studying the interference between travelling wave packets and superconducting devices [27, 29, 31].

3.2 Transmission line terminated by an impedance

In this section, we consider a semi-infinite transmission line ($x \geq 0$) with characteristic impedance Z_c terminated by an impedance $Z_0(\omega)$ at $x = 0$ as shown in Fig. 3.2. First, we calculate the classical reflection coefficient, and then we calculate the quantum mechanical reflection coefficient in two special cases and compare them to the classical result.

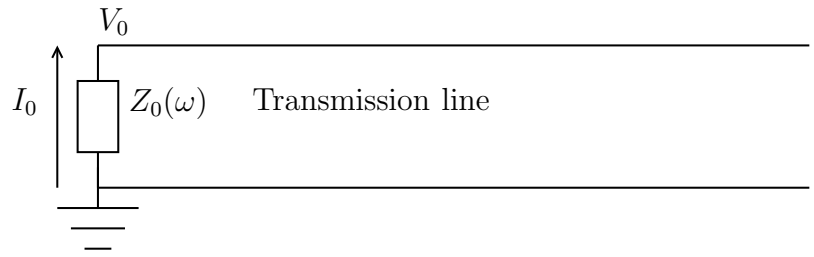

Figure 3.2: Transmission line terminated by an impedance $Z_0(\omega)$.

3.2.1 Classical reflection coefficient

The classical reflection coefficient for waves of single frequency ω is a well-known result [30],

$$r(\omega) = \frac{Z_0(\omega) - Z_c}{Z_0(\omega) + Z_c}. \quad (3.54)$$

Nevertheless, since the quantum treatment resembles the derivation of the classical reflection coefficient, it is instructive to derive the above equation explicitely.

The wave equation (3.2) holds inside the semi-infinite transmission line, and we may write

$$Q(x,t) = Q_L(t + x/v) + Q_R(t - x/v), \quad (3.55)$$

as in Eq. (3.3). Fourier expanding Q, we obtain

$$Q_L(t+x/v) = \int_{-\infty}^{\infty} d\omega\, A_{L\omega} e^{i\omega(t+x/v)}, \tag{3.56}$$

$$Q_R(t-x/v) = \int_{-\infty}^{\infty} d\omega\, (-A_{R\omega}) e^{i\omega(t-x/v)}, \tag{3.57}$$

$$Q(x,t) = \int_{-\infty}^{\infty} d\omega\, A_{L\omega} e^{i\omega(t+x/v)} - A_{R\omega} e^{i\omega(t-x/v)}. \tag{3.58}$$

The left- and right-going voltage waves defined in Eqs. (3.6) and (3.7) are

$$V_L(x,t) = Z_c \int_{-\infty}^{\infty} d\omega\, i\omega A_{L\omega} e^{i\omega(t+x/v)} = \int_{-\infty}^{\infty} d\omega\, V_{L\omega}(x) e^{i\omega t}, \tag{3.59}$$

$$V_R(x,t) = -Z_c \int_{-\infty}^{\infty} d\omega\, i\omega(-A_{R\omega}) e^{i\omega(t-x/v)} = \int_{-\infty}^{\infty} d\omega\, V_{R\omega}(x) e^{i\omega t}, \tag{3.60}$$

where $V_{L\omega}(x) = i\omega Z_c A_{L\omega} e^{i\omega x/v}$ and $V_{R\omega}(x) = i\omega Z_c A_{R\omega} e^{-i\omega x/v}$ are the Fourier coefficients of the voltage at x related to frequency ω.

The total voltage at $x = 0$ can be written as

$$\begin{aligned} V_0(t) = V_L(0,t) + V_R(0,t) &= \int_{-\infty}^{\infty} d\omega\, i\omega Z_c (A_{L\omega} + A_{R\omega}) e^{i\omega t} \\ &= \int_{-\infty}^{\infty} d\omega\, V_{0\omega} e^{i\omega t}, \end{aligned} \tag{3.61}$$

where $V_{0\omega} = i\omega Z_c (A_{L\omega} + A_{R\omega})$. The current at $x = 0$ can be written as

$$\begin{aligned} I_0(t) = -\partial_t [Q_L(t) + Q_R(t)] &= -\int_{-\infty}^{\infty} d\omega\, i\omega (A_{L\omega} - A_{R\omega}) e^{i\omega t} \\ &= \int_{-\infty}^{\infty} d\omega\, I_{0\omega} e^{i\omega t}, \end{aligned} \tag{3.62}$$

where $I_{0\omega} = -i\omega(A_{L\omega} - A_{R\omega})$.

Using these expansions, the boundary condition caused by the impedance is

$$V_{0\omega} = -Z_0(\omega) I_{0\omega} \tag{3.63}$$

$$\Leftrightarrow \qquad i\omega Z_c (A_{L\omega} + A_{R\omega}) = -Z_0(\omega)[-i\omega(A_{L\omega} - A_{R\omega})], \tag{3.64}$$

where the minus sign is due to the fact that the direction of the current I_0 is from ground to $V(0,t)$. The reflection coefficient for the voltage waves is

$$r(\omega) = \frac{V_{R\omega}(0)}{V_{L\omega}(0)} = \frac{Z_c i\omega A_{R\omega}}{Z_c i\omega A_{L\omega}} = \frac{Z_0(\omega) - Z_c}{Z_0(\omega) + Z_c}, \tag{3.65}$$

which is equivalent to Eq. (3.54). Because the voltage of a classical wave is real, Eq. (3.59) yields $A_{L\omega} = A^*_{L-\omega}$, and thus

$$V_L(x,t) = \int_0^\infty d\omega\, i\omega Z_c A_{L\omega} e^{i\omega(t+x/v)} + \text{c.c.} = \int_0^\infty d\omega\, V_{L\omega}(0) e^{i\omega(t+x/v)} + \text{c.c.}, \quad (3.66)$$

$$\begin{aligned} V_R(x,t) &= \int_0^\infty d\omega\, i\omega Z_c A_{R\omega} e^{i\omega(t-x/v)} + \text{c.c.} \\ &= \int_0^\infty d\omega\, r(\omega) V_{L\omega}(0) e^{i\omega(t-x/v)} + \text{c.c.}, \end{aligned} \quad (3.67)$$

where c.c. denotes the complex conjugate.

3.2.2 Single LC element at the end of the transmission line

We consider a semi-infinite transmission line ($x > 0$) with characteristic impedance Z_c terminated by an LC element with an inductance L_0 and a capacitance C_0 in series as shown in Fig. 3.3. First, we derive the corresponding Lagrangian and Hamiltonian, and then we quantize the system and find the quantum reflection coefficient. Finally, we define the field operators for this case and briefly study the reflection of wave packets.

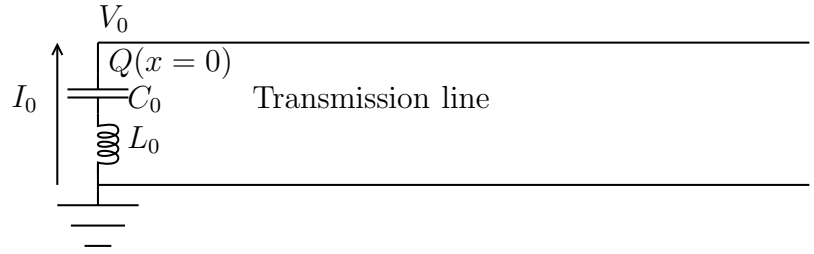

Figure 3.3: Transmission line terminated by a capacitor C_0 and an inductor L_0 in series.

Lagrangian

Here, $Q(0,t)$ becomes the charge on the capacitor and $-\partial_t Q(0,t)$ is the current at the inductor from ground towards the transmission line. The equation of motion at $x = 0$ is thus

$$\frac{1}{c}\partial_x Q(0^+,t) = V(0,t) = V_{\text{inductor}} + V_{\text{capacitor}} = L_0\partial_t^2 Q(0,t) + \frac{1}{C_0}Q(0,t), \quad (3.68)$$

and the wave equation for the transmission line for $x > 0$ remains the same,

$$l\partial_t^2 Q(x) = \frac{1}{c}\partial_x^2 Q(x). \quad (3.69)$$

These equations are also obtained by the Lagrangian [28]

$$\mathcal{L}(x) = \delta(x)\left[\frac{L_0}{2}\dot{Q}^2 - \frac{1}{2C_0}Q^2\right] + \theta(x)\left[\frac{l}{2}\dot{Q}^2 - \frac{1}{2c}(\partial_x Q)^2\right], \quad (3.70)$$

where θ is the Heaviside step function defined in App. A. The $\delta(x)$ term corresponds to the LC element and the $\theta(x)$ term corresponds to the transmission line. The Euler-Lagrange equation is

$$\begin{aligned} 0 &= \frac{d}{dt}\frac{\delta\mathcal{L}}{\delta(\partial_t Q)} + \frac{d}{dx}\frac{\delta\mathcal{L}}{\delta(\partial_x Q)} - \frac{\delta\mathcal{L}}{\delta Q} \\ &= \delta(x)\left[L_0\ddot{Q} - \frac{1}{c}\partial_x Q + \frac{1}{C_0}Q\right] + \theta(x)\left[l\ddot{Q} - \frac{1}{c}\partial_x^2 Q\right]. \end{aligned} \tag{3.71}$$

The canonical conjugate variable to Q is Π_Q, defined by

$$\Pi_Q(x) = \frac{\delta\mathcal{L}(x)}{\delta\dot{Q}(x)} = [L_0\delta(x) + l\theta(x)]\dot{Q}(x). \tag{3.72}$$

The conjugate variable $\Pi_Q(x)$ corresponds to the magnetic field per unit length in the transmission line for $x > 0$ and to the magnetic field in the inductor at the end of the transmission line for $x = 0$. To obtain a real value for the magnetic field at $x = 0$, we define

$$\Pi_0 = \lim_{\epsilon\to 0}\int_{-\epsilon}^{\epsilon} dx\, \Pi_Q(x) = L_0\dot{Q}(0). \tag{3.73}$$

For convenience, we also define

$$\tilde{\Pi}_Q(x) = \begin{cases} \Pi_Q(x) = l\dot{Q}(x), & x > 0, \\ 0, & x \le 0. \end{cases} \tag{3.74}$$

Because the δ term dominates at $x = 0$, we may write

$$\Pi_Q(x) = \delta(x)\Pi_0 + \tilde{\Pi}_Q(x). \tag{3.75}$$

The Hamiltonian is

$$\begin{aligned} \mathcal{H} &= \int dx\, \left[\Pi_Q(x)\dot{Q}(x) - \mathcal{L}(x)\right] \\ &= \int dx \left\{\delta(x)\left[\frac{1}{2L_0}\Pi_0^2 + \frac{1}{2C_0}Q(0)^2\right]\right. \\ &\quad \left. +\theta(x)\left[\frac{1}{2l}[\tilde{\Pi}_Q(x)]^2 + \frac{1}{2c}[\partial_x Q(x)]^2\right]\right\}. \end{aligned} \tag{3.76}$$

Quantization

The conjugate variables Q and Π_Q become operators $\hat{Q}(x)$ and $\hat{\Pi}_Q$ satisfying the canonical commutation relations

$$\begin{aligned} [\hat{Q}(x), \hat{\Pi}_Q(x')] &= i\hbar\delta(x - x'), \\ [\hat{Q}(x), \hat{Q}(x')] = [\hat{\Pi}_Q(x), \hat{\Pi}_Q(x')] &= 0. \end{aligned} \tag{3.77}$$

We may also define the operators $\hat{\Pi}_0$ and $\hat{\tilde{\Pi}}_Q(x)$ as above. The commutation relations become

$$[\hat{Q}(x), \hat{\tilde{\Pi}}_Q(x')] = i\hbar\delta(x-x'), \text{ for } x' > 0,$$
$$[\hat{Q}(x), \hat{\Pi}_0] = \begin{cases} 0, & x > 0, \\ i\hbar, & x = 0. \end{cases} \tag{3.78}$$

In the Heisenberg picture,

$$\begin{aligned}
\partial_t \hat{Q}(0,t) =& -\frac{i}{\hbar}\left[\hat{Q}(0,t), \hat{\mathcal{H}}(t)\right] \\
=& -\frac{i}{\hbar}\int dx \left\{\delta(x)\left(\frac{1}{2L_0}\left[\hat{Q}(0,t), \hat{\Pi}_0(t)^2\right] + \frac{1}{2C_0}\left[\hat{Q}(0,t), \hat{Q}(0,t)^2\right]\right) + \right. \\
& \left. \theta(x)\left(\frac{1}{2l}\left[\hat{Q}(0,t), [\hat{\tilde{\Pi}}_Q(x,t)]^2\right] + \frac{1}{2c}\left[\hat{Q}(0,t), [\partial_x \hat{Q}(x,t)]^2\right]\right)\right\} \\
=& -\frac{i}{\hbar}\int dx\, \delta(x)\frac{1}{2L_0}\left[\left[\hat{Q}(0,t), \hat{\Pi}_0(t)\right], \hat{\Pi}_0(t)\right]_+ \\
=& \frac{1}{L_0}\hat{\Pi}_0(t),
\end{aligned} \tag{3.79}$$

and for $x > 0$,

$$\begin{aligned}
\partial_t \hat{Q}(x,t) =& -\frac{i}{\hbar}\left[\hat{Q}(x,t), \hat{\mathcal{H}}(t)\right] \\
=& -\frac{i}{\hbar}\int dx' \left\{\delta(x')\left(\frac{1}{2L_0}\left[\hat{Q}(x,t), \hat{\Pi}_0(t)^2\right] + \frac{1}{2C_0}\left[\hat{Q}(x,t), \hat{Q}(0,t)^2\right]\right) + \right. \\
& \left. \theta(x')\left(\frac{1}{2l}\left[\hat{Q}(x,t), [\hat{\tilde{\Pi}}_Q(x',t)]^2\right] + \frac{1}{2c}\left[\hat{Q}(x,t), [\partial_x \hat{Q}(x',t)]^2\right]\right)\right\} \\
=& -\frac{i}{\hbar}\int dx'\, \theta(x')\frac{1}{2l}\left[\left[\hat{Q}(x,t), \hat{\tilde{\Pi}}_Q(x',t)\right], \hat{\tilde{\Pi}}_Q(x',t)\right]_+ \\
=& \frac{1}{l}\hat{\Pi}_Q(x,t),
\end{aligned} \tag{3.80}$$

Further, we obtain

$$\begin{aligned}
\partial_t \hat{\Pi}_0(t) =& -\frac{i}{\hbar}\left[\hat{\Pi}_0(t), \hat{\mathcal{H}}(t)\right] \\
=& -\frac{i}{\hbar}\int dx \left\{\delta(x)\left(\frac{1}{2L_0}\left[\hat{\Pi}_0(t), \hat{\Pi}_0(t)^2\right] + \frac{1}{2C_0}\left[\hat{\Pi}_0(t), \hat{Q}(0,t)^2\right]\right) + \right. \\
& \left. \theta(x)\left(\frac{1}{2l}\left[\hat{\Pi}_0(t), [\hat{\tilde{\Pi}}_Q(x,t)]^2\right] + \frac{1}{2c}\left[\hat{\Pi}_0(t), [\partial_x \hat{Q}(x,t)]^2\right]\right)\right\} \\
=& -\frac{i}{\hbar}\int dx \left\{\delta(x)\frac{1}{2C_0}\left[\left[\hat{\Pi}_0(t), \hat{Q}(0,t)\right], \hat{Q}(0,t)\right]_+ \right. \\
& \left. +\theta(x)\frac{1}{2c}\left[\left[\hat{\Pi}_0(t), \partial_x \hat{Q}(x,t)\right], \partial_x \hat{Q}(x,t)\right]_+\right\}
\end{aligned}$$

$$
\begin{aligned}
&= -\frac{i}{\hbar}\int dx\left\{\delta(x)\frac{1}{2C_0}\left[\left[\hat{\Pi}_0(t),\hat{Q}(0,t)\right],\hat{Q}(0,t)\right]_+\right.\\
&\quad\left.+\theta(x)\frac{1}{2c}\left[\left[\hat{\Pi}_0(t),\partial_x\hat{Q}(x,t)\right],\partial_x\hat{Q}(x,t)\right]_+\right\}\\
&= -\frac{1}{C_0}\hat{Q}(0,t)-\frac{i}{\hbar}\int dx\,\theta(x)\frac{1}{2c}\left[\left[\hat{\Pi}_0(t),\partial_x\hat{Q}(x,t)\right],\partial_x\hat{Q}(x,t)\right]_+\\
&= -\frac{1}{C_0}\hat{Q}(0,t)+\frac{i}{\hbar}\int dx\left\{\delta(x)\frac{1}{2c}\left[\left[\hat{\Pi}_0(t),\hat{Q}(x,t)\right],\partial_x\hat{Q}(x,t)\right]_+\right.\\
&\quad\left.+\,\theta(x)\frac{1}{2c}\left[\left[\hat{\Pi}_0(t),\hat{Q}(x,t)\right],\partial_x^2\hat{Q}(x,t)\right]_+\right\}\\
&= -\frac{1}{C_0}\hat{Q}(0,t)+\frac{1}{c}\partial_x\hat{Q}(0,t).
\end{aligned}
\tag{3.81}
$$

where $\partial_x\hat{Q}(0,t)=\lim_{x\to 0^+}\hat{Q}(x,t)$. Finally, for $x>0$, we obtain

$$
\begin{aligned}
\partial_t\hat{\tilde{\Pi}}_Q(x,t) &= -\frac{i}{\hbar}\left[\hat{\tilde{\Pi}}_Q(x,t),\hat{\mathcal{H}}(t)\right]\\
&= -\frac{i}{\hbar}\int dx'\left\{\delta(x')\left(\frac{1}{2L_0}\left[\hat{\tilde{\Pi}}_Q(x,t),\hat{\Pi}_0(t)^2\right]+\frac{1}{2C_0}\left[\hat{\tilde{\Pi}}_Q(x,t),\hat{Q}(0,t)^2\right]\right)+\right.\\
&\quad\left.\theta(x')\left(\frac{1}{2l}\left[\hat{\tilde{\Pi}}_Q(x,t),[\hat{\tilde{\Pi}}_Q(x',t)]^2\right]+\frac{1}{2c}\left[\hat{\tilde{\Pi}}_Q(x,t),[\partial_x\hat{Q}(x',t)]^2\right]\right)\right\}\\
&= -\frac{i}{\hbar}\int dx'\theta(x')\frac{1}{2c}\left[\left[\hat{\tilde{\Pi}}_Q(x,t),\partial_x\hat{Q}(x',t)\right],\partial_x\hat{Q}(x',t)\right]\\
&= \frac{i}{\hbar}\int dx'\frac{1}{2c}\left\{\delta(x')\left[\left[\hat{\tilde{\Pi}}_Q(x,t),\hat{Q}(x',t)\right],\partial_x\hat{Q}(x',t)\right]\right.\\
&\quad\left.+\theta(x')\left[\left[\hat{\tilde{\Pi}}_Q(x,t),\hat{Q}(x',t)\right],\partial_x^2\hat{Q}(x',t)\right]\right\}\\
&= \frac{1}{c}\partial_x^2\hat{Q}(x,t),
\end{aligned}
\tag{3.82}
$$

where the δ term in the last integral vanishes because $\delta(x')\left[\hat{\tilde{\Pi}}_Q(x,t),\hat{Q}(x',t)\right]=\delta(x')\delta(x-x')=0$ for $x>0$.

Combining the Heisenberg equations of motion, we obtain

$$
L_0\ddot{\hat{Q}}+\frac{1}{C_0}\hat{Q}-\frac{1}{c}\partial_x\hat{Q}=0,\ \text{for } x=0, \tag{3.83}
$$

$$
l\ddot{\hat{Q}}-\frac{1}{c}\partial_x^2\hat{Q}=0,\ \text{for } x>0. \tag{3.84}
$$

Since the charge $\hat{Q}(x,t)$ satisfies the wave equation for $x>0$, is continuous at $x=0$, and is Hermitian, it has for $x\geq 0$ the general form identical to Eq. (3.26)

$$
\hat{Q}(x,t)=\sqrt{\frac{\hbar}{4\pi Z_c}}\int_0^\infty d\omega\frac{1}{\sqrt{\omega}}\left(\hat{A}_{L\omega}e^{-i\omega(x/v+t)}-\hat{A}_{R\omega}e^{-i\omega(-x/v+t)}+\text{h.c.}\right). \tag{3.85}
$$

Fourier transforming the boundary condition (3.83), we obtain

$$\begin{aligned} 0 &= -\omega^2 L_0(\hat{A}_{L\omega} - \hat{A}_{R\omega}) + \frac{1}{C_0}(\hat{A}_{L\omega} - \hat{A}_{R\omega}) - \frac{1}{c}\frac{-i\omega}{v}(\hat{A}_{L\omega} + \hat{A}_{R\omega}) \\ &= i\omega\left(i\omega L_0 + \frac{1}{i\omega C_0}\right)(\hat{A}_{L\omega} - \hat{A}_{R\omega}) + i\omega Z_c(\hat{A}_{L\omega} + \hat{A}_{R\omega}), \end{aligned} \tag{3.86}$$

which gives the quantum equivalent to the classical reflection coefficient,

$$\hat{A}_{R\omega} = \frac{Z_0(\omega) + Z_c}{Z_0(\omega) - Z_c}\hat{A}_{L\omega}, \tag{3.87}$$

where $Z_0(\omega) = i\omega L_0 + 1/(i\omega C_0)$ is the impedance at the end of the transmission line. Using the classical reflection coefficient defined in Eq. (3.65), we may rewrite this as

$$\hat{A}_{R\omega} = r(\omega)^* \hat{A}_{L\omega}, \tag{3.88}$$

which is the complex conjugate of Eq. (3.65) for classical voltage waves. The difference is due to the fact that the annihilation operators are associated with the negative frequency term $e^{-i\omega t}$ whereas the classical amplitudes $A_{L\omega}$ and $A_{R\omega}$ in Eq. (3.65) are associated with the positive frequency term $e^{i\omega t}$. For the creation operators, we obtain

$$\hat{A}^\dagger_{R\omega} = r(\omega)\hat{A}^\dagger_{L\omega}. \tag{3.89}$$

The parts of the voltage operator $\hat{V}(x,t)$ corresponding to the left- and right-moving waves are

$$\hat{V}_L(x,t) \propto \int_0^\infty d\omega\, \hat{A}^\dagger_{L\omega} e^{i\omega(t+x/v)} + \text{h.c.}, \tag{3.90}$$

$$\hat{V}_R(x,t) \propto \int_0^\infty d\omega\, r(\omega)\hat{A}^\dagger_{L\omega} e^{i\omega(t-x/v)} + \text{h.c.}, \tag{3.91}$$

which are similar to Eqs. (3.66) and (3.67), respectively. Because $Z_0(\omega)$ is purely imaginary in this case, we have $|r(\omega)| = 1$ and thus $r(\omega)^* = r(\omega)^{-1}$.

Hamiltonian

Here, we derive the Hamiltonian in terms of the photon annihilation and creation operators. The term for the LC element in the Hamiltonian in Eq. (3.76) can be

written as

$$
\begin{aligned}
&\frac{L_0}{2}[\partial_t\hat{Q}(0,t)]^2+\frac{1}{2C_0}\hat{Q}(0,t)^2\\
=&\frac{\hbar}{4\pi Z_c}\int_0^\infty d\omega\int_0^\infty d\omega'\frac{1}{\sqrt{\omega\omega'}}\Big\{\\
&\frac{L_0}{2}\left[-i\omega\left(\hat{A}_{L\omega}e^{-i\omega t}-\hat{A}_{R\omega}e^{-i\omega t}-\text{h.c.}\right)\right]\times\\
&\left[-i\omega'\left(\hat{A}_{L\omega'}e^{-i\omega' t}-\hat{A}_{R\omega'}e^{-i\omega' t}-\text{h.c.}\right)\right]+\\
&\frac{1}{2C_0}\left[\hat{A}_{L\omega}e^{-i\omega t}-\hat{A}_{R\omega}e^{-i\omega t}+\text{h.c.}\right]\left[\hat{A}_{L\omega'}e^{-i\omega' t}-\hat{A}_{R\omega'}e^{-i\omega' t}+\text{h.c.}\right]\Big\}\\
=&\frac{\hbar}{4\pi Z_c}\int_0^\infty d\omega\int_0^\infty d\omega'\frac{1}{\sqrt{\omega\omega'}}\Big\{\\
&\frac{-\omega\omega' L_0}{2}\left[\left[1-r(\omega)^*\right]\hat{A}_{L\omega}e^{-i\omega t}-\text{h.c.}\right]\left[\left[1-r(\omega')^*\right]\hat{A}_{L\omega'}e^{-i\omega' t}-\text{h.c.}\right]+\\
&\frac{1}{2C_0}\left[\left[1-r(\omega)^*\right]\hat{A}_{L\omega}e^{-i\omega t}+\text{h.c.}\right]\left[\left[1-r(\omega')^*\right])\hat{A}_{L\omega'}e^{-i\omega' t}+\text{h.c.}\right]\Big\}\\
=&\frac{\hbar}{4\pi Z_c}\int_0^\infty d\omega\int_0^\infty d\omega'\frac{1}{\sqrt{\omega\omega'}}\Big\{\\
&\left[\frac{-\omega\omega' L_0}{2}+\frac{1}{2C_0}\right]\left[1-r(\omega)^*\right]\left[1-r(\omega')^*\right]\hat{A}_{L\omega}\hat{A}_{L\omega'}e^{-i(\omega+\omega')t}\\
&+\left[\frac{\omega\omega' L_0}{2}+\frac{1}{2C_0}\right]\left[1-r(\omega)^*\right]\left[1-r(\omega')\right]\hat{A}_{L\omega}\hat{A}^\dagger_{L\omega'}e^{-i(\omega-\omega')t}\\
&+\left[\frac{\omega\omega' L_0}{2}+\frac{1}{2C_0}\right]\left[1-r(\omega)\right]\left[1-r(\omega')^*\right]\hat{A}^\dagger_{L\omega}\hat{A}_{L\omega'}e^{-i(-\omega+\omega')t}\\
&+\left[\frac{-\omega\omega' L_0}{2}+\frac{1}{2C_0}\right]\left[1-r(\omega)\right]\left[1-r(\omega')\right]\hat{A}^\dagger_{L\omega}\hat{A}^\dagger_{L\omega'}e^{i(\omega\omega')t}\Big\}.
\end{aligned}
\tag{3.92}
$$

The transmission line term in the Hamiltonian can be written as

$$
\begin{aligned}
&\int_0^\infty dx\left[\frac{l}{2}(\partial_t\hat{Q})^2+\frac{1}{2c}(\partial_x\hat{Q})^2\right]\\
=&\frac{\hbar}{4\pi Z_c}\int_0^\infty dx\int_0^\infty d\omega\int_0^\infty d\omega'\frac{1}{\sqrt{\omega\omega'}}\Big\{\\
&\frac{l}{2}\left[-i\omega\left(\hat{A}_{L\omega}e^{-i\omega(t+x/v)}-\hat{A}_{R\omega}e^{-i\omega(t-x/v)}-\text{h.c.}\right)\right]\times\\
&\left[-i\omega'\left(\hat{A}_{L\omega'}e^{-i\omega'(t+x/v)}-\hat{A}_{R\omega'}e^{-i\omega'(t-x/v)}-\text{h.c.}\right)\right]+\\
&\frac{1}{2c}\left[\frac{-i\omega}{v}\left(\hat{A}_{L\omega}e^{-i\omega(t+x/v)}+\hat{A}_{R\omega}e^{-i\omega(t-x/v)}-\text{h.c.}\right)\right]\times\\
&\left[\frac{-i\omega'}{v}\left(\hat{A}_{L\omega'}e^{-i\omega'(t+x/v)}+\hat{A}_{R\omega'}e^{-i\omega'(t-x/v)}-\text{h.c.}\right)\right]\Big\}\\
=&\frac{\hbar l}{8\pi Z_c}\int_0^\infty dx\int_0^\infty d\omega\int_0^\infty d\omega'(-\sqrt{\omega\omega'})\Big\{
\end{aligned}
$$

$$
\begin{aligned}
&\left(\hat{A}_{L\omega}e^{-i\omega(t+x/v)} - \hat{A}_{R\omega}e^{-i\omega(t-x/v)} - \text{h.c.}\right)\times \\
&\left(\hat{A}_{L\omega'}e^{-i\omega'(t+x/v)} - \hat{A}_{R\omega'}e^{-i\omega'(t-x/v)} - \text{h.c.}\right) + \\
&\left(\hat{A}_{L\omega}e^{-i\omega(t+x/v)} + \hat{A}_{R\omega}e^{-i\omega(t-x/v)} - \text{h.c.}\right)\times \\
&\left(\hat{A}_{L\omega'}e^{-i\omega'(t+x/v)} + \hat{A}_{R\omega'}e^{-i\omega'(t-x/v)} - \text{h.c.}\right)\Big\} \\
=&\frac{\hbar l}{4\pi Z_c}\int_0^\infty dx\int_0^\infty d\omega\int_0^\infty d\omega'(-\sqrt{\omega\omega'})\Big\{ \\
&\hat{A}_{L\omega}\hat{A}_{L\omega'}e^{-i(\omega+\omega')(t+x/v)} - \hat{A}_{L\omega}\hat{A}^\dagger_{L\omega'}e^{-i(\omega-\omega')(t+x/v)} \\
&- \hat{A}^\dagger_{L\omega}\hat{A}_{L\omega'}e^{-i(-\omega+\omega')(t+x/v)} + \hat{A}^\dagger_{L\omega}\hat{A}^\dagger_{L\omega'}e^{i(\omega+\omega')(t+x/v)} \\
&+ \hat{A}_{R\omega}\hat{A}_{R\omega'}e^{-i(\omega+\omega')(t-x/v)} - \hat{A}_{R\omega}\hat{A}^\dagger_{R\omega'}e^{-i(\omega-\omega')(t-x/v)} \\
&-\hat{A}^\dagger_{R\omega}\hat{A}_{R\omega'}e^{-i(-\omega+\omega')(t-x/v)} + \hat{A}^\dagger_{R\omega}\hat{A}^\dagger_{R\omega'}e^{i(\omega+\omega')(t-x/v)}\Big\} \\
=&\frac{\hbar l}{4\pi Z_c}\int_0^\infty dx\int_0^\infty d\omega\int_0^\infty d\omega'(-\sqrt{\omega\omega'})\Big\{ \\
&\hat{A}_{L\omega}\hat{A}_{L\omega'}e^{-i(\omega+\omega')(t+x/v)} - \hat{A}_{L\omega}\hat{A}^\dagger_{L\omega'}e^{-i(\omega-\omega')(t+x/v)} \\
&- \hat{A}^\dagger_{L\omega}\hat{A}_{L\omega'}e^{-i(-\omega+\omega')(t+x/v)} + \hat{A}^\dagger_{L\omega}\hat{A}^\dagger_{L\omega'}e^{i(\omega+\omega')(t+x/v)} \\
&+ r(\omega)^*r(\omega')^*\hat{A}_{L\omega}\hat{A}_{L\omega'}e^{-i(\omega+\omega')(t-x/v)} - r(\omega)^*r(\omega')\hat{A}_{L\omega}\hat{A}^\dagger_{L\omega'}e^{-i(\omega-\omega')(t-x/v)} \\
&-r(\omega)r(\omega')^*\hat{A}^\dagger_{L\omega}\hat{A}_{L\omega'}e^{-i(-\omega+\omega')(t-x/v)} + r(\omega)r(\omega')\hat{A}^\dagger_{L\omega}\hat{A}^\dagger_{L\omega'}e^{i(\omega+\omega')(t-x/v)}\Big\} \\
=&\frac{\hbar l}{4\pi Z_c}\int_0^\infty d\omega\int_0^\infty d\omega'(-\sqrt{\omega\omega'})v\Big\{ \\
&\left[\left[1+r(\omega)^*r(\omega')^*\right]\pi\delta(\omega+\omega') + \frac{1-r(\omega)^*r(\omega')^*}{i(\omega+\omega')}\right]\hat{A}_{L\omega}\hat{A}_{L\omega'}e^{-i(\omega+\omega')t} \\
&- \left[\left[1+r(\omega)^*r(\omega')\right]\pi\delta(\omega-\omega') + \frac{1-r(\omega)^*r(\omega')}{i(\omega-\omega')}\right]\hat{A}_{L\omega}\hat{A}^\dagger_{L\omega'}e^{-i(\omega-\omega')t} \\
&- \left[\left[1+r(\omega)r(\omega')^*\right]\pi\delta(-\omega+\omega') + \frac{1-r(\omega)r(\omega')^*}{i(-\omega+\omega')}\right]\hat{A}^\dagger_{L\omega}\hat{A}_{L\omega'}e^{-i(-\omega+\omega')t} \\
&+ \left[\left[1+r(\omega)r(\omega')\right]\pi\delta(-\omega-\omega') + \frac{1-r(\omega)r(\omega')}{i(-\omega-\omega')}\right]\hat{A}^\dagger_{L\omega}\hat{A}^\dagger_{L\omega'}e^{i(\omega+\omega')t}\Big\} \\
=&\frac{\hbar l}{4\pi Z_c}\int_0^\infty d\omega\int_0^\infty d\omega'(-\sqrt{\omega\omega'})v\Big\{ \\
&\left[\frac{1-r(\omega)^*r(\omega')^*}{i(\omega+\omega')}\right]\hat{A}_{L\omega}\hat{A}_{L\omega'}e^{-i(\omega+\omega')t} \\
&- \left[\frac{1-r(\omega)^*r(\omega')}{i(\omega-\omega')}\right]\hat{A}_{L\omega}\hat{A}^\dagger_{L\omega'}e^{-i(\omega-\omega')t} \\
&- \left[\frac{1-r(\omega)r(\omega')^*}{i(-\omega+\omega')}\right]\hat{A}^\dagger_{L\omega}\hat{A}_{L\omega'}e^{-i(-\omega+\omega')t} \\
&+ \left[\frac{1-r(\omega)r(\omega')}{i(-\omega-\omega')}\right]\hat{A}^\dagger_{L\omega}\hat{A}^\dagger_{L\omega'}e^{i(\omega+\omega')t}\Big\}
\end{aligned}
$$

$$
\begin{aligned}
&+\frac{\hbar l}{4\pi Z_c}\int_0^\infty d\omega\,\omega\pi v\left\{[1+r(\omega)^* r(\omega)]\hat{A}_{L\omega}\hat{A}^\dagger_{L\omega}+[1+r(\omega)r(\omega)^*]\hat{A}^\dagger_{L\omega}\hat{A}_{L\omega}\right\}\\
=&\frac{\hbar}{4\pi}\int_0^\infty d\omega\int_0^\infty d\omega'(-\sqrt{\omega\omega'})\Big\{\\
&\frac{1-r(\omega)^* r(\omega')^*}{i(\omega+\omega')}\hat{A}_{L\omega}\hat{A}_{L\omega'}e^{-i(\omega+\omega')t}-\frac{1-r(\omega)^* r(\omega')}{i(\omega-\omega')}\hat{A}_{L\omega}\hat{A}^\dagger_{L\omega'}e^{-i(\omega-\omega')t}\\
&-\frac{1-r(\omega)r(\omega')^*}{i(-\omega+\omega')}\hat{A}^\dagger_{L\omega}\hat{A}_{L\omega'}e^{-i(-\omega+\omega')t}+\frac{1-r(\omega)r(\omega')}{i(-\omega-\omega')}\hat{A}^\dagger_{L\omega}\hat{A}^\dagger_{L\omega'}e^{i(\omega+\omega')t}\Big\}\\
&+\int_0^\infty d\omega\frac{1}{2}\hbar\omega\left\{\hat{A}_{L\omega}\hat{A}^\dagger_{L\omega}+\hat{A}^\dagger_{L\omega}\hat{A}_{L\omega}\right\}.
\end{aligned}
\tag{3.93}
$$

Using identities

$$
\begin{aligned}
&\frac{1}{Z_c\sqrt{\omega\omega'}}\left[\frac{-\omega\omega' L_0}{2}+\frac{1}{2C_0}\right]\left[1-r(\omega)^*\right]\left[1-r(\omega')^*\right]\\
=&-\left(-\sqrt{\omega\omega'}\right)\left[\frac{1-r(\omega)^* r(\omega')^*}{i(\omega+\omega')}\right],
\end{aligned}
\tag{3.94}
$$

$$
\begin{aligned}
&\frac{1}{Z_c\sqrt{\omega\omega'}}\left[\frac{-\omega\omega' L_0}{2}+\frac{1}{2C_0}\right]\left[1-r(\omega)^*\right]\left[1-r(\omega')\right]\\
=&\left(-\sqrt{\omega\omega'}\right)\left[\frac{1-r(\omega^*)r(\omega')}{i(\omega-\omega')}\right],
\end{aligned}
\tag{3.95}
$$

and their complex conjugates, the term in Eq. (3.92) of the Hamiltonian cancels the first integral in the Eq. (3.93), and the total Hamiltonian becomes

$$
\hat{\mathcal{H}}(t)=\int_0^\infty d\omega\frac{1}{2}\hbar\omega\left\{\hat{A}_{L\omega}\hat{A}^\dagger_{L\omega}+\hat{A}^\dagger_{L\omega}\hat{A}_{L\omega}\right\}=\int_0^\infty d\omega\,\hbar\omega\hat{A}^\dagger_{L\omega}\hat{A}_{L\omega}+\text{const.},
\tag{3.96}
$$

which is the Hamiltonian of a combination of Harmonic oscillators, similar to Eq. (3.30). However, in this case, the direction of a single photon with well-defined frequency is not well defined, and thus there are no separate terms for left- and right-going photons. Nevertheless, a wave packet localized in space can be expressed in terms of the field operators derived below.

Field operators and reflection of wave packets

We may define the field operators for $x \geq 0$, similar to the ones for the infinite transmission line in Eqs. (3.36) and (3.38), by

$$
\hat{\psi}_L(x)=\frac{1}{\sqrt{2\pi v}}\int_0^\infty d\omega\,e^{-i\omega x/v}\hat{A}_{L\omega},
\tag{3.97}
$$

$$
\hat{\psi}_R(x)=\frac{1}{\sqrt{2\pi v}}\int_0^\infty d\omega\,e^{i\omega x/v}\hat{A}_{R\omega}.
\tag{3.98}
$$

However, in this case the left- and right-going fields are not independent and the time evolution of a state described by

$$|s\rangle = \int_0^\infty dx \left[\xi_L(x)\hat{\psi}_L^\dagger(x) + \xi_R(x)\hat{\psi}_R^\dagger(x)\right]|0\rangle \tag{3.99}$$

is nontrivial. Here, we study a simple special case of the reflection of a localized left-moving wave packet. We solve the wave function of the reflected wave after a long time, i.e., when the reflected wave is far from the origin.

For notational simplicity, we extend the definition of $\hat{\psi}_L$ for $x \in \mathbb{R}$ by

$$\hat{\tilde{\psi}}_L(x) = \frac{1}{\sqrt{2\pi v}} \int_0^\infty d\omega e^{-i\omega x/v} \hat{A}_{L\omega}. \tag{3.100}$$

As in Sec. 3.1.4, any single photon state can be expressed as

$$|s\rangle = \int_{-\infty}^\infty dx\, \xi(x)\hat{\tilde{\psi}}_L^\dagger(x)|0\rangle. \tag{3.101}$$

However, here the x variable takes both positive and negative values, and thus $\xi(x)$ does not correspond directly to a field in space. In the Heisenberg picture,

$$\hat{\tilde{\psi}}_L(x,t) = \frac{1}{\sqrt{2\pi v}} \int_0^\infty d\omega\, e^{-i\omega(x/v+t)} \hat{A}_{L\omega}, \tag{3.102}$$

and in the Schrödinger picture,

$$|s(t)\rangle = \int_{-\infty}^\infty dx\, \xi(x+vt)\hat{\tilde{\psi}}_L^\dagger(x)|0\rangle. \tag{3.103}$$

For $x \geq 0$, the field operators $\hat{\psi}_L$ and $\hat{\tilde{\psi}}_L$ are equal. For $x > 0$, we may write

$$\begin{aligned}
\hat{\tilde{\psi}}_L(-x) &= \frac{1}{\sqrt{2\pi v}} \int_0^\infty d\omega\, e^{i\omega x/v} \hat{A}_{L\omega} \\
&= \frac{1}{\sqrt{2\pi v}} \int_0^\infty d\omega\, e^{i\omega x/v} r(\omega) \hat{A}_{R\omega} \\
&= \frac{1}{\sqrt{2\pi v}} \int_0^\infty d\omega\, e^{i\omega x/v} \int_{-\infty}^\infty d\tau\, \tilde{r}(\tau) e^{-i\tau\omega} \hat{A}_{R\omega} \\
&= \frac{1}{\sqrt{2\pi v}} \int_{-\infty}^\infty d\tau\, \tilde{r}(\tau) \int_0^\infty d\omega\, e^{i\omega(x/v-\tau)} \hat{A}_{R\omega} \\
&= \frac{1}{\sqrt{2\pi v}} \int_0^\infty d\tau\, \tilde{r}(\tau) \int_0^\infty d\omega\, e^{i\omega(x/v-\tau)} \hat{A}_{R\omega} \\
&\approx \frac{1}{\sqrt{2\pi v}} \int_0^{x/v} d\tau\, \tilde{r}(\tau) \hat{\psi}_R(x - \tau v),
\end{aligned} \tag{3.104}$$

where $\tilde{r}$ is the inverse Fourier transform of the reflection coefficient derived in App. B and the approximation on the limit of the integral over τ is valid if $x \gg x_0$ where $x_0 = v\tau_0$ and τ_0 is the time scale of $\tilde{r}$, given in Eq. (B.9).

Consider a left-moving wave packet localized between $x_{\min}$ and $x_{\max}$ (where $0 < x_{\min} < x_{\max}$) at $t = 0$. It can be described by

$$|s(0)\rangle = \int_{x_{\min}}^{x_{\max}} dx\, \xi(x)\hat{\psi}_L^\dagger(x)|0\rangle = \int_{x_{\min}}^{x_{\max}} dx\, \xi(x)\hat{\tilde{\psi}}_L^\dagger(x)|0\rangle. \tag{3.105}$$

Using Eq. (3.103), the time evolution of the state can be expressed as

$$|s(t)\rangle = \int_{x_{\min}-vt}^{x_{\max}-vt} dx\, \xi(x+vt)\hat{\tilde{\psi}}_L^\dagger(x)|0\rangle. \tag{3.106}$$

For t sufficiently large such that $vt - x_{\max} \gg x_0$, we may use Eq. (3.104) to obtain

$$|s(t)\rangle = \int_{x_{\min}-vt}^{x_{\max}-vt} dx\, \xi(x+vt)\left[\frac{1}{\sqrt{2\pi v}}\int_0^{-x/v} d\tau\, \tilde{r}(\tau)^*\hat{\psi}_R^\dagger(-x-\tau v)\right]|0\rangle. \tag{3.107}$$

Here, it should be noted that no left-moving photons exist for sufficiently long time after the reflection. Making the change of variables from (x, τ) to $(y = -x - \tau v, \tau)$ and changing the order of integrals, the system state assumes the form

$$|s(t)\rangle = \int_0^{vt-x_{\min}} dy \left[\frac{1}{\sqrt{2\pi v}}\int_{\max\left(0, t-\frac{y+x_{\max}}{v}\right)}^{t-\frac{y+x_{\min}}{v}} d\tau\, \xi(vt-y-v\tau)\tilde{r}(\tau)^*\right]\hat{\psi}_R^\dagger(y)|0\rangle. \tag{3.108}$$

Noting that the limits of the inner integral can be extended to $\pm\infty$ because the integrand is zero in other points, we may write the term as a convolution

$$|s(t)\rangle = \int_0^{vt-x_{\min}} dy \left[\frac{1}{\sqrt{2\pi v}}(\tilde{\xi} * \tilde{r}^*)(t - y/v)\right]\hat{\psi}_R^\dagger(y)|0\rangle, \tag{3.109}$$

where we defined $\tilde{\xi}(\tau) = \xi(v\tau)$ to obtain equal units for the convolution. The wave function of the reflected wave of a wave packet can thus be approximated by the convolution of the wave function of the incident wave and the inverse Fourier transform of the reflection coefficient.

3.2.3 Multiple LCR elements at the end of the transmission line

In this section, we consider a transmission line with inductance per unit length l, capacitance per unit length c, characteristic impedance $Z_c = \sqrt{l/c}$, and velocity $v = 1/\sqrt{lc}$, terminated by n parallel LCR elements (inductance L_k, capacitance C_k, resistance R_k for $k = 1, 2, \cdots, n$), as shown in Fig. 3.4. Each LCR element acts as a band-pass filter and the total admittance at the end of the main transmission line is the sum of the admittances of the LCR elements. We assume that a frequency-dependent admittance can be approximated by the sum of the admittances of the

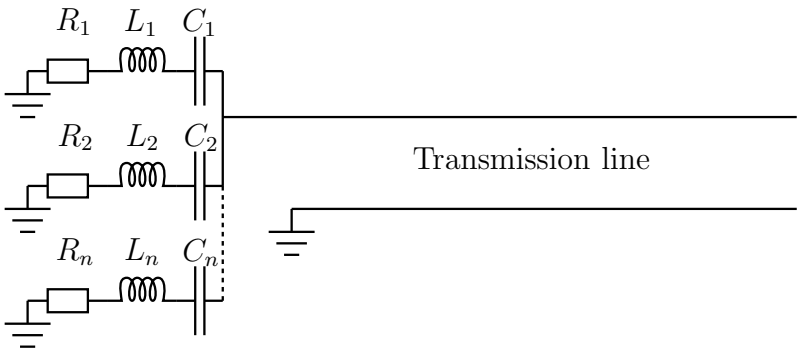

Figure 3.4: Transmission line terminated by n parallel LCR elements.

band-pass filters in some frequency range, and thus this model can be used to model the impedance $Z_0(\omega)$ at the end of the transmission line[2]. First, we show that a noisy resistor can be modelled as a semi-infinite transmission line, and then we model the circuit with the n resistors replaced by transmission lines.

Resistor modelled as transmission line

For a semi-infinite transmission line with characteristic impedance Z_c shown in Fig. 3.5(a), the current $I_0(t)$ going into the transmission line can be expressed using Eq. (3.9) as

$$\begin{aligned} I_0(t) &= -\partial_t Q(0,t) = -\frac{1}{Z_c}\left[V_L(t) - V_R(t)\right] \\ &= -\frac{1}{Z_c}\left[2V_L(t) - V(0,t)\right], \end{aligned} \tag{3.110}$$

which can further be written as

$$V_0(t) = 2V_L(t) + Z_c I_0(t), \tag{3.111}$$

where $V_0(t) = V(0,t)$ is the voltage at the end of the transmission line.

A noisy resistor can be modelled as an ideal resistor and a voltage source in series as shown in Fig. 3.5(b). The voltage-current relation is

$$V_0(t) = V(t) + RI_0(t), \tag{3.112}$$

which is similar to Eq. (3.111) with resistance R replaced by Z_c, the characteristic impedance of the transmission line, and V replaced by $2V_L$, twice the voltage of the incoming wave. A noisy resistor can thus be modelled as semi-infinite transmission line with characteristic impedance equal to the resistance of the resistor. The power of the right-going wave radiates into infinity, effectively dissipating energy. The

[2]Any realizable purely reactive frequency-dependent impedance can be implemented with parallel series-LC elements, in so-called Foster II form [32]. Here, we model the dissipation in the system by inserting a resistor into each LC element.

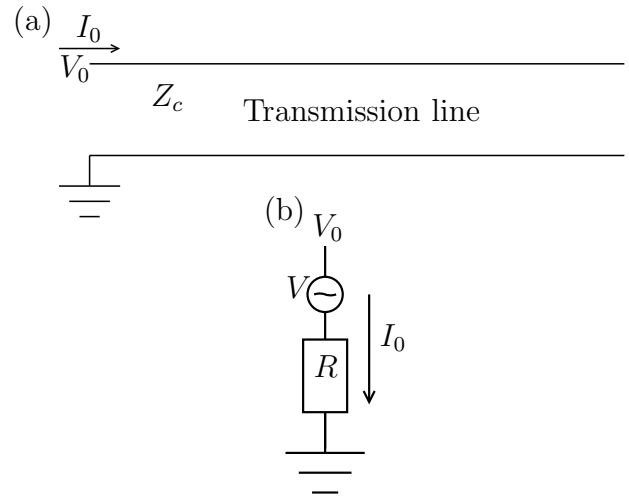

Figure 3.5: (a) Semi-infinite transmission line with voltage V_0 at the end and current I_0 goint into the transmission line. (b) A model of a noisy resistor consisting of a voltage source with voltage V and an ideal resistor with resistance R .

left-going wave can be used to model the fluctuations in the resistor. This model is useful when quantizing a circuit with resistors, for example the Johnson-Nyquist noise [33, 34] of a resistor can be derived using this model by assuming that the left-going waves are in thermal equilibrium [35].

Classical case

We model the resistors in the circuit in Fig. 3.4 by semi-infinite transmission lines with inductance and capacitance per unit length l_k and c_k, respectively. The characteristic impedance equals the resistance of the resistor, $R_k = \sqrt{l_k/c_k}$. Since we have one condition for two parameters, we may choose the speed of propagation in each of the transmission lines arbitrarily. For convenience, we choose $v = 1/\sqrt{lc} = 1/\sqrt{l_k c_k}$. These conditions result in $l_k = R_k/v$ and $c_k = 1/(R_k v)$.

Each transmission line modeling a resistor is described by the variable $Q_k(x)$ with $x \geq 0$ where $Q_k(0)$ is the charge at the kth capacitor, positive on the side of the kth resistor. The Kirchoff's law gives the boundary condition $\dot{Q}(0) + \sum_k \dot{Q}_k(0) = 0$. Since the exact value of $Q(0)$ has no physical meaning here, we may choose $Q(0) = -\sum_k Q_k(0)$ which is the total charge on the capacitors on the side of the main transmission line. This is illustrated for the case $n = 2$ in Fig. 3.6.

Equations of motion are the wave equations for the transmission lines and the voltage at the end of the main transmission line,

$$\ddot{Q}_k(x,t) = v^2 \partial_x^2 Q_k(x,t), \qquad x > 0 \tag{3.113}$$

$$\ddot{Q}(x,t) = v^2 \partial_x^2 Q(x,t), \qquad x > 0 \tag{3.114}$$

$$\frac{1}{c}\partial_x Q(x,t)|_{x=0} = \frac{1}{c_k}\partial_x Q_k(x,t)|_{x=0} - \frac{1}{C_k} Q_k(0,t) - L_k \ddot{Q}_k(0), \tag{3.115}$$

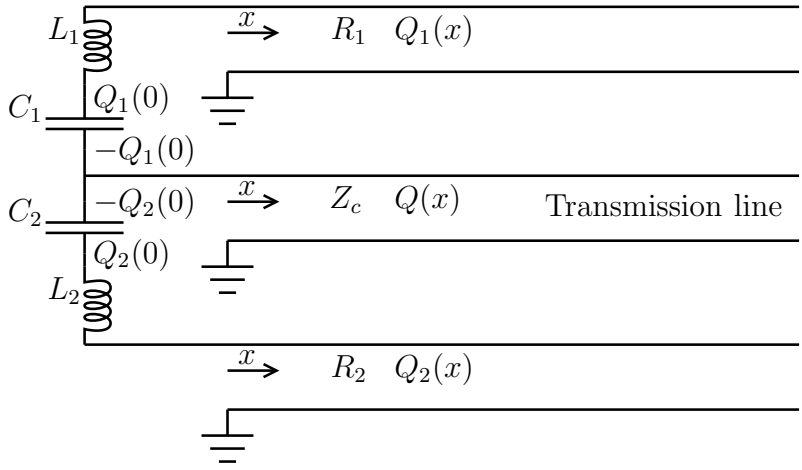

Figure 3.6: Transmission line terminated by two parallel LCR elements where each resistor is replaced with a transmission line. The charge at the kth capacitor is $Q_k(0)$ on the side of the resistor and $-Q_k(0)$ on the side of the main trasmission line.

which are to be satisfied for each k. The left-hand side of Eq. (3.115) is the voltage at the end of the main transmission line, and the terms on the right-hand side are the voltage at the end of the transmission line modeling the kth resistor, the voltage over the kth capacitor, and the voltage over the kth inductor, respectively.

These equations are also given by the Lagrangian

$$\begin{aligned}\mathcal{L}(x) =&\delta(x)\left\{\sum_k \frac{L_k}{2}\dot{Q}_k(x)^2 - \frac{1}{2C_k}Q_k(x)^2\right\}\\ &+\theta(x)\left\{\left[\sum_k \frac{l_k}{2}\dot{Q}_k(x)^2 - \frac{1}{2c_k}[\partial_x Q_k(x)]^2\right]+\right.\\ &\left.\left[\frac{l}{2}\dot{Q}(x)^2 - \frac{1}{2c}[\partial_x Q(x)]^2\right]\right\}. \end{aligned} \tag{3.116}$$

For the main transmission line, we may write

$$Q(x,t) = Q_L(t+x/v) + Q_R(t-x/v) \tag{3.117}$$

as in Eq. (3.3). Fourier expanding Q, we obtain

$$Q_L(t+x/v) = \int_{-\infty}^{\infty} d\omega\, A_{L\omega} e^{i\omega(t+x/v)}, \tag{3.118}$$

$$Q_R(t-x/v) = \int_{-\infty}^{\infty} d\omega\, (-A_{R\omega}) e^{i\omega(t-x/v)}, \tag{3.119}$$

$$Q(x,t) = \int_{-\infty}^{\infty} d\omega\, A_{L\omega} e^{i\omega(t+x/v)} - A_{R\omega} e^{i\omega(t-x/v)}. \tag{3.120}$$

For the transmission lines modeling the resistors, we write

$$Q_k(x,t) = Q_{k\mathrm{in}}(t+x/v) + Q_{k\mathrm{out}}(t-x/v), \tag{3.121}$$

where $Q_{k\text{in}}$ is the wave in the transmission line modeling the kth resistor coming into the circuit connecting the main transmission line with the resistors, and $Q_{k\text{out}}$ is the outgoing wave at the same resistor, propagating to infinity. Fourier expanding Q_k, we obtain

$$Q_{k\text{in}}(t+x/v) = \int_{-\infty}^{\infty} d\omega\, A_{k\text{in}\omega} e^{i\omega(t+x/v)}, \tag{3.122}$$

$$Q_{k\text{out}}(t-x/v) = \int_{-\infty}^{\infty} d\omega\, (-A_{k\text{out}\omega}) e^{i\omega(t-x/v)}, \tag{3.123}$$

$$Q_k(x,t) = \int_{-\infty}^{\infty} d\omega A_{k\text{in}\omega}\, e^{i\omega(t+x/v)} - A_{k\text{out}\omega} e^{i\omega(t-x/v)}. \tag{3.124}$$

The boundary condition $Q(0) = -\sum_k Q_k(0)$ yields

$$A_{L\omega} - A_{R\omega} = -\sum_k (A_{k\text{in}\omega} - A_{k\text{out}\omega}), \tag{3.125}$$

and the boundary condition in Eq. (3.115) yields for all k,

$$\begin{aligned}
&\frac{i\omega}{cv}(A_{L\omega} + A_{R\omega}) = \frac{i\omega}{c_k v}(A_{k\text{in}\omega} + A_{k\text{out}\omega}) - \left(\frac{1}{C_k} - L_k\omega^2\right)(A_{k\text{in}\omega} - A_{k\text{out}\omega}) \\
\Leftrightarrow\quad &Z_c(A_{L\omega} + A_{R\omega}) = R_k(A_{k\text{in}\omega} + A_{k\text{out}\omega}) - \left(\frac{1}{i\omega C_k} + i\omega L_k\right)(A_{k\text{in}\omega} - A_{k\text{out}\omega}) \\
\Leftrightarrow\quad &Z_c(A_{L\omega} + A_{R\omega}) = Z_k(\omega)^* A_{k\text{in}\omega} + Z_k(\omega) A_{k\text{out}\omega},
\end{aligned} \tag{3.126}$$

where we wrote $Z_c = 1/(cv)$ and $R_k = 1/(c_k v)$, and defined $Z_k(\omega) = R_k + i\omega L_k + \frac{1}{i\omega C_k}$. Solving $A_{k\text{out}\omega}$ in Eq. (3.126) and inserting it into Eq. (3.125), we obtain

$$A_{R\omega} = \frac{1 - \frac{Z_c}{Z(\omega)}}{1 + \frac{Z_c}{Z(\omega)}} A_{L\omega} + \frac{1}{1 + \frac{Z_c}{Z(\omega)}} \sum_k \frac{2R_k}{Z_k(\omega)} A_{k\text{in}\omega}, \tag{3.127}$$

where $Z(\omega) = [\sum_k 1/Z_k(\omega)]^{-1}$ is the total impedance at the end of the main transmission line. Inserting this into Eq. (3.126), we obtain

$$A_{k\text{out}\omega} = \frac{Z_c}{Z_k(\omega)[1 + Z_c/Z(\omega)]} \left(2A_{L\omega} + \sum_l \frac{2R_l}{Z_l(\omega)} A_{l\text{in}\omega}\right) - \frac{Z_k(\omega)^*}{Z_k(\omega)} A_{k\text{in}\omega}. \tag{3.128}$$

If we assume that the resistors are noiseless, $A_{k\text{in}\omega} = 0$. With this assumption, we obtain the reflection coefficient

$$r(\omega) = \frac{A_{R\omega}}{A_{L\omega}} = \frac{V_{R\omega}(0)}{V_{L\omega}(0)} = \frac{Z(\omega) - Z_c}{Z(\omega) + Z_c}, \tag{3.129}$$

which is of course equivalent to the one we found for the general impedance in Eq. (3.65).

Quantization

The conjugate variable of $Q(x)$, $x > 0$ is $\Pi_Q(x) = l\dot{Q}(x)$, and the conjugate variable of $Q_k(x)$, is $\Pi_{Qk}(x) = [\delta(x)L_k + \theta(x)l_k]\dot{Q}_k(x)$. Note that $Q(0)$ is not an independent variable. The Hamiltonian becomes

$$\begin{aligned}\mathcal{H}(x) = \theta(x)&\left\{\frac{l}{2}\dot{Q}^2 + \frac{1}{2c}(\partial_x Q)^2\right\}\\ &+ \theta(x)\sum_k\left\{\frac{l_k}{2}\dot{Q}_k^2 + \frac{1}{2c_k}(\partial_x Q_k)^2\right\}\\ &+ \delta(x)\sum_k\left\{\frac{L_k}{2}\dot{Q}_k^2 + \frac{1}{2C_k}Q_k^2\right\}.\end{aligned} \tag{3.130}$$

Quantizing the system, we obtain the operators $\hat{Q}(x)$, $\hat{\Pi}_Q(x)$, $\hat{Q}_k(x)$, and $\hat{\Pi}_{Qk}(x)$ with the usual commutation relations. The boundary condition for $\hat{Q}(0)$ holds in the quantum case as well,

$$\hat{Q}(0) = -\sum_k \hat{Q}_k(0). \tag{3.131}$$

The Heisenberg equations of motion inside the transmission lines are similar to the ones in Sec. 3.2.2, yielding the wave equations for $\hat{Q}$ and $\hat{Q}_k$, and as above, we obtain the expressions

$$\hat{Q} = \int_0^\infty d\omega\sqrt{\frac{\hbar}{4\pi Z_c\omega}}\left(\hat{A}_{L\omega}e^{-i\omega(t+x/v)} - \hat{A}_{R\omega}e^{-i\omega(t-x/v)} + \text{h.c.}\right), \tag{3.132}$$

$$\hat{Q}_k = \int_0^\infty d\omega\sqrt{\frac{\hbar}{4\pi R_k\omega}}\left(\hat{A}_{k\text{in}\omega}e^{-i\omega(t+x/v)} - \hat{A}_{k\text{out}\omega}e^{-i\omega(t-x/v)} + \text{h.c.}\right). \tag{3.133}$$

The boundary condition $\hat{Q}(0,t) = -\sum_k \hat{Q}_k(0,t)$ yields

$$\frac{1}{\sqrt{Z_c}}(\hat{A}_{L\omega} - \hat{A}_{R\omega}) = -\sum_k \frac{1}{\sqrt{R_k}}(\hat{A}_{k\text{in}\omega} - \hat{A}_{k\text{out}\omega}). \tag{3.134}$$

The remaining equation of motion is similar to the classical boundary condition [28],

$$\frac{1}{c}\partial_x\hat{Q}|_{x=0} = \frac{1}{c_k}\partial_x\hat{Q}_k|_{x=0} - L_k\ddot{\hat{Q}}_k(0) - \frac{1}{C_k}\hat{Q}_k(0), \tag{3.135}$$

which yields

$$\begin{aligned}\frac{-i}{cv}\sqrt{\frac{\omega}{Z_c}}\left(\hat{A}_{L\omega} + \hat{A}_{R\omega}\right) =&\sqrt{\frac{1}{\omega R_k}}\left[\frac{-i\omega}{c_k v}(\hat{A}_{k\text{in}\omega} + \hat{A}_{k\text{out}\omega}) + L_k\omega^2\left(\hat{A}_{k\text{in}\omega} - \hat{A}_{k\text{out}\omega}\right)\right.\\ &\left. - \frac{1}{C_k}\left(\hat{A}_{k\text{in}\omega} - \hat{A}_{k\text{out}\omega}\right)\right],\end{aligned} \tag{3.136}$$

$$\Leftrightarrow \qquad \sqrt{Z_c}\left(\hat{A}_{L\omega} + \hat{A}_{R\omega}\right) = \sqrt{\frac{1}{R_k}}\left[Z_k(\omega)\hat{A}_{k\text{in}\omega} + Z_k(\omega)^*\hat{A}_{k\text{out}\omega}\right], \tag{3.137}$$

where $Z_k[\omega] = R_k + i\omega L_k + 1/(i\omega C_k)$ is the impedance of the kth LCR element.

Equations (3.134) and (3.137) are similar to Eqs. (3.125) and (3.126), and the solution is

$$\left(1 + \frac{Z_c}{Z(\omega)^*}\right)\hat{A}_{R\omega} = \left(1 - \frac{Z_c}{Z(\omega)^*}\right)\hat{A}_{L\omega} + \sqrt{Z_c}\sum_k \frac{2\sqrt{R_k}}{Z_k(\omega)^*}\hat{A}_{k\mathrm{in}\omega}, \tag{3.138}$$

$$\begin{aligned}\hat{A}_{k\mathrm{out}\omega} =& \frac{\sqrt{Z_c R_k}}{Z_k(\omega)^*[1 + Z_c/Z(\omega)^*]}\left(2\hat{A}_{L\omega} + \sqrt{Z_c}\sum_l \frac{2\sqrt{R_l}}{Z_l(\omega)^*}\hat{A}_{l\mathrm{in}\omega}\right) \\ & - \frac{Z_k(\omega)}{Z_k(\omega)^*}\hat{A}_{k\mathrm{in}\omega},\end{aligned} \tag{3.139}$$

where $Z(\omega) = [\sum_k 1/Z_k(\omega)]^{-1}$ is the total impedance at the end of the main transmission line. The explicit solution to the outgoing field in the main transmission line is

$$\hat{A}_{R\omega} = \frac{Z(\omega)^* - Z_c}{Z(\omega)^* + Z_c}\hat{A}_{L\omega} + \frac{\sqrt{Z_c}}{1 + \frac{Z_c}{Z(\omega)^*}}\sum_k \frac{2\sqrt{R_k}}{Z_k(\omega)^*}\hat{A}_{k\mathrm{in}\omega}. \tag{3.140}$$

Taking into account the factors $\sqrt{Z_c}$ and $\sqrt{Z_k}$ in the expressions of the charge operators $\hat{Q}$ and $\hat{Q}_k$ in Eqs. (3.132) and (3.133), respectively, this equation is equivalent to the complex conjugate of Eq. (3.127). If the resistors are noiseless, i.e., $\hat{A}_{k\mathrm{in}\omega} = 0$, the reflection coefficient is equal to the classical one without dissipation.

3.3 Networks of transmission lines

In networks with N finite or semi-infinite transmission lines, each transmission line can be characterized by a variable Q_k ($k = 1, 2, \ldots, N$) similar to the cases above. Given the inductance per unit length l_k and the capacitance per unit length c_k of the kth transmission line, the part of the Lagrangian that depends on Q_k at the points inside the kth transmission line is of the form $\int dx \left\{\frac{l_k}{2}\dot{Q}_k(x)^2 - \frac{1}{2c_k}[\partial_x Q_k(x)]^2\right\}$, where the integration limits are 0 and L_k for a finite transmission line of length L_k, and 0 and ∞ for a semi-infinite transmission line. Therefore, the conjugate of $Q_k(x)$ is $l_k\dot{Q}_k(x)$ for points inside the transmission line, and thus the equation of motion for the kth transmission line is the wave equation,

$$\partial_t^2 Q_k(x,t) = v_k^2 \partial_x^2 Q_k(x,t), \tag{3.141}$$

where $v_k = 1/\sqrt{l_k c_k}$ is the velocity of propagation for the kth transmission line. In addition, the Lagrangian contains terms that depend on the values of Q_k and $\dot{Q}_k$ at the endpoints of the kth transmission line. The equations of motion derived from these terms are the boundary conditions that relate the transmission lines to each other.

Quantizing the network, the Heisenberg equations of motion for $\hat{Q}_k(x)$ points inside the transmission lines yield the wave equation similar to the one for the infinite

transmission line [28], and therefore we may write

$$\hat{Q}_k(x,t) = \sqrt{\frac{\hbar}{4\pi Z_k}} \int_0^\infty d\omega \frac{1}{\sqrt{\omega}} \left(\hat{A}_{Lk\omega} e^{-i\omega(t+x/v_k)} - \hat{A}_{Rk\omega} e^{-i\omega(t-x/v_k)} + \text{h.c.} \right), \tag{3.142}$$

where $Z_k = \sqrt{l_k/c_k}$ is the characteristic impedance of the kth transmission line.

For sufficiently simple networks, the Heisenberg equations of motion yield boundary conditions similar to the classical ones [28]. For each circuit connecting transmission lines, the boundary conditions are most conveniently written in terms of the photon annihilation operators obtained from Eq. (3.142) for each connected transmission line in the coordinate system where $x \geq 0$ and the origin is at the end connected to the circuit in question.

For each circuit connecting transmission lines, the operators for the outgoing photons can be solved in terms of the operators for the incoming photons. Furthermore, for each finite transmission line connected to a circuit at both ends, we have the relation between the operators at both ends of a finite transmission line (to be derived in Sec. 3.3.1). Combining these equations yield the scattering parameters of the network, i.e., the operators for the photons going out of the system into the semi-infinite transmission lines in terms of the operators for the photons coming into the system from the semi-infinite transmission lines.

In Secs. 3.3.2 and 3.3.3, we solve the scattering parameters for the case where multiple transmission lines are connected to a single junction and the case where a single indcutor breaks a transmission line, respectively.

3.3.1 Phase shift on a finite transmission line

Consider a transmission line of length d connecting systems A and B, shown in Fig. 3.7(a). Choosing the coordinates such that $x = 0$ is at system A and $x = d$ is at system B, we have

$$\hat{Q}(x,t) = \sqrt{\frac{\hbar}{4\pi Z_c}} \int_0^\infty d\omega \frac{1}{\sqrt{\omega}} \left(\hat{A}_{L\omega} e^{-i\omega(t+x/v)} - \hat{A}_{R\omega} e^{-i\omega(t-x/v)} + \text{h.c.} \right), \tag{3.143}$$

for $0 \leq x \leq d$. At $x = 0$, the operators $\hat{A}_{L\omega}$ and $\hat{A}_{R\omega}$ correspond to the modes incoming to and outgoing from system A, respectively. To obtain similar operators for the other end of the transmission line, we apply a coordinate transformation $\xi = d - x$ and $\tilde{Q}(\xi, t) = -Q(d - \xi, t)$ to obtain

$$\begin{aligned} \tilde{Q}(\xi,t) =& -\sqrt{\frac{\hbar}{4\pi Z_c}} \int_0^\infty d\omega \frac{1}{\sqrt{\omega}} \left(\hat{A}_{L\omega} e^{-i\omega(t+(d-\xi)/v)} - \hat{A}_{R\omega} e^{-i\omega(t-(d-\xi)/v)} + \text{h.c.} \right) \\ =& \sqrt{\frac{\hbar}{4\pi Z_c}} \int_0^\infty d\omega \frac{1}{\sqrt{\omega}} \times \\ & \left(e^{i\omega d/v} \hat{A}_{R\omega} e^{-i\omega(t+\xi/v)} - e^{-i\omega d/v} \hat{A}_{L\omega} e^{-i\omega(t-\xi/v)} + \text{h.c.} \right). \end{aligned} \tag{3.144}$$

Thus the operators $e^{-i\omega d/v}\hat{A}_{L\omega}$ and $e^{i\omega d/v}\hat{A}_{R\omega}$ correspond to the outgoing and incoming modes at system B, respectively, as shown in Fig. 3.7(b). In other words, the photons acquire a phase shift of $\varphi = \omega d/v$ when travelling through the transmission line.

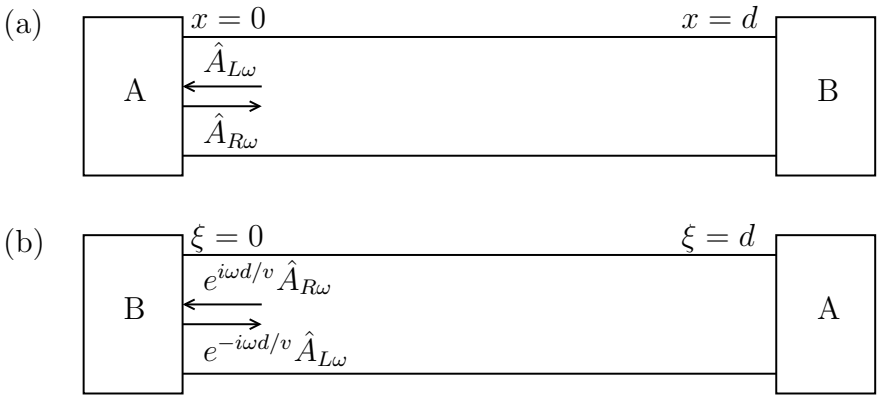

Figure 3.7: Finite transmission line of length d between systems A and B (a) in original coordinates and (b) in transformed coordinates.

3.3.2 Junction of multiple transmission lines

Consider the special case where n semi-infinite or finite transmission lines are connected at one end in a single point. The kth transmission line with impedance Z_k and velocity v_k is described by the operators

$$\begin{aligned}\hat{Q}_k(x,t) =& \sqrt{\frac{\hbar}{4\pi Z_k}}\int_0^\infty d\omega \frac{1}{\sqrt{\omega}}\times \\ & \left(\hat{A}_{k\mathrm{in}\omega}e^{-i\omega(t+x/v_k)} - \hat{A}_{k\mathrm{out}\omega}e^{-i\omega(t-x/v_k)} + \mathrm{h.c.}\right),\end{aligned} \tag{3.145}$$

where $x \in [0, L_k]$ for a finite transmission line of length L_k and $x \geq 0$ for a semi-infinite transmission line. The boundary conditions are the conservation of charge,

$$\sum_{k=1}^{n} \partial_t \hat{Q}_k(0,t) = 0, \tag{3.146}$$

and the equality of voltages,

$$\frac{1}{c_1}\partial_x \hat{Q}_1(0,t) = \frac{1}{c_2}\partial_x \hat{Q}_2(0,t) = \ldots = \frac{1}{c_n}\partial_x \hat{Q}_n(0,t). \tag{3.147}$$

Fourier transforming the boundary conditions, we obtain

$$\sum_{k=1}^{n} \frac{1}{\sqrt{Z_k}}(\hat{A}_{k\mathrm{in}\omega} - \hat{A}_{k\mathrm{out}\omega}) = 0, \tag{3.148}$$

$$\begin{aligned}\sqrt{Z_1}(\hat{A}_{1\mathrm{in}\omega} + \hat{A}_{1\mathrm{out}\omega}) &= \sqrt{Z_2}(\hat{A}_{2\mathrm{in}\omega} + \hat{A}_{2\mathrm{out}\omega}) \\ &= \ldots = \sqrt{Z_n}(\hat{A}_{n\mathrm{in}\omega} + \hat{A}_{n\mathrm{out}\omega}).\end{aligned} \tag{3.149}$$

The solution for the outgoing operators is

$$\hat{A}_{l\text{out}\omega} = -\hat{A}_{l\text{in}\omega} + \frac{2\sum_{k=1}^{n}\frac{1}{\sqrt{Z_l Z_k}}\hat{A}_{k\text{in}\omega}}{\sum_{k=1}^{n}\frac{1}{Z_k}}. \tag{3.150}$$

An interesting special case is $n = 2$ which is equal to one transmission line with a sudden impedance change at a single point. The solution is

$$\hat{A}_{1\text{out}\omega} = \frac{Z_2 - Z_1}{Z_2 + Z_1}\hat{A}_{1\text{in}\omega} + \frac{2\sqrt{Z_1 Z_2}}{Z_2 + Z_1}\hat{A}_{2\text{in}\omega}. \tag{3.151}$$

For classical voltages, [30]

$$V_{1\text{out}\omega} = \frac{Z_2 - Z_1}{Z_2 + Z_1}V_{1\text{in}\omega} + \frac{2Z_1}{Z_2 + Z_1}V_{2\text{in}\omega}, \tag{3.152}$$

where $V_{1\text{in(out)}\omega}$ is the amplitude of the incoming (outgoing) voltage wave in the transmission line 1, and $V_{2\text{out}\omega}$ is the amplitude of the outgoing voltage wave in the transmission line 2. Taking into account the factors $\sqrt{Z_{1,2}}$ in the expression of the voltage operators for the transmission lines, the Hermitian conjugate of Eq. (3.151) for the creation operators is equivalent to Eq. (3.152) for the classical voltage amplitudes, as in Sec. 3.2.2.

3.3.3 Inductor on a transmission line

Consider an inductor with inductance L breaking at some point an infinite transmission line with characteristic impedance Z_c. The system can be modelled as two separate semi-infinite transmission lines, described by the variables $\hat{Q}_a(x,t)$ and $\hat{Q}_b(x,t)$ for $x > 0$, connected by the inductor. Here, $\hat{I}_a(0,t)$ and $\hat{I}_b(0,t)$ are the currents from the inductor to the transmission lines a and b, respectively. The boundary conditions can be obtained from the Heisenberg equations of motion and are similar to the classical ones [28],

$$\hat{I}_a(0,t) + \hat{I}_b(0,t) = 0, \tag{3.153}$$

$$\hat{V}_a(0,t) - \hat{V}_b(0,t) = -L\partial_t \hat{I}_a(0,t). \tag{3.154}$$

Writing

$$\hat{Q}_a(x,t) = \sqrt{\frac{\hbar}{4\pi Z_c}}\int_0^\infty d\omega \frac{1}{\sqrt{\omega}}\left(\hat{a}_\omega^{\text{in}} e^{-i\omega(t+x/v)} - \hat{a}_\omega^{\text{out}} e^{-i\omega(t-x/v)} + \text{h.c.}\right), \tag{3.155}$$

$$\hat{Q}_b(x,t) = \sqrt{\frac{\hbar}{4\pi Z_c}}\int_0^\infty d\omega \frac{1}{\sqrt{\omega}}\left(\hat{b}_\omega^{\text{in}} e^{-i\omega(t+x/v)} - \hat{b}_\omega^{\text{out}} e^{-i\omega(t-x/v)} + \text{h.c.}\right), \tag{3.156}$$

where $\hat{a}_\omega^{\text{in,out}}$ and $\hat{b}_\omega^{\text{in,out}}$ are the annihilation operators for incident and outgoing photons of frecuency ω in transmission lines a and b, respectively, the boundary conditions become

$$\hat{a}_\omega^{\text{in}} - \hat{a}_\omega^{\text{out}} + \hat{b}_\omega^{\text{in}} - \hat{b}_\omega^{\text{out}} = 0, \tag{3.157}$$

$$Z_c \left[(\hat{a}_\omega^{\text{in}} + \hat{a}_\omega^{\text{out}}) - (\hat{b}_\omega^{\text{in}} + \hat{b}_\omega^{\text{out}}) \right] = -i\omega L (\hat{a}_\omega^{\text{in}} - \hat{a}_\omega^{\text{out}}). \tag{3.158}$$

These boundary conditions can be used also for an inductor breaking a finite transmission line in a more complex network.

Chapter 4

Quantum gates for microwave photons

In this section, we present devices for microwave photons that can be used as quantum gates in the dual-rail representation. The branch-line coupler used normally as a power divider for microwaves can be used as a beam splitter gate for single photons in the dual-rail representation. In addition, we present a novel idea for a tunable phase shifter for microwave photons, which can be used as a tunable phase shift gate. Further, we show how the tunable phase shifter can be used to create a tunable beam splitter. We conclude this chapter by discussing the idea of using nonlinear phase shifter in a conditional phase shift gate.

4.1 Branch-line coupler

4.1.1 Design

The branch-line coupler [30] shown in Fig. 4.1 has two inputs and two outputs, connected with four $\lambda/4$ transmission line sections. Because of its design, the branch-line coupler is a convenient choice for a beam splitter for microwave photons in the dual-rail representation. For example, the output ports in the 180° Hybrid ring [36] are not adjacent, which would introduce a technical challenge for the physical realization of quantum networks in a circuit. The branch-line coupler is normally used as a 50:50 power splitter with characteristic impedances $Z_1 = Z_4 = Z_0$ and $Z_2 = Z_3 = Z_0/\sqrt{2}$. For example, in Ref. [22], the branch-line coupler was used as a beam splitter for single microwave photons.

With proper selection of impedances, arbitrary power division ratio can be obtained. Here, we derive the scattering formulas for the beam splitter and the impedance choices using only the requirement that no photons from inputs c and d in Fig. 4.1 are reflected back into c or d.

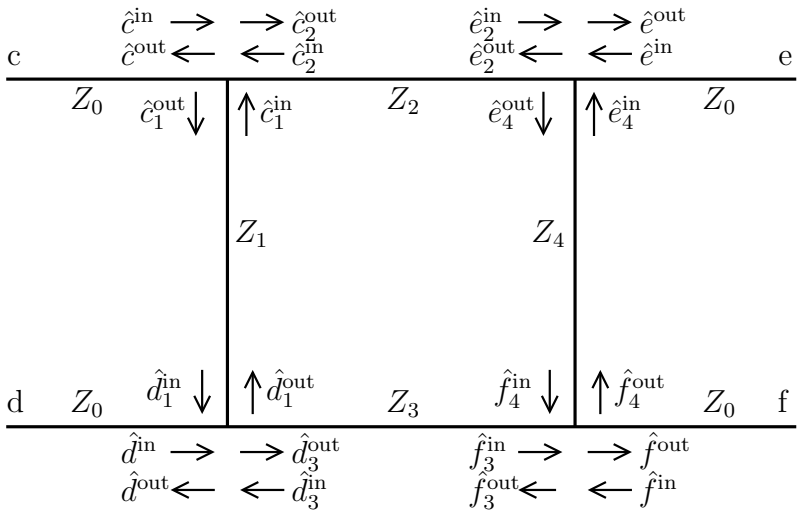

Figure 4.1: Branch-line coupler. The input lines c and d and the output lines e and f are connected with transmission lines 1, 2, 3 and 4 of length $\lambda/4 = \pi v_k/(2\omega)$ with characteristic impedances Z_1, Z_2, Z_3 and Z_4. The mode in the kth ($k = 1, 2, 3, 4$) $\lambda/4$ section in the end near input/output a ($a = c, d, e, f$) is denoted by a_k.

We are considering only photons with single frequency $\omega = \omega_0$ so we omit the indices ω for clarity. The input transmission lines are c and d with photon annihilation operators $\hat{c}^{\rm in,out}$ and $\hat{d}^{\rm in,out}$, and the output transmission lines are e and f with $\hat{e}^{\rm in,out}$ and $\hat{f}^{\rm in,out}$, where the indices in and out correspond to photons coming into and going out of the beam splitter, respectively. The characteristic impedance of each input and output transmission line is equal, Z_0.

The input lines c and d are connected with the transmission line 1 with impedance Z_1. The input c and output e are connected with the transmission line 2 with impedance Z_2, d and f are connected with the transmission line 3 with impedance Z_3, and the outputs e and f are connected with the transmission line 4 with impedance Z_4. We denote by $\hat{a}_k^{\rm in}(\hat{a}_k^{\rm out})$ the annihilation operator of a photon in the incoming (outgoing) mode of transmission line $k = 1, 2, 3, 4$ that is connected to input/output $a = c, d, e, f$. Here, the indices in and out correspond to the photons coming into and going out of the junction of transmission lines.

For each of the 4 junctions, we have Eq. (3.148) and Eq. (3.149), resulting in

$$\begin{aligned}
\frac{1}{\sqrt{Z_0}}(\hat{c}^{\rm in} - \hat{c}^{\rm out}) + \frac{1}{\sqrt{Z_1}}(\hat{c}_1^{\rm in} - \hat{c}_1^{\rm out}) + \frac{1}{\sqrt{Z_2}}(\hat{c}_2^{\rm in} - \hat{c}_2^{\rm out}) &= 0, \\
\sqrt{Z_0}(\hat{c}^{\rm out} + \hat{c}^{\rm in}) = \sqrt{Z_1}(\hat{c}_1^{\rm out} + \hat{c}_1^{\rm in}) &= \sqrt{Z_2}(\hat{c}_2^{\rm out} + \hat{c}_2^{\rm in}), \\
\frac{1}{\sqrt{Z_0}}(\hat{d}^{\rm in} - \hat{d}^{\rm out}) + \frac{1}{\sqrt{Z_1}}(\hat{d}_1^{\rm in} - \hat{d}_1^{\rm out}) + \frac{1}{\sqrt{Z_3}}(\hat{d}_3^{\rm in} - \hat{d}_3^{\rm out}) &= 0, \\
\sqrt{Z_0}(\hat{d}^{\rm out} + \hat{d}^{\rm in}) = \sqrt{Z_1}(\hat{d}_1^{\rm out} + \hat{d}_1^{\rm in}) &= \sqrt{Z_3}(\hat{d}_3^{\rm out} + \hat{d}_3^{\rm in}), \\
\frac{1}{\sqrt{Z_0}}(\hat{e}^{\rm in} - \hat{e}^{\rm out}) + \frac{1}{\sqrt{Z_2}}(\hat{e}_2^{\rm in} - \hat{e}_2^{\rm out}) + \frac{1}{\sqrt{Z_4}}(\hat{e}_4^{\rm in} - \hat{e}_4^{\rm out}) &= 0,
\end{aligned}$$

$$\sqrt{Z_0}(\hat{e}^{\text{out}} + \hat{e}^{\text{in}}) = \sqrt{Z_2}(\hat{e}_2^{\text{out}} + \hat{e}_2^{\text{in}}) = \sqrt{Z_4}(\hat{e}_4^{\text{out}} + \hat{e}_4^{\text{in}}),$$
$$\frac{1}{\sqrt{Z_0}}(\hat{f}^{\text{in}} - \hat{f}^{\text{out}}) + \frac{1}{\sqrt{Z_3}}(\hat{f}_3^{\text{in}} - \hat{f}_3^{\text{out}}) + \frac{1}{\sqrt{Z_4}}(\hat{f}_4^{\text{in}} - \hat{f}_4^{\text{out}}) = 0,$$
$$\sqrt{Z_0}(\hat{f}^{\text{out}} + \hat{f}^{\text{in}}) = \sqrt{Z_3}(\hat{f}_3^{\text{out}} + \hat{f}_3^{\text{in}}) = \sqrt{Z_4}(\hat{f}_4^{\text{out}} + \hat{f}_4^{\text{in}}).$$

Due to the finite lengths of the transmission lines, photons of given frequency accumulate a phase φ_k when traveling through transmission line $k = 1, 2, 3, 4$, yielding

$$\hat{c}_1^{\text{in}} = e^{i\varphi_1}\hat{d}_1^{\text{out}}, \qquad \hat{d}_1^{\text{in}} = e^{i\varphi_1}\hat{c}_1^{\text{out}},$$
$$\hat{c}_2^{\text{in}} = e^{i\varphi_2}\hat{e}_2^{\text{out}}, \qquad \hat{e}_2^{\text{in}} = e^{i\varphi_2}\hat{c}_2^{\text{out}},$$
$$\hat{d}_3^{\text{in}} = e^{i\varphi_3}\hat{f}_3^{\text{out}}, \qquad \hat{f}_3^{\text{in}} = e^{i\varphi_3}\hat{d}_3^{\text{out}},$$
$$\hat{e}_4^{\text{in}} = e^{i\varphi_4}\hat{f}_4^{\text{out}}, \qquad \hat{f}_4^{\text{in}} = e^{i\varphi_4}\hat{e}_4^{\text{out}},$$

as shown in Sec. 3.3.1. We select the lengths of the sections of the beam splitter to be $\lambda/4$, yielding phase shifts $\varphi_1 = \varphi_2 = \varphi_3 = \varphi_4 = \pi/2$.

We can solve analytically the output operators $\hat{c}^{\text{out}}$, $\hat{d}^{\text{out}}$, $\hat{e}^{\text{out}}$, and $\hat{f}^{\text{out}}$ as linear combinations of the input operators $\hat{c}^{\text{in}}$, $\hat{d}^{\text{in}}$, $\hat{e}^{\text{in}}$, and $\hat{f}^{\text{in}}$. However, the equations are too long to be expressed here.

For the beam splitter to be unitary, nothing from the input lines c and d may be reflected back into the input lines c and d. This yields the requirement

$$\frac{\partial(\hat{c}^{\text{out}}, \hat{d}^{\text{out}})}{\partial(\hat{c}^{\text{in}}, \hat{d}^{\text{in}})} = 0, \tag{4.1}$$

which implies that

$$Z_2 = Z_3 = \frac{Z_0 Z_1}{\sqrt{Z_0^2 + Z_1^2}}, \tag{4.2}$$
$$Z_4 = Z_1. \tag{4.3}$$

This form suggests that we write the impedances in terms of $\theta \in (0, \pi/2)$ such that $Z_4 = Z_1 = Z_0 \cot\theta$ and $Z_2 = Z_3 = Z_0 \cos\theta$. This yields

$$\hat{e}^{\text{out}} = i\cos\theta\hat{c}^{\text{in}} - \sin\theta\hat{d}^{\text{in}}, \tag{4.4}$$
$$\hat{f}^{\text{out}} = -\sin\theta\hat{c}^{\text{in}} + i\cos\theta\hat{d}^{\text{in}}. \tag{4.5}$$

Note that the outgoing operators $\hat{e}^{\text{out}}$ and $\hat{f}^{\text{out}}$ do not depend on $\hat{e}^{\text{in}}$ and $\hat{f}^{\text{in}}$, i.e., the photons incoming from the output modes e and f are not reflected back. This was not explicitely assumed but is a trivial consequence of symmetry and the requirement that the incident input waves are not reflected back into the input lines.

The branch-line coupler works without reflection only for photons of single frequency ω_0 for which it is designed. For wave packets, for which the spread in the frequency

$\Delta\omega$ is low compared to the center frequency ω_0, i.e., the extent of the wave packet in time is $\tau_0 \gg 2\pi/\omega_0$, the effect is not significant. However, for shorter wave packets, the finite length may significantly affect the operation of the beam splitter. Nevertheless, the time scale for an experimentally realistic frequency $\omega_0 = 2\pi \times 10$ GHz is 100 ps which is very short compared with the typical wave packets realized experimentally. Solving the scattering equations for the chosen impedances and phase shifts $\phi_1 = \phi_2 = \phi_3 = \phi_4 = \frac{\omega}{\omega_0}\frac{\lambda}{4}$ for $\omega \neq \omega_0$, one can obtain the scattering matrix for all frequencies, and use this to treat realistic wave packets. However, the precies treatment is beyond the scope of this thesis.

4.1.2 Single-qubit beam splitter gate

In the dual-rail representation, the branch-line coupler can be used as a single qubit gate as explained in Sec. 2.2.2. It performs the gate

$$B = \begin{pmatrix} i\cos\theta & -\sin\theta \\ -\sin\theta & i\cos\theta \end{pmatrix}, \tag{4.6}$$

where $\theta \in (0, \pi/2)$. Choosing $\theta = \pi/4$ for the 50 : 50 beam splitter, the transform is

$$B = \frac{1}{\sqrt{2}} \begin{pmatrix} i & -1 \\ -1 & i \end{pmatrix}. \tag{4.7}$$

Adding phase shifters, the Hadamard gate can be written as

$$\begin{aligned} H &= \frac{1}{\sqrt{2}} \begin{pmatrix} 1 & 1 \\ 1 & -1 \end{pmatrix} \\ &= -i \begin{pmatrix} 1 & 0 \\ 0 & -i \end{pmatrix} \frac{1}{\sqrt{2}} \begin{pmatrix} i & -1 \\ -1 & i \end{pmatrix} \begin{pmatrix} 1 & 0 \\ 0 & -i \end{pmatrix} \\ &= -iR(-\frac{\pi}{2})BR(-\frac{\pi}{2}). \end{aligned} \tag{4.8}$$

The Hadamard gate can thus be constructed with the beam splitter and $-\pi/2$ phase shifters.

Contrary to the Hadamard gate, applying the 50 : 50 beam splitter twice yields the NOT gate,

$$B^2 = \frac{1}{2} \begin{pmatrix} i & -1 \\ -1 & i \end{pmatrix} \begin{pmatrix} i & -1 \\ -1 & i \end{pmatrix} = \begin{pmatrix} 0 & -i \\ -i & 0 \end{pmatrix}, \tag{4.9}$$

where the additional global phase shift $-\pi/2$ can be ignored.

4.1.3 Hong–Ou–Mandel effect

It can be shown that two photons entering the 50 : 50 beam splitter in different modes exit the beam splitter in the same mode. Using the same notation as in

Sec. 2.2.2, the state of the system is $|11\rangle_{\text{in}}$. It can be rewritten as

$$|11\rangle_{\text{in}} = \hat{c}^\dagger \hat{d}^\dagger |0\rangle = \frac{1}{2}(i\hat{e}^\dagger - \hat{f}^\dagger)(-\hat{e}^\dagger + i\hat{f}^\dagger)|0\rangle$$
$$= \frac{-i}{2}\left[(\hat{e}^\dagger)^2 + (\hat{f}^\dagger)^2\right]|0\rangle = \frac{-i}{\sqrt{2}}(|20\rangle_{\text{out}} + |02\rangle_{\text{out}}). \tag{4.10}$$

The absence of the $|11\rangle_{\text{out}}$ term is called the Hong–Ou–Mandel effect [37]. This effect can be used for probabilistic linear optical quantum computing [10] and it may prove useful for nonlinear optical quantum computing.

4.2 Tunable phase shifter

4.2.1 Design

The phase shifter for fixed frequency $\omega > 0$ shown in Fig. 4.2 consists of three SQUIDs $\lambda/4$ apart from each other in a transmission line with impedance Z_0. The tunable inductance of the middle SQUID is L_2 and the tunable inductances of the other ones is equal to L_1. We denote the left transmission line modes at the first SQUID by $\hat{a}^{\text{in}}$ and $\hat{a}^{\text{out}}$, and the right transmission line modes at the last SQUID by $\hat{d}^{\text{in}}$ and $\hat{d}^{\text{out}}$. The modes at left and right end of the $\lambda/4$ sections are denoted by $\hat{b}_{l,r}^{\text{in,out}}$ and $\hat{c}_{l,r}^{\text{in,out}}$.

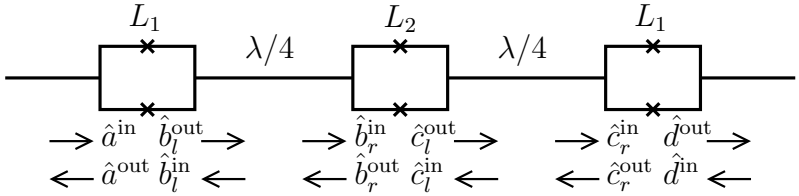

Figure 4.2: Tunable phase shifter consists of three SQUIDs with tunable inductances L_1, L_2, and L_1 separated with $\lambda/4$ transmission line sections.

In the $\lambda/4$ sections, the waves accumulate a phase shift of $\pi/2$, i.e.

$$\hat{b}_r^{\text{in}} = i\hat{b}_l^{\text{out}}, \tag{4.11}$$
$$\hat{b}_l^{\text{in}} = i\hat{b}_r^{\text{out}}, \tag{4.12}$$
$$\hat{c}_r^{\text{in}} = i\hat{c}_l^{\text{out}}, \tag{4.13}$$
$$\hat{c}_l^{\text{in}} = i\hat{c}_r^{\text{out}}. \tag{4.14}$$

For the SQUIDs, Eqs. (3.157) and (3.158) yield

$$\hat{a}^{\rm in} - \hat{a}^{\rm out} + \hat{b}_l^{\rm in} - \hat{b}_l^{\rm out} = 0, \tag{4.15}$$

$$Z_0\left[(\hat{a}^{\rm in} + \hat{a}^{\rm out}) - (\hat{b}_l^{\rm in} + \hat{b}_l^{\rm out})\right] = -i\omega L_1(\hat{a}^{\rm in} - \hat{a}^{\rm out}), \tag{4.16}$$

$$\hat{b}_r^{\rm in} - \hat{b}_r^{\rm out} + \hat{c}_l^{\rm in} - \hat{c}_l^{\rm out} = 0, \tag{4.17}$$

$$Z_0\left[(\hat{b}_r^{\rm in} + \hat{b}_r^{\rm out}) - (\hat{c}_l^{\rm in} + \hat{c}_l^{\rm out})\right] = -i\omega L_2(\hat{b}_r^{\rm in} - \hat{b}_r^{\rm out}), \tag{4.18}$$

$$\hat{c}_r^{\rm in} - \hat{c}_r^{\rm out} + \hat{d}^{\rm in} - \hat{d}^{\rm out} = 0, \tag{4.19}$$

$$Z_0\left[(\hat{c}_r^{\rm in} + \hat{c}_r^{\rm out}) - (\hat{d}^{\rm in} + \hat{d}^{\rm out})\right] = -i\omega L_1(\hat{c}_r^{\rm in} - \hat{c}_r^{\rm out}). \tag{4.20}$$

Solving Eqs. (4.11)–(4.20) yields

$$\hat{d}^{\rm out} = \frac{2i\hat{a}^{\rm in}Z_0^3 + \hat{d}^{\rm in}\omega(L_1^2L_2\omega^2 - 2L_1Z_0^2 + L_2Z_0^2)}{(L_1\omega + iZ_0)(L_1L_2\omega^2 + (iL_2\omega - 2Z_0)Z_0)}. \tag{4.21}$$

Requiring that no reflection occurs, $\partial\hat{d}^{\rm out}/\partial\hat{d}^{\rm in} = 0$ yields

$$L_1^2L_2\omega^2 - 2L_1Z_0^2 + L_2Z_0^2 = 0 \tag{4.22}$$

$$\Rightarrow\ \omega L_2 = \frac{2\omega L_1 Z_0^2}{(\omega L_1)^2 + Z_0^2}. \tag{4.23}$$

Choosing $\omega L_1 = Z_0 \tan\theta/2$ with some $\theta \in (0, \pi)$ yields

$$\omega L_2 = \frac{2Z_0 \tan\frac{\theta}{2}}{\tan^2\frac{\theta}{2} + 1} = Z_0 \sin\theta, \tag{4.24}$$

which implies that the condition in Eq. (4.23) is satisfied. With these choices,

$$\hat{d}^{\rm out} = \frac{2i\hat{a}^{\rm in}Z_0^3}{(L_1\omega + iZ_0)(L_1L_2\omega^2 + (iL_2\omega - 2Z_0)Z_0)} = -e^{i\theta}\hat{a}^{\rm in} = e^{i(\theta+\pi)}\hat{a}^{\rm in}, \tag{4.25}$$

so a phase shift of $\theta + \pi \in (\pi, 2\pi)$ with no reflection occurs. The total length of the phase shifter is $\lambda/2$ corresponding to a phase shift of π without the SQUIDs. Thus the extra phase shift introduced by the SQUIDs is θ, which can be tuned with controlling the inductances L_1 and L_2. It should be noted that one or two SQUIDs on a transmission line are not enough to yield a tunable phase shifter with no reflection.

4.2.2 Single-qubit phase shift gate

The tunable phase shifter yields a phase shift of $\theta \in (\pi, 2\pi)$. Inserting a transmission line section of length $\lambda/2$ in the $|0_Q\rangle$ wire and the tunable phase shifter in the $|1_Q\rangle$ wire yields the phase shift gate $R(\theta)$ with an additional irrelevant $e^{i\pi}$ global phase.

Negative values of phase shift can be obtained by inserting the phase shifter into the $|0_Q\rangle$ wire instead of the $|1_Q\rangle$ wire.

Physical limitations for the SQUIDs may yield a minimum and a maximum value for the angle θ on the phase shifter. For the phase shift gate, this can be overcome by inserting multiple phase shifters in both wires. If $\theta \in [\alpha, \beta]$ is the tunable angle for a single phase shifter, n phase shifters in both wires can be tuned to yield the phase shift gate $R(\phi)$ where $\phi \in [n(\alpha - \beta), n(\beta - \alpha)]$. Therefore, for an arbitrary tunable phase shift gate, at least $\lceil \pi/(\beta - \alpha) \rceil$ phase shifters in both wires are required.

4.2.3 Experimental parameters

We assume that the critical currents of the Josephson junctions in all of the SQUIDs are equal and denote it by I_{c0}. With zero bias current, combining Eqs. (2.41) and (2.48), we obtain the inductance of a SQUID as a function of the magnetic flux Φ threading it,

$$L_J(\Phi) = \frac{\Phi_0/2\pi}{2I_{c0}\left|\cos\left(\pi\frac{\Phi}{\Phi_0}\right)\right|}. \tag{4.26}$$

Let I_{c1} be the critical current of the left and right SQUIDs determined by the magnetic fluxes threading the SQUIDs and I_{c2} be the corresponding critical current of the middle SQUID. The equations for a phase shift of θ for photons with frequency ω yield

$$I_{c1} = \frac{\omega\Phi_0}{2\pi Z_0 \tan(\theta/2)}, \tag{4.27}$$

$$I_{c2} = \frac{\omega\Phi_0}{2\pi Z_0 \sin\theta}. \tag{4.28}$$

Assuming realistic values $Z_0 = 50\,\Omega$ and $\omega = 2\pi \times 6.566\,\text{GHz}$ [22], the values needed for the critical currents of the SQUIDs for different phase shifts θ are shown in Fig. 4.3. The values for the critical currents are of the order of 300 nA for phase shifts near $\pi/2$, which is still plausible for SQUIDs. For example, in Ref. [15], SQUIDs with critical current of the same magnitude were used inside microwave cavities. However, phase shifts close to 0 or π require extremely high critical currents so they are not easily achieveable with a single phase shifter.

In a real SQUID, the critical current can be tuned between a maximum value $I_c^{\max}$ and a minimum value $I_c^{\min}$, where the minimum value is caused, for example, by asymmetry in the critical currents of the Josephson junctions of the SQUIDs. However, even with these restrictions, tunable phase shifts of wide range can be achieved with standard components.

If a bias current I_b is applied in a SQUID, the critical current I_c is replaced by $\sqrt{I_c^2 - I_b^2}$ in the expression of the SQUID inductance in Eq. (2.47). In Fig. 4.3, this corresponds to changing the vertical axis variable to $\sqrt{I_c^2 - I_b^2}$.

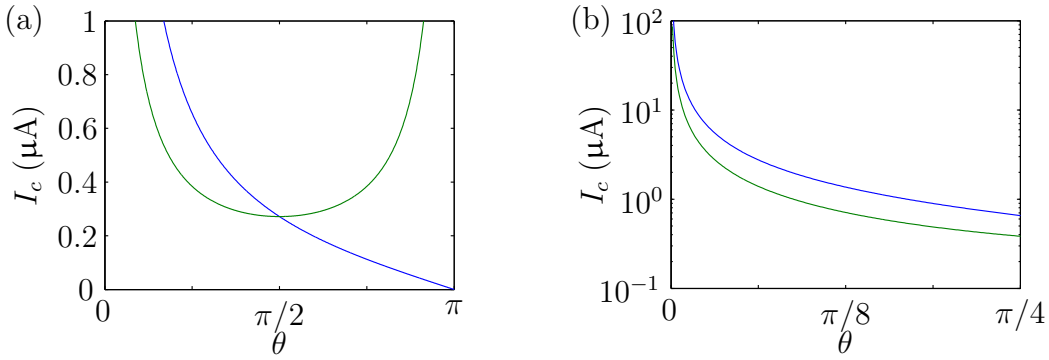

Figure 4.3: Required critical currents for the left and right SQUIDs (blue) and for the middle SQUID (green) as a function of the obtained phase shift θ (a) for $\theta \in (0, \pi)$ and (b) logarithmic plot for $\theta \in (0, \pi/4)$. The system parameters are $Z_0 = 50\,\Omega$ and $\omega = 2\pi \times 6.566$ GHz.

The Josephson energy of a SQUID with critical current 300 nA is $E_J \approx 600$ μeV. This is significantly higher than the energy of the photon $\hbar\omega_0 \approx 30$ μeV. Thus we are in the low-power regime of the SQUID and the approximation of the SQUID as a linear inductor is valid.

As the branch-line coupler, the tunable phase shifter is only designed to work with a single frequency ω_0. The treatment of wave packets involving significant contribution of frequencies far from ω_0 is beyond the scope of this thesis.

4.2.4 Nonlinear phase shifter

The nonlinear inductance of the SQUID results in nonlinear behaviour in the phase shifter discussed here. However, the effect of the nonlinearity on single photons is nontrivial and thus it is beyond the scope of this thesis. If the incoming photons do not scatter into photons with different frequencies, the nonlinear behaviour could in principle be utilized to create a nonlinear phase shifter combining multiple SQUIDs in such way that no reflection occurs for one and two incoming photons. The nonlinear phase shifter can then be characterized by the phase shifts it applies to incoming states with one and two photons, φ_1 and φ_2, respectively. In Sec. 4.4, we show how a conditional phase shift gate can be realized with the components discussed here assuming an ideal nonlinear phase shifter.

4.3 Tunable beam splitter

As explained in Sec. 2.1.4, any single-qubit gate can be constructed using phase shifters and two Hadamard gates. Similarly, we may create a tunable beam splitter using 50 : 50 beam splitters and tunable phase shifters. Connecting two 50 : 50 beam splitters by inserting a tunable phase shifter in one line and a constant phase

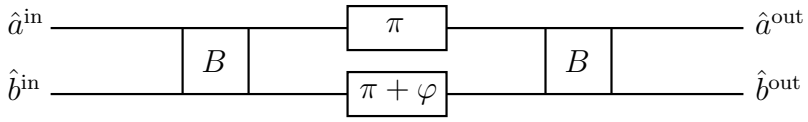

Figure 4.4: Tunable beam splitter consisting of two 50 : 50 beam splitters (B) and a constant phase shifter of π and a tunable phase shifter of $\pi + \varphi$.

shifter of π on the other line as in Fig. 4.4 yields the transformation

$$\begin{aligned} Be^{i\pi}R(\phi)B &= \frac{1}{2}e^{i\pi}\begin{pmatrix} i & -1 \\ -1 & i \end{pmatrix}\begin{pmatrix} 1 & 0 \\ 0 & e^{i\phi} \end{pmatrix}\begin{pmatrix} i & -1 \\ -1 & i \end{pmatrix} \\ &= e^{i(\phi/2+\pi/2)}\begin{pmatrix} -\sin\frac{\phi}{2} & \cos\frac{\phi}{2} \\ \cos\frac{\phi}{2} & \sin\frac{\phi}{2} \end{pmatrix}, \end{aligned} \tag{4.29}$$

where the global phase can be ignored. The tunable beam splitter also provides another convenient way to experimentally demonstrate the tunable phase shifter.

4.4 Conditional phase shift gate

The Hong–Ou–Mandel effect along with a nonlinear phase shifter can be used to create an entangling two-qubit gate in the dual-rail representation. Consider the system shown in Fig. 4.5, where the $|1_Q\rangle$ modes of two qubits are connected with two beam splitters and nonlinear phase shifters with angles φ_1 and φ_2 for one and two photons, respectively, in between. Here, the 2-qubit input states are defined as

$$\begin{aligned} |00_Q\rangle &= \hat{a}^\dagger_{\text{in}}\hat{d}^\dagger_{\text{in}}|0\rangle, & |01_Q\rangle &= \hat{a}^\dagger_{\text{in}}\hat{c}^\dagger_{\text{in}}|0\rangle, \\ |10_Q\rangle &= \hat{b}^\dagger_{\text{in}}\hat{d}^\dagger_{\text{in}}|0\rangle, & |11_Q\rangle &= \hat{b}^\dagger_{\text{in}}\hat{c}^\dagger_{\text{in}}|0\rangle, \end{aligned} \tag{4.30}$$

where $|0\rangle$ is the ground state of the system.

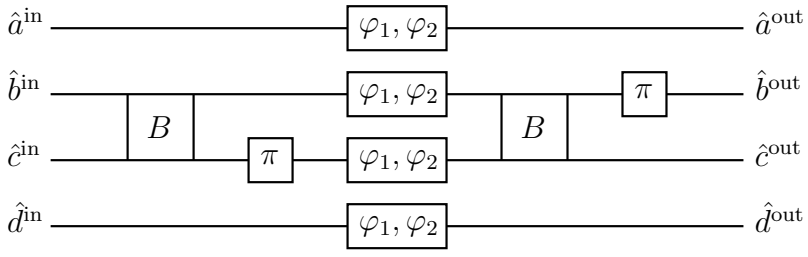

Figure 4.5: Conditional phase shift gate consisting of 50:50 beam splitters (B), linear phase shifters of angle π, and nonlinear phase shifters (angle φ_1 for one photon and φ_2 for two photons). The first qubit is represented by the lines a and b and the second qubit is represented by the lines c and d.

For input states $|00_Q\rangle$, $|01_Q\rangle$ and $|10_Q\rangle$, each line contains at most one photon, and the nonlinear effect is not observed. In the linear case, the system can be described

by the scattering equations

$$\hat{a}_{\text{out}} = e^{i\varphi_1}\hat{a}_{\text{in}}, \tag{4.31}$$

$$\hat{d}_{\text{out}} = e^{i\varphi_1}\hat{d}_{\text{in}}, \tag{4.32}$$

$$\begin{aligned}\begin{pmatrix}\hat{b}_{\text{out}}\\ \hat{c}_{\text{out}}\end{pmatrix} &= \begin{pmatrix}-1 & 0\\ 0 & 1\end{pmatrix}\frac{1}{\sqrt{2}}\begin{pmatrix}i & -1\\ -1 & i\end{pmatrix}\begin{pmatrix}e^{i\varphi_1} & 0\\ 0 & e^{i\varphi_1}\end{pmatrix}\begin{pmatrix}1 & 0\\ 0 & -1\end{pmatrix}\frac{1}{\sqrt{2}}\begin{pmatrix}i & -1\\ -1 & i\end{pmatrix}\begin{pmatrix}\hat{b}_{\text{in}}\\ \hat{c}_{\text{in}}\end{pmatrix}\\ &= \begin{pmatrix}e^{i\varphi_1}\hat{b}_{\text{in}}\\ e^{i\varphi_1}\hat{c}_{\text{in}}\end{pmatrix}.\end{aligned} \tag{4.33}$$

Thus the state of the 2-qubit system changes only by a global phase $e^{i2\varphi_1}$. However, the nonlinear effect for the input state $|11_Q\rangle$ cannot be taken into account by the scattering equations for the operators. Here, the evolution of the system is described by the b and c modes. Denoting by $|mn\rangle$ the Fock state with m photons in the b mode and n photons in the c mode, the step-by-step transformation according to Fig. 4.5 is

$$|11\rangle \to \frac{i}{\sqrt{2}}(|20\rangle + |02\rangle) \tag{4.34}$$

$$\to \frac{i}{\sqrt{2}}(|20\rangle + e^{i2\pi}|02\rangle) \tag{4.35}$$

$$\to \frac{i}{\sqrt{2}}(e^{i\varphi_2}|20\rangle + e^{i\varphi_2}|02\rangle) \tag{4.36}$$

$$\to -e^{i\varphi_2}|11\rangle \tag{4.37}$$

$$\to e^{i\varphi_2}|11\rangle, \tag{4.38}$$

where the first and fourth lines are the transformations by the beam splitters, the second and fifth lines are the transformations by the phase shifters of angle π and the third line is the transformation by the nonlinear phase shifter. This corresponds to the mapping $|11_Q\rangle \to e^{i\varphi_2}|11_Q\rangle$ for the qubit states. Therefore, the total 2-qubit gate is described by the matrix

$$CZ(\varphi_2 - 2\varphi_1) = \begin{pmatrix}1 & & & \\ & 1 & & \\ & & 1 & \\ & & & e^{i(\varphi_2-2\varphi_1)}\end{pmatrix}, \tag{4.39}$$

where we neglected the total global phase $2\varphi_1$. If the nonlinearity is small, i.e., $|\varphi_2 - 2\varphi_1|$ is small, compining multiple similar gates will in principle result in larger conditional phase shift. However, this can also cumulate the effect of error sources, and thus the nonlinear phase shift of the phase shifter should be rather high compared to the reflection and other nonidealities in the nonlinear phase shifter.

Chapter 5

Discussion

In this thesis, we presented studies on superconducting microwave transmission lines in the single-photon regime. The results can be used in the research of microwave photons, which may prove useful both in realizing a quantum computer and in the general study of quantum mechanics using circuit quantum electrodynamics.

The reflection in a transmission line terminated by impedance was studied. This includes the effect of a purely reactive LC element on the shape of the single photon wave packet. In addition, the LCR oscillator approach can be used for example for treating dissipation in the single photon regime in circuits with resistive elements. The effect of reflection on wave packets was treated only briefly, and thus further research is required. Nevertheless, only very general assumptions were used in these observations, and thus the approach can be directly utilized in many systems using superconducting transmission lines.

In addition, we presented quantum gates for qubits consisting of microwave photons in the dual-rail representation. Starting from the model of a transmission line, we reviewed the result that the branch-line coupler, used typically as a power divider for classical microwaves, can be directly used as a beam splitter gate for microwave photons.

We introduced a novel idea for a tunable phase shifter consisting of SQUIDs that are treated as tunable inductors. The tunable phase shifter can be used as a quantum phase shift gate and in many applications in the study of microwave photons. Previously, a tunable phase shifter based on the nonlinear kinetic inductance of the superconducting centre conductor of the transmission line has been demonstrated [38,39]. Compared to that, our suggestion uses only a small number of SQUIDs. The discrete number of free parameters in the phase shifter presented here may be useful in fine-tuning the physical realization which is necessarily nonideal. Further, the approach can in principle be extended using more than three SQUIDs in the same formation, possibly yielding a more controllable phase shifter. The drawback is that our phase shifter can only be used with a single frequency. A possible improvement

is using the kinetic inductance to adjust the phase velocity of the transmission line in the phase shifter to match the chosen frequency.

The parameters required for the phase shifter to yield measurable phase shifts in the single-photon regime are attainable using existing technology for superconducting circuits. Further, the phase shifter can be experimentally studied combining it with the beam splitter, yielding the tunable beam splitter. Beam splitters are an essential part in various single-photon microwave experiments, and thus the effect of the tunable phase shifter should be easy to demonstrate and utilize experimentally.

The idea of an entangling two-qubit gate using nonlinear phase shifter was briefly discussed. However, the nonlinear behaviour of the tunable phase shifter was not studied in detail, and further research is required.

References

[1] R. Feynman. Simulating physics with computers. *Int. J. Theor. Phys.* **21**:467, 1982.

[2] D. Deutsch. Quantum Theory, the Church–Turing Principle and the Universal Quantum Computer. *Proc. R. Soc. London, Ser. A* **400**:97, 1985.

[3] P. Shor. Algorithms for quantum computation: discrete logarithms and factoring. *Proceedings 35th Annual Symposium on Foundations of Computer Science*, p. 124. IEEE Press, Los Alamitos, 1994.

[4] M. A. Nielsen and I. L. Chuang. *Quantum Computation and Quantum Information*. Cambridge University Press, Cambridge, 2000.

[5] H. Walther, B. T. H. Varcoe, B.-G. Englert, and T. Becker. Cavity quantum electrodynamics. *Rep. Prog. Phys.* **69**:1325, 2006.

[6] E. Knill, R. Laflamme, and G. J. Milburn. A scheme for efficient quantum computation with linear optics. *Nature* **409**:46, 2001.

[7] A. Blais, R.-S. Huang, A. Wallraff, S. Girvin, and R. Schoelkopf. Cavity quantum electrodynamics for superconducting electrical circuits: An architecture for quantum computation. *Phys. Rev. A* **69**:062320, 2004.

[8] D. I. Schuster. Circuit Quantum Electrodynamics. Ph.D. thesis. Yale University, 2007.

[9] K. S. Thorne, R. W. P. Drever, C. M. Caves, M. Zimmermann, and V. D. Sandberg. Quantum Nondemolition Measurements of Harmonic Oscillators. *Phys. Rev. Lett.* **40**:667, 1978.

[10] P. Kok, K. Nemoto, T. C. Ralph, J. P. Dowling, and G. J. Milburn. Linear optical quantum computing with photonic qubits. *Rev. Mod. Phys.* **79**:135, 2007.

[11] M. Tinkham. *Introduction to Superconductivity*. 2nd edition. Dover Publications, New York, 2004.

[12] J. Johansson, G. Johansson, C. Wilson, and F. Nori. Dynamical Casimir Effect in a Superconducting Coplanar Waveguide. *Phys. Rev. Lett.* **103**:147003, 2009.

[13] V. Manucharyan, E. Boaknin, M. Metcalfe, R. Vijay, I. Siddiqi, and M. Devoret. Microwave bifurcation of a Josephson junction: Embedding-circuit requirements. *Phys. Rev. B* **76**:014524, 2007.

[14] S. Kumar and D. DiVincenzo. Exploiting Kerr cross nonlinearity in circuit quantum electrodynamics for nondemolition measurements. *Phys. Rev. B* **82**:014512, 2010.

[15] A. Palacios-Laloy, F. Nguyen, F. Mallet, P. Bertet, D. Vion, and D. Esteve. Tunable Resonators for Quantum Circuits. *J. Low Temp. Phys.* **151**:1034, 2008.

[16] P. Jones, J. Huhtamäki, M. Partanen, K. Tan, and M. Möttönen. Tunable single-photon heat conduction in electrical circuits. *Phys. Rev. B* **86**:035313, 2012.

[17] A. Blais, J. Gambetta, A. Wallraff, D. Schuster, S. Girvin, M. Devoret, and R. Schoelkopf. Quantum-information processing with circuit quantum electrodynamics. *Phys. Rev. A* **75**:032329, 2007.

[18] F. Helmer, M. Mariantoni, A. G. Fowler, J. von Delft, E. Solano, and F. Marquardt. Cavity grid for scalable quantum computation with superconducting circuits. *Europhys. Lett.* **85**:50007, 2009.

[19] A. A. Houck, D. I. Schuster, J. M. Gambetta, J. A. Schreier, B. R. Johnson, J. M. Chow, L. Frunzio, J. Majer, M. H. Devoret, S. M. Girvin, and R. J. Schoelkopf. Generating single microwave photons in a circuit. *Nature* **449**:328, 2007.

[20] M. Hofheinz, E. M. Weig, M. Ansmann, R. C. Bialczak, E. Lucero, M. Neeley, A. D. O'Connell, H. Wang, J. M. Martinis, and A. N. Cleland. Generation of Fock states in a superconducting quantum circuit. *Nature* **454**:310, 2008.

[21] J. Koch, T. Yu, J. Gambetta, A. Houck, D. Schuster, J. Majer, A. Blais, M. Devoret, S. Girvin, and R. Schoelkopf. Charge-insensitive qubit design derived from the Cooper pair box. *Phys. Rev. A* **76**:042319, 2007.

[22] D. Bozyigit, C. Lang, L. Steffen, J. M. Fink, C. Eichler, M. Baur, R. Bianchetti, P. J. Leek, S. Filipp, M. P. da Silva, A. Blais, and A. Wallraff. Antibunching of microwave-frequency photons observed in correlation measurements using linear detectors. *Nature Phys.* **7**:154, 2011.

[23] C. Eichler, D. Bozyigit, C. Lang, L. Steffen, J. Fink, and A. Wallraff. Experimental State Tomography of Itinerant Single Microwave Photons. *Phys. Rev. Lett.* **106**:220503, 2011.

[24] I.-C. Hoi, C. Wilson, G. Johansson, T. Palomaki, B. Peropadre, and P. Delsing. Demonstration of a Single-Photon Router in the Microwave Regime. *Phys. Rev. Lett.* **107**:073601, 2011.

[25] F. Helmer, M. Mariantoni, E. Solano, and F. Marquardt. Quantum nondemolition photon detection in circuit QED and the quantum Zeno effect. *Phys. Rev. A* **79**:052115, 2009.

[26] J.-T. Shen and S. Fan. Coherent Single Photon Transport in a One-Dimensional Waveguide Coupled with Superconducting Quantum Bits. *Phys. Rev. Lett.* **95**:213001, 2005.

[27] G. Romero, J. García-Ripoll, and E. Solano. Microwave Photon Detector in Circuit QED. *Phys. Rev. Lett.* **102**:173602, 2009.

[28] B. Yurke and J. Denker. Quantum network theory. *Phys. Rev. A* **29**:1419, 1984.

[29] G. Romero, J. J. García-Ripoll, and E. Solano. Photodetection of propagating quantum microwaves in circuit QED. *Phys. Scr.* **T137**:014004, 2009.

[30] D. M. Pozar. *Microwave Engineering*. 2nd edition. Wiley, New York, 1998.

[31] B. Peropadre, G. Romero, G. Johansson, C. Wilson, E. Solano, and J. García-Ripoll. Approaching perfect microwave photodetection in circuit QED. *Phys. Rev. A* **84**:063834, 2011.

[32] A. I. Zverev. *Handbook of filter synthesis*. Wiley, New York, 1967.

[33] J. Johnson. Thermal Agitation of Electricity in Conductors. *Phys. Rev.* **32**:97, 1928.

[34] H. Nyquist. Thermal Agitation of Electric Charge in Conductors. *Phys. Rev.* **32**:110, 1928.

[35] A. A. Clerk, S. M. Girvin, F. Marquardt, and R. J. Schoelkopf. Introduction to quantum noise, measurement, and amplification. *Rev. Mod. Phys.* **82**:1155, 2010.

[36] E. Hoffmann, F. Deppe, T. Niemczyk, T. Wirth, E. P. Menzel, G. Wild, H. Huebl, M. Mariantoni, T. Weißl, A. Lukashenko, A. P. Zhuravel, A. V. Ustinov, A. Marx, and R. Gross. A superconducting 180° hybrid ring coupler for circuit quantum electrodynamics. *Appl. Phys. Lett.* **97**:222508, 2010.

[37] C. K. Hong, Z. Y. Ou, and L. Mandel. Measurement of subpicosecond time intervals between two photons by interference. *Phys. Rev. Lett.* **59**:2044, 1987.

[38] S. M. Anlage, H. J. Snortland, and M. R. Beasley. A current controlled variable delay superconducting transmission line. *IEEE Trans. Magn.* **25**:1388, 1989.

[39] B. Ho Eom, P. K. Day, H. G. LeDuc, and J. Zmuidzinas. A wideband, low-noise superconducting amplifier with high dynamic range. *Nature Phys.* **8**:623, 2012.

[40] F. W. Byron and R. W. Fuller. *Mathematics of Classical and Quantum Physics*. Dover Publications, New York, 1992.

[41] L. Råde and B. Westergren. *Mathematics Handbook for Science and Engineering*. Studentlitteratur, Lund, 2004.

Appendix A

Mathematical tools

A.1 Dirac delta and Heaviside step function

The Dirac delta distribution δ is defined to satisfy

$$\int_{-\infty}^{\infty} dx\, \delta(x) f(x) = f(0), \tag{A.1}$$

for all smooth functions $f : \mathbb{R} \to \mathbb{R}$. It can be considered as a limit of Gaussian functions $\varphi_\sigma(x) = e^{-x^2/(2\sigma^2)}/\sqrt{2\pi\sigma^2}$ for $\sigma \to 0$, for which

$$\int_{-\infty}^{\infty} dx\, \delta(x) f(x) := \lim_{\sigma\to 0} \int_{-\infty}^{\infty} dx\, \varphi_\sigma(x) f(x) = f(0). \tag{A.2}$$

The Dirac delta behaves as a function in most cases, and in the context of physics, it is usually treated as a function for which $\delta(x) = 0$ for $x \neq 0$ [40].

The Heaviside step function θ is defined by

$$\theta(x) = \begin{cases} 1, & x > 0, \\ \frac{1}{2}, & x = 0, \\ 0, & x < 0. \end{cases} \tag{A.3}$$

The definition of $\theta(0)$ varies, but in distribution theory it is most conveniently defined as here to satisfy

$$\begin{aligned} \theta(0) &= \int_{-a}^{a} dx\, \delta(x)\theta(x) = [\theta(x)\theta(x)]_{x=-a}^{a} - \int_{-a}^{a} dx\, \theta(x)\delta(x) \\ &= 1 - 0 - \theta(0). \end{aligned} \tag{A.4}$$

Here, we used integration by parts and the fact that δ is the distribution derivative of θ, i.e.,

$$\int_{-\infty}^{\infty} dx\, \delta(x) f(x) = -\int_{-\infty}^{\infty} dx\, \theta(x) f'(x), \tag{A.5}$$

for all square-integrable smooth functions f on $\mathbb{R}$. This definition of $\theta(0)$ is also convenient if we define θ as a limit of the integrals of the Gaussian functions $\varphi_\sigma(x)$.

A.2 Fourier transform

The definition of the Fourier transform and the formulas used here can be found in many mathematics handbooks, e.g., [41].

A.2.1 Definition

In this thesis, the Fourier transform of a function $f : \mathbb{R} \to \mathbb{C}$ is defined by

$$F(\omega) = \mathcal{F}[f](\omega) = \int_{-\infty}^{\infty} dx e^{-i\omega x} f(x). \tag{A.6}$$

The Fourier transform is defined for square-integrable functions, distributions, and for some other special cases, too. The inverse Fourier transform is

$$f(x) = \mathcal{F}^{-1}[F](x) = \frac{1}{2\pi} \int_{-\infty}^{\infty} d\omega e^{i\omega x} F(\omega). \tag{A.7}$$

For most physical functions, the Fourier transform is well-defined, and the function may be expanded using Eq. (A.7). The Fourier transform may be defined for quantum operators as well, with a similar inverse formula.

A.2.2 Fourier transform formulas

Some Fourier transform formulas used in this thesis. Here, F is the Fourier transform of f and G is the Fourier transform of g.

$$\mathcal{F}[\alpha f(x) + \beta g(x)](\omega) = \alpha F(\omega) + \beta G(\omega), \tag{A.8}$$

$$\mathcal{F}[f(x-a)](\omega) = e^{-ia\omega} F(\omega), \qquad a \in \mathbb{R}, \tag{A.9}$$

$$\mathcal{F}[f(ax)](\omega) = \frac{1}{|a|} F\left(\frac{\omega}{a}\right), \qquad a \in \mathbb{R} \setminus \{0\}, \tag{A.10}$$

$$\mathcal{F}\left[e^{iax} f(x)\right](\omega) = F(\omega - a), \qquad a \in \mathbb{R}, \tag{A.11}$$

$$\mathcal{F}[F(\omega)](\xi) = 2\pi f(-\xi), \tag{A.12}$$

$$\mathcal{F}\left[\int_{-\infty}^{\infty} d\xi\, f(\xi) g(x-\xi)\right](\omega) = F(\omega) G(\omega), \tag{A.13}$$

$$\mathcal{F}[f(x)g(x)](\omega) = \frac{1}{2\pi} \int_{-\infty}^{\infty} d\nu F(\nu) G(\omega - \nu), \tag{A.14}$$

$$\mathcal{F}\left[\frac{d^n}{dx^n} f(x)\right](\omega) = (i\omega)^n F(\omega). \tag{A.15}$$

Fourier transforms of some functions and distributions:

$$\mathcal{F}\left[\delta(x)\right](\omega) = 1, \tag{A.16}$$

$$\mathcal{F}\left[\mathrm{sgn}(x)\right](\omega) = \frac{2}{i\omega}, \tag{A.17}$$

$$\mathcal{F}\left[1\right](\omega) = 2\pi\delta(\omega), \tag{A.18}$$

$$\mathcal{F}\left[\theta(x)\right](\omega) = \frac{1}{i\omega} + \pi\delta(\omega), \tag{A.19}$$

$$\mathcal{F}\left[e^{-ax}\theta(x)\right](\omega) = \frac{1}{a+i\omega}, \qquad a > 0, \tag{A.20}$$

$$\mathcal{F}\left[e^{-ax^2}\right](\omega) = \sqrt{\frac{\pi}{\alpha}}e^{-\frac{\omega^2}{4a}}, \qquad a > 0, \tag{A.21}$$

$$\mathcal{F}\left[e^{-ax^2}\theta(x)\right](\omega) = \sqrt{\frac{\pi}{\alpha}}e^{-\frac{\omega^2}{2a}}, \qquad a > 0, \tag{A.22}$$

$$\mathcal{F}\left[xe^{-ax}\theta(x)\right](\omega) = \frac{1}{(a+i\omega)^2}, \qquad a > 0. \tag{A.23}$$

Appendix B

Inverse Fourier transform of the reflection coefficient

In this Appendix, we derive the inverse Fourier transform of the reflection coefficient,

$$\tilde{r}(\tau) = \frac{1}{2\pi}\int_{-\infty}^{\infty} d\omega\, r(\omega) e^{i\omega\tau}. \tag{B.1}$$

The reflection coefficient in the case of a semi-infinite transmission line terminated by a single LC element is

$$r(\omega) = \frac{Z_0(\omega) - Z_c}{Z_0(\omega) + Z_c} = \frac{iL_0\omega + \frac{1}{iC_0\omega} - Z_c}{iL_0\omega + \frac{1}{iC_0\omega} + Z_c} = \frac{C_0L_0(i\omega)^2 - C_0Z_c(i\omega) + 1}{C_0L_0(i\omega)^2 + C_0Z_c(i\omega) + 1}, \tag{B.2}$$

where $Z_0(\omega)$ is the total impedance of the LC element, L_0 and C_0 are the inductance of the inductor and the capacitance of the capacitor in the LC element, respectively, and Z_c is the characteristic impedance of the transmission line. Let a and b be the complex-valued roots of the polynomial $C_0L_0x^2 - C_0Z_0x + 1$,

$$a = \frac{C_0Z_c + \sqrt{C_0^2Z_c^2 - 4C_0L_0}}{2C_0L_0}, \tag{B.3}$$

$$b = \frac{C_0Z_c - \sqrt{C_0^2Z_c^2 - 4C_0L_0}}{2C_0L_0}. \tag{B.4}$$

If $C_0^2Z_c^2 < 4C_0L_0$, the square roots are imaginary and $\Re(a) = \Re(b) = \frac{Z_c}{2L_0} > 0$. If $C_0^2Z_c^2 > 4C_0L_0$, then a and b are real and $a, b > 0$. Thus if $C_0^2Z_c^2 \neq 4C_0L_0$, we may write

$$\begin{aligned} r(\omega) &= \frac{C_0L_0(i\omega - a)(i\omega - b)}{C_0L_0(i\omega + a)(i\omega + b)} = \frac{(i\omega - a)(i\omega - b)}{(i\omega + a)(i\omega + b)} \\ &= 1 - \frac{2(a+b)}{a-b}\left(\frac{a}{a + i\omega} - \frac{b}{b + i\omega}\right). \end{aligned} \tag{B.5}$$

Using Eq. (A.20), we obtain the inverse Fourier transform,

$$\begin{aligned}\tilde{r}(\tau) &= \delta(\tau) - \frac{a+b}{a-b}\left[ae^{-a\tau}\theta(\tau) - be^{-b\tau}\theta(\tau)\right] \\ &= \delta(\tau) - \frac{a+b}{a-b}\left(ae^{-a\tau} - be^{-b\tau}\right)\theta(\tau). \end{aligned} \tag{B.6}$$

If $C_0^2 Z_c^2 = 4C_0 L_0$, we have $a = b = \frac{Z_c}{2L_0}$, and thus

$$r(\omega) = \frac{(i\omega - a)^2}{(i\omega + a)^2} = 1 - \frac{4i\omega a}{(i\omega + a)^2}. \tag{B.7}$$

Using Eqs. (A.15) and (A.23), we obtain

$$\tilde{r}(\tau) = \delta(\tau) - 4a\frac{d}{d\tau}\left[\tau e^{-a\tau}\theta(\tau)\right] = \delta(\tau) - 4a(1 - a\tau)e^{-a\tau}\theta(\tau). \tag{B.8}$$

In both cases, $\tilde{r}(\tau)$ is zero for $\tau < 0$ and vanishes exponentially for $\tau \to \infty$. Therefore, we may define the characteristic time scale for the reflection to be

$$\tau_0 = \frac{1}{\min[\Re(a), \Re(b)]}. \tag{B.9}$$

This time scale is used in the approximations for the reflection of wave packets.